Tumor characterization using radiolabeled anti-cancer drugs in NSCLC patients

Bahce, I.

2017

document version
Publisher's PDF, also known as Version of record

بسم الله الرحمن الرحيم

Tumor characterization using radiolabeled anti-cancer drugs in NSCLC patients

Idris Bahce

VRIJE UNIVERSITEIT

Tumor characterization using radiolabeled anti-cancer drugs in NSCLC patients.

ACADEMISCH PROEFSCHRIFT

ter verkrijging van de graad Doctor aan
de Vrije Universiteit Amsterdam,
op gezag van de rector magnificus
prof.dr. V. Subramaniam,
in het openbaar te verdedigen
ten overstaan van de promotiecommissie
van de Faculteit der Geneeskunde
op maandag 22 mei 2017 om 15.45 uur
in de aula van de universiteit,
De Boelelaan 1105

door
Idris Bahce
geboren te Zele

promotoren:	prof.dr. N.H. Hendrikse
	prof.dr. E.F. Smit
	prof.dr. A.A. Lammertsma
copromotor:	dr.ir. M.M. Yaqub

Table of Contents

Chapter 1.

Introduction and outline of the thesis

Background

Lung cancer epidemiology

Lung cancer is one of the most prevalent cancers worldwide, and it accounts for ~20% of all cancer-related mortality worldwide. North America and Europe have the highest incidences, reaching ~13% of all cancer diagnoses [1]. In the Netherlands, approximately 12.000 new cases of lung cancer are diagnosed each year according to the Netherlands Cancer Registry (Integraal Kankercentrum Nederland). Moreover, the incidence of lung cancer is still rising. Finally, the mortality incidence of lung cancer in the Netherlands is higher than 10.000 patients per year .

Cytotoxic chemotherapy

Lung cancer can be divided into 2 major histological types, i.e. small cell lung cancer and non-small cell lung cancer (NSCLC), comprising roughly 15% and 85% of patients, respectively. In approximately half of the newly diagnosed cases of NSCLC, patients have advanced metastatic disease, and the remaining patients have local or locally advanced disease, of whom the majority eventually develops advanced metastatic disease [2].

Systemic therapy is the corner stone of treatment in metastatic NSCLC. Historically, cytotoxic chemotherapy was the only option, albeit controversial. The survival advantages in NSCLC associated with the use of cisplatin were known as early as the seventies [3]. However, due to refractory emetogenicity, cisplatin was not broadly used until the nineties, when a new class of potent anti-emetics, i.e. serotonin antagonists, became available, making cisplatin therapy more tolerable [4, 5]. Various platinum containing regimens were investigated, and a preference according to histological classification was seen [6–10]. Furthermore, maintenance therapies using cytotoxic agents appeared to provide some benefit with respect to clinical outcome [11–13].

To date, the proportion of patients receiving chemotherapy for advanced stage NSCLC is only ~50% in the Netherlands [14]. The objective response rate to first line chemotherapy is ~30%. The median duration of response to first line chemotherapy is between 3.5 and 5.5 months [14]. So, even though the use of cytotoxic chemotherapy in NSCLC has improved outcome in advanced stage disease, gains have been limited. In addition, the gain in survival outcome seems to have reached a plateau. Therefore, more efficient systemic treatment options are urgently needed.

New treatment strategies to improve outcome for patients are under investigation. In the past decade, research on cancer immune therapy and molecular targeted therapy has led to significant clinical improvements in various subsets of NSCLC patients.

Targeted therapy

In recent years, targeted therapies against NSCLC, comprising tyrosine kinase inhibitors (TKIs) and monoclonal antibodies (mAbs), were introduced. As opposed to classical cytotoxic chemotherapeutic drugs that cause damage to all proliferating cells in a nonspecific manner, these targeted drugs act against specific targets.

Tyrosine kinases inhibitors (TKIs) are small molecules that can easily enter cells and subsequently inhibit intracellular tyrosine kinase enzymes that activate signal transduction cascades. Overall, TKIs can operate through different mechanisms. For example, TKIs can compete with adenosine triphosphate (ATP) for the ATP-binding pocket or they can affect TK activity by causing a conformational change. In addition, TKIs can interfere with the TK's Hsp90 molecular chaperone system, which causes ubiquitination and degradation of the TK.

In NSCLC, TKIs directed against EGFR, ALK, and ROS1 are used in routine clinical practice. Patients harboring a sensitizing EGFR mutation or a sensitizing ALK or ROS1 translocation (~10%, ~5% and ~1% of NSCLC patients in the Western population, respectively) respond much better to TKIs than to cytotoxic chemotherapy [15]. Typically, the response rate in these sensitive subgroups is around 70%. Furthermore, the duration of response is much longer than with cytotoxic chemotherapy [16–19]. TKIs directed against BRAF, MEK, MET, Her2, and RET are in various stages of development. Patients with sensitizing DNA alterations in these genes also respond to TKIs, although the response rates are usually lower than in patients with EGFR, ALK or ROS1 aberrations, with the exception of BRAF [20–22].

Monoclonal antibodies are large molecules that usually do not enter cells, but primarily bind to extracellular targets, such as cell surface proteins. Therapeutic mAbs can act through different mechanisms. For example, mAbs can block the function of a targeted molecule or modulate signaling pathways, which can lead to inhibition of cell proliferation. In addition, mAbs can bind to cancer cells and induce an immune response.

In NSCLC, at present, mAbs directed against EGFR, VEGF, VEGFR and PD-1 are used in routine clinical practice [23]. Monoclonal antibodies directed against EGFR, VEGF and VEGFR have shown modest clinical benefit when added to cytotoxic

chemotherapy regimens. The increase in median overall survival by adding these mAbs was between 1.4 and 2.0 months [24–26]. In general, there are no predictive biomarkers in use that allow for selecting sensitive subgroups, however, there is some evidence to suggest that target expression levels could predict for higher response rates. For example, EGFR-expression in non-squamous NSCLC tumors correlated with treatment efficacy of necitumumab, an anti-EGFR mAb, combined with first line chemotherapy [27].

Monoclonal antibodies directed against PD-1 are currently approved for use in second line as monotherapy in patients with NSCLC. Approximately ~20% of NSCLC patients responds to anti-PD-1 therapy with a 1-year survival rate of approximately 40-50% [28–30]. In anti-PD-1/PD-L1 therapy, the role of PD-L1 expression as a predictive marker is becoming ever more important. For example, nivolumab was approved for all NSCLC patients, irrespective of tumor PD-L1 expression. However, the use of pembrolizumab in second line, another anti-PD1 mAb, is approved in patients with a PD-L1 positive tumor (Tumor Proportion Score (TPS) greater than or equal to 1%). Furthermore, the FDA recently approved the use of pembrolizumab in first line in patients whose tumors have high PD-L1 expression (TPS greater than or equal to 50%) as determined by an FDA-approved test. This indicates that PD-L1 has predictive capacity [31].

Selecting the right therapy

Targeted agents, mainly TKIs and anti-PD1 mAbs, can provide superior efficacy in specific subgroups of sensitive patients. Molecular analysis of tumor specimens can detect these patients by identifying sensitizing DNA mutations, gene rearrangements or protein expressions.

In the absence of a sensitizing molecular alteration, these targeted agents perform worse than cytotoxic chemotherapy. Therefore, they should only be given to patients with a proven sensitive tumor. This poses a challenge, as it is often difficult to obtain representative tumor biopsies in sufficient quantities.

Without having proof for these sensitizing molecular alterations, patients should not receive targeted agents, as this may cause unnecessary toxicity and delay more effective cytotoxic chemotherapy. In addition, costs of targeted therapy are much higher than those of chemotherapy. For example, in 2015 the quality adjusted life year costs of nivolumab was estimated at € 134,000 by the Netherlands National Health Care Institute (Zorginstituut Nederland).

Therefore, identification of sensitive patients for targeted therapy is essential. As classical biopsy based analyses are associated with the abovementioned

limitations, non-biopsy based predictive biomarkers are needed. An imaging biomarker based on positron emission tomography (PET) and radiolabeled targeted drugs may offer a solution.

PET and radiolabeled targeted agents

PET is an imaging technique that is based on the simultaneous detection of two coincident gamma rays, resulting from the annihilation of a positron emitted by a positron emitting radionuclide. By labelling a compound with such a positron emitter, its distribution in the human body can be measured non-invasively. In addition, by performing repetitive scans (i.e. a dynamic scan) after injection its pharmacokinetic behavior can also be measured. PET using TKIs and mAbs labelled with a positron emitter may offer a new (non-invasive) approach to identify sensitive patients.

Aim and outline

The aim of this thesis is to investigate the potential of PET using radiolabeled targeting agents, i.e. TKI PET using [^{11}C]erlotinib and immunoPET using [^{89}Zr]bevacizumab, directed against NSCLC, as a means to characterize tumors and determine their sensitivity to targeting agents.

Chapter 2 reviews the current literature on TKI PET and immunoPET in NSCLC, and provides an overview of the most relevant preclinical and clinical studies.

Chapter 3 investigates uptake and pharmacokinetics of [^{11}C]erlotinib, a radiolabeled EGFR TKI, in NSCLC tumors. The aims of this study were to assess (1) whether tumor tracer uptake can be quantified, and (2) whether tracer uptake levels can predict the presence of activating tumor EGFR mutations.

Chapter 4 describes the optimal pharmacokinetic model for quantification of uptake and evaluates various simplified methods for routine analysis of [^{11}C]erlotinib uptake in NSCLC patients.

Chapter 5 compares uptake of [^{11}C]erlotinib in NSCLC patients off and on erlotinib therapy. The aims of this study were to evaluate the effects of erlotinib therapy on tumor [^{11}C]erlotinib uptake. A secondary aim was to investigate the use of venous blood samples.

Chapter 6 discusses the potential role of [^{11}C]erlotinib PET in detecting tumor TKI resistance and heterogeneity, as illustrated in the case of an EGFR mutation positive patient that progressed after erlotinib therapy.

Chapter 7 studies uptake of [^{89}Zr]bevacizumab in NSCLC patients, who subsequently are treated with a bevacizumab containing chemotherapy regimen. The aim of this pilot study was to evaluate whether uptake of [^{89}Zr]bevacizumab in NSCLC can be visualized and quantified. In addition, the correlation between tumor [^{89}Zr]bevacizumab uptake and tumor response to therapy with a bevacizumab based regimen was explored.

Abbreviations

ALK	Anaplastic Lymphoma Kinase
ATP	Adenosine Triphosphate
BRAF	B-RAF (Rapidly Accelerated Fibrosarcoma) (proto-oncogene)
EGFR	Epidermal Growth Factor Receptor
HER2	Human Epidermal growth factor Receptor 2
mAb	monoclonal Antibody
MEK	MAPK/ERK Kinase
MET	hepatocyte growth factor receptor (proto-oncogene)
NSCLC	Non-Small Cell Lung Cancer
PD-1	Programmed cell Death protein-1
PD-L1	Programmed cell Death-Ligand 1
PET	Positron Emission Tomography
RET	Rearranged during transfection (proto-oncogene)
ROS1	ROS Proto-Oncogene 1, Receptor Tyrosine Kinase (proto-oncogene)
TKI	Tyrosine Kinase Inhibitor
VEGF	Vascular Endothelial Growth Factor
VEGFR	Vascular Endothelial Growth Factor Receptor

Bibliography

1. Ferlay J, Soerjomataram I, Dikshit R, Eser S, Mathers C, Rebelo M, et al. Cancer incidence and mortality worldwide: sources, methods and major patterns in GLOBOCAN 2012. Int J Cancer. 2015, 136: E359–86.

2. SEER Cancer Statistics Factsheets: Lung and Bronchus Cancer. National Cancer Institute. 2016, http://seer.cancer.gov/statfacts/html/lungb.html.

3. Eagan R, Ingle JN, Frytak S, Rubin J, Kvols L, Carr D, et al. Platinum based polychemotherapy versus dianhydrogalactitol in advanced non-small cell lung cancer. Cancer treatment reports. 1977, 61: 1339–1345.

4. Hainsworth J, Harvey W, Pendergrass K, Kasimis B, Oblon D, Monaghan G, et al. A single-blind comparison of intravenous ondansetron, a selective serotonin antagonist, with intravenous metoclopramide in the prevention of nausea and vomiting associated with high-dose cisplatin chemotherapy. Journal of clinical oncology. 1991, 9: 721–728.

5. De Mulder PH, Seynaeve C, Vermorken JB, van Liessum PA, Mols-Jevdevic S, Allman EL, et al. Ondansetron compared with high-dose metoclopramide in prophylaxis of acute and delayed cisplatin-induced nausea and vomiting: a multicenter, randomized, double-blind, crossover study. Annals of internal medicine. 1990, 113: 834–840.

6. Scagliotti GV, Parikh P, Von Pawel J, Biesma B, Vansteenkiste J, Manegold C, et al. Phase III study comparing cisplatin plus gemcitabine with cisplatin plus pemetrexed in chemotherapy-naive patients with advanced-stage non-small-cell lung cancer. Journal of Clinical Oncology. 2008, 26: 3543–3551.

7. Scagliotti G, De Marinis F, Rinaldi M, Crino L, Gridelli C, Ricci S, et al. Phase III randomized trial comparing three platinum-based doublets in advanced non-small-cell lung cancer. Journal of Clinical Oncology. 2002, 20: 4285–4291.

8. Schiller JH, Harrington D, Belani CP, Langer C, Sandler A, Krook J, et al. Comparison of four chemotherapy regimens for advanced non-small-cell lung cancer. New England Journal of Medicine. 2002, 346: 92–98.

9. Pujol J-L, Barlesi F, Daurès J-P. Should chemotherapy combinations for advanced non-small cell lung cancer be platinum-based? A meta-analysis of phase III randomized trials. Lung cancer. 2006, 51: 335–345.

10. D'Addario G, Pintilie M, Leighl NB, Feld R, Cerny T, Shepherd FA. Platinum-based versus non-platinum-based chemotherapy in advanced non-small-cell lung cancer: a meta-analysis of the published literature. Journal of clinical oncology. 2005, 23: 2926–2936.

11. Cappuzzo F, Ciuleanu T, Stelmakh L, Cicenas S, Szczésna A, Juhász E, et al. Erlotinib as maintenance treatment in advanced non-small-cell lung cancer: a multicentre, randomised, placebo-controlled phase 3 study. The lancet oncology. 2010, 11: 521–529.

12. Paz-Ares L, de Marinis F, Dediu M, Thomas M, Pujol JL, Bidoli P, et al. Maintenance therapy with pemetrexed plus best supportive care versus placebo plus best supportive care after induction therapy with pemetrexed plus cisplatin for advanced non-squamous non-small-cell lung cancer (PARAMOUNT): a double-blind, phase 3, randomised controlled trial. The lancet oncology. 2012, 13: 247–55.

13. Ciuleanu T, Brodowicz T, Zielinski C, Kim JH, Krzakowski M, Laack E, et al. Maintenance pemetrexed plus best supportive care versus placebo plus best supportive care for non-small-cell lung cancer: a randomised, double-blind, phase 3 study. The Lancet. 2009, 374: 1432–1440.

14. Aarts MJ, van den Borne BE, Biesma B, Kloover JS, Aerts JG, Lemmens VE. Improvement in population-based survival of stage IV NSCLC due to increased use of chemotherapy. International Journal of Cancer. 2015, 136: E387–E395.

15. Laenger F, Dickgreber N, Lehmann U. Molecular pathology. ERS monogr. 2015, 68: 95–118.

16. Shaw AT, Ou S-HI, Bang Y-J, Camidge DR, Solomon BJ, Salgia R, et al. Crizotinib in ROS1-rearranged non-small-cell lung cancer. New England Journal of Medicine. 2014, 371: 1963–1971.

17. Shaw AT, Kim D-W, Nakagawa K, Seto T, Crinó L, Ahn M-J, et al. Crizotinib versus chemotherapy in advanced ALK-positive lung cancer. New England Journal of Medicine. 2013, 368: 2385–2394.

18. Rosell R, Carcereny E, Gervais R, Vergnenegre A, Massuti B, Felip E, et al. Erlotinib versus standard chemotherapy as first-line treatment for European patients with advanced EGFR mutation-positive non-small-cell lung cancer (EURTAC): a multicentre, open-label, randomised phase 3 trial. The lancet oncology. 2012, 13: 239–246.

19. Mok TS, Wu YL, Thongprasert S, Yang CH, Chu DT, Saijo N, et al. Gefitinib or carboplatin-paclitaxel in pulmonary adenocarcinoma. New England Journal of Medicine. 2009, 361: 947–957.

20. Pérol M. Negative results of METLung study: an opportunity to better understand the role of MET pathway in advanced NSCLC. Translational lung cancer research. 2014, 3: 392.

21. Mazières J, Peters S, Lepage B, Cortot AB, Barlesi F, Beau-Faller M, et al. Lung cancer that harbors an HER2 mutation: epidemiologic characteristics and therapeutic perspectives. Journal of Clinical Oncology. 2013, 31: 1997–2003.

22. Tsuta K, Kohno T, Yoshida A, Shimada Y, Asamura H, Furuta K, et al. RET-rearranged non-small-cell lung carcinoma: a clinicopathological and molecular analysis. British journal of cancer. 2014, 110: 1571–1578.

23. Bahce I, Yaqub M, Smit E, Lammertsma A, van Dongen G, Hendrikse N. Personalizing NSCLC therapy by characterizing tumors using TKI-PET and immuno-PET. Lung Cancer. 2016, doi: 10.1016/j.lungcan.2016.05.025.

24. Sandler A, Gray R, Perry MC, Brahmer J, Schiller JH, Dowlati A, et al. Paclitaxel-carboplatin alone or with bevacizumab for non-small-cell lung cancer. N Engl J Med. 2006, 355: 2542–50.

25. Garon EB, Ciuleanu T-E, Arrieta O, Prabhash K, Syrigos KN, Goksel T, et al. Ramucirumab plus docetaxel versus placebo plus docetaxel for second-line treatment of stage IV non-small-cell lung cancer after disease progression on platinum-based therapy (REVEL): a multicentre, double-blind, randomised phase 3 trial. The Lancet. 2014, 384: 665–673.

26. Thatcher N, Hirsch FR, Luft AV, Szczesna A, Ciuleanu TE, Dediu M, et al. Necitumumab plus gemcitabine and cisplatin versus gemcitabine and cisplatin alone as first-line therapy in patients with stage IV squamous non-small-cell lung cancer (SQUIRE): an open-label, randomised, controlled phase 3 trial. The lancet oncology. 2015, 16: 763–774.

27. Paz-Ares L, Socinski M, Shahidi J, Hozak R, Soldatenkova V, Kurek R, et al. Correlation of EGFR-expression with safety and efficacy outcomes in SQUIRE: a randomized, multicenter, open-label, phase III study of gemcitabine-cisplatin plus necitumumab versus gemcitabine-cisplatin alone in the first-line treatment of patients with stage IV squamous non-small cell lung cancer. Annals of Oncology. 2016, doi: 10.1093/annonc/mdw214.

28. Garon EB, Rizvi NA, Hui R, Leighl N, Balmanoukian AS, Eder JP, et al. Pembrolizumab for the treatment of non-small-cell lung cancer. New England Journal of Medicine. 2015, 372: 2018–2028.

29. Borghaei H, Paz-Ares L, Horn L, Spigel DR, Steins M, Ready NE, et al. Nivolumab versus docetaxel in advanced nonsquamous non-small-cell lung cancer. New England Journal of Medicine. 2015, 373: 1627–1639.

30. Brahmer J, Reckamp KL, Baas P, Crinò L, Eberhardt WE, Poddubskaya E, et al. Nivolumab versus docetaxel in advanced squamous-cell non-small-cell lung cancer. New England Journal of Medicine. 2015, 373: 123–135.

31. Reck M, Rodriguez-Abreu D, Robinson AG, Hui R, Csoszi T, Fülöp A, et al. Pembrolizumab versus Chemotherapy for PD-L1-Positive Non-Small-Cell Lung Cancer. New England Journal of Medicine. 2016, doi: 10.1056/NEJMoa1606774.

Chapter 2

Personalizing NSCLC therapy by characterizing tumors using TKI-PET and immuno-PET

Idris Bahce

Maqsood Yaqub

Egbert F. Smit

Adriaan A. Lammertsma

Guus A.M.S. van Dongen

N.Harry Hendrikse

Lung Cancer. 2016 May 31. doi: 10.1016/j.lungcan.2016.05.025.

Abstract

Non-small cell lung cancer (NSCLC) therapy has entered a rapidly advancing era of precision medicine with an ever increasing number of drugs directed against a variety of specific tumor targets. Amongst these new agents, tyrosine kinase inhibitors (TKIs) and monoclonal antibodies (mAbs) are most frequently used. However, as only a sensitive subgroup of patients benefits from targeting drugs, predictive biomarkers are needed. Positron emission tomography (PET) may offer such a biomarker for predicting therapy efficacy. Some of the TKIs and mAbs that are in clinical use can be radioactively labeled and used as tracers. PET can visualize and quantify tumor specific uptake of radiolabeled targeting drugs, allowing for characterization of their pharmacokinetic behavior. In this review, the clinical potential of PET using radiolabeled TKIs (TKI-PET) and mAbs (immuno-PET) in NSCLC is discussed, and an overview is provided of the most relevant preclinical and clinical studies.

1. Introduction

Non-small cell lung cancer (NSCLC) causes the highest cancer-related mortality worldwide [1]. Until a decade ago, the number of systemic treatment options was limited. However, with advancements in molecular genotyping of NSCLC tumors, ever more actionable molecular targets are being identified. Highly specific drugs directed against these targets are rapidly being developed and approved (see Table 1). Targeting drugs like tyrosine kinase inhibitors (TKIs) and monoclonal antibodies (mAbs) have demonstrated to improve clinical outcome in target-positive tumors. For example, epidermal growth factor receptor (EGFR) TKIs achieve response rates up to 70% in patients with activating EGFR mutations [2]. Furthermore, mAbs directed against immune checkpoint targets such as PD1, PDL1 or CTLA4 may achieve very long durations of response, even reaching several years in a limited number of patients [3]. However, in patients with target-negative tumors, most targeting drugs perform worse than cytotoxic agents. In addition, the costs of these new targeting drugs are much higher as compared to classical cytotoxic agents. For example, in 2015 the quality adjusted life year cost of nivolumab was estimated at 134.000 € by the Netherlands National Health Care Institute. These facts highlight the necessity for limiting the use of these drugs to sensitive patients, i.e. personalizing therapy.

Table 1. NSCLC targeted therapies and FDA-approval status.

Drug class	Generic name	Trade name	Target	T½	Cancer indication	FDA approval status (date)
TKI	Erlotinib	Tarceva	EGFR	36 hrs	NSCLC with activating EGFR mutations[b], 1st line	Approved May, 2013
TKI	Afatinib	Gilotrif (Giotrif) [a]	EGFR / ERBB2	37 hrs	NSCLC with activating EGFR mutations[b],	Approved Jul, 2013

					1st line	
TKI	Gefitinib	Iressa	EGFR	48 hrs	NSCLC with activating EGFR mutations[b], 1st line	Approved Jul, 2015
TKI	Osimertinib	Tagrisso	EGFR	48 hrs	NSCLC with T790M mutation-positive EGFR, in 2nd line after PD on treatment with an FDA-approved, EGFR TKI.	Approved Nov, 2015
TKI	Rociletinib		EGFR	2-4 hrs	NSCLC with T790M mutation-positive EGFR, in 2nd line after PD on treatment with an FDA-approved, EGFR TKI.	Breakthrough Therapy Designation May, 2014
TKI	BI1482694 (HM61713)		EGFR		NSCLC with T790M mutation-positive EGFR, in 2nd line after PD on treatment	Breakthrough Therapy Designation December, 2015

					with an FDA-approved, EGFR TKI.	
TKI	Crizotinib	Xalkori	ALK	42 hrs	NSCLC with ALK activation	Approved Nov, 2013
TKI	Ceritinib	Zykadia	ALK	41 hrs	NSCLC with ALK activation, 2nd line when not able to be treated with crizotinib or PD while on crizotinib	Approved Apr, 2014
TKI	Alectinib	Alecensa	ALK	20 hrs	NSCLC with ALK activation, 2nd line when not able to be treated with crizotinib or PD while on crizotinib	Approved Dec, 2015
TKI	Brigatinib		ALK		NSCLC with ALK activation, 2nd line when not able to be treated with crizotinib or PD while on	Breakthrough Therapy Designation Oct, 2014

					crizotinib	
TKI	Dabrafenib	Tafinlar	BRAF	8 hrs	NSCLC with BRAF V600E mutations, in 2nd line after platinum containing regimen.	Breakthrough Therapy Designation Jan, 2014
mAb	Necitumumab	Portrazza	EGFR	14 days	NSCLC squamous, in 1st line combined with doublet	Approved Nov, 2015
mAb	Bevacizumab	Avastin	VEGF	20 days	NSCLC, in 1st line combined with carboplatin and paclitaxel	Approved Oct, 2006
mAb	Ramucirumab	Cyramza	VEGFR	15 days	NSCLC, in 2nd line with docetaxel after platinum containing regimen.	Approved Dec, 2014
mAb	Pembrolizumab	Keytruda	PD1	26 days	NSCLC (non-EGFR, non-ALK)[c] with PD-L1 in 2nd line after platinum containing	Approved Oct, 2015

					regimen.	
mAb	Nivolumab	Opdivo	PD1	27 days	NSCLC (non-EGFR, non-ALK)[c] in second line after platinum containing regimen.	Approved Oct, 2015
mAb	Atezolizumab		PD-L1	21 days	NSCLC (non-EGFR, non-ALK)[c] with PD-L1 in 2nd line after platinum containing regimen.	Breakthrough Therapy Designation Feb, 2015

FDA approved drugs and drugs granted Breakthrough Therapy Designation status as of February 2016 are listed.

***Abbreviations**: ALK = anaplastic lymphoma kinase; EGFR = epidermal growth factor receptor; FDA = U.S. Food and Drug Administration; NSCLC = non-small cell lung cancer; PD = progressive disease; PD1 = programmed death-1; PD-L1 = programmed death ligand-1; T½ = mean biological elimination half life according to FDA prescribing information; VEGF = vascular endothelial growth factor; VEGFR = VEGF receptor.*

*(**a**)Trade name is Giotrif is in Europe.*
*(**b**) Patients harboring an EGFR exon 19 deletion or an exon 21 (L858R) substitution mutation as detected by an FDA-approved test.*
*(**c**) Patients with EGFR or ALK genomic tumor aberrations should have PD on FDA-approved therapy for these aberrations.*

A promising new approach for personalizing therapy is the use of positron emission tomography (PET) and radioactively labeled drugs. Classically, pharmacokinetic (PK) analysis of newly developed drugs is performed by serial assessment of drug and metabolites concentrations in plasma and sometimes in urine or stool samples after administrating the drug orally or intravenously. Using PET, radiolabeled drugs

can be used as PET tracers that allow for PK studies [4]. Compared to preclinical and clinical PK studies, PET provides a faster and more cost-effective approach, moreover, it provides additional information e.g. on drug modeling and on the drug tissue distribution, particularly on drug uptake in tumors. These PK insights are now being used to study the potential of PET as a predictive imaging biomarker.

This review will mention some of the general principles of PET and then focus on the current research and potential clinical implications of PET using radiolabeled mAbs (immuno-PET) and TKIs (TKI-PET) in personalizing NSCLC therapy. Literature searches were performed in PubMed and references from relevant articles using the search terms “NSCLC”, "immuno", “TKI”, "radionuclide imaging", “PET”, and their synonyms (see Supplementary table 1 and Supplementary table 2). Only publications in English, up to February, 2016, were included.

2. General principles of PET, possibilities and limitations

PET is an imaging technique that utilizes gamma rays, emitted by positron emitting tracers, to produce 3-dimensional images (see Figure 1). Using PET, the PK behavior of tracers can be imaged *in vivo*. For example, the most often used PET tracer in NSCLC is fluorine-18 labeled fluorodeoxyglucose ([^{18}F]FDG or FDG), a glucose analog that accumulates in cells with high glucose metabolism. FDG was the first widely used PET tracer to improve disease staging, i.e. by better identifying lymph node metastases and distant metastases. This improvement in disease staging led to a decrease in futile thoracotomies, e.g. a 20% decrease in the absolute number of thoracotomies was seen in the Amsterdam region [5, 6]. Besides staging, FDG PET was also used to assess metabolic response. For example, metabolic changes after chemoradiotherapy could predict residual vital tumor cells in NSCLC tumors [7]. However, FDG is only specific for glucose metabolism. To identify the previously mentioned actionable molecular targets, specific PET tracers are needed.

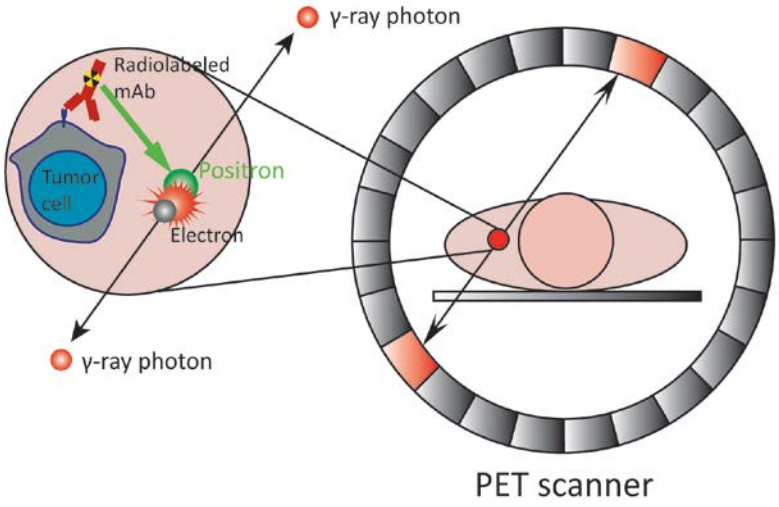

Fig. 1. The basic mechanism of action of PET is shown. A patient with a tumor, in which a radiolabeled mAb is bound to a tumor cell, is depicted. The radionuclide emits a positron that annihilates with a nearby electron, hereby producing 2 gamma ray photons, each with an energy of 511 keV. The oppositely directed photons are detected by the PET scanner. Calculating each of the synchronously detected pairs of photons allows for a 3-dimensional reconstruction of the tracer distribution.

A great advantage of PET is that targeting drugs themselves can be used as PET tracers, provided that they can be labeled with a positron emitting radionuclide. The PK behavior of these radiolabeled drugs can then be studied. These PK insights are both useful for developing new drugs, as well as for clinical use, as the binding of radiolabeled drugs to tumors possibly predicts for tumor sensitivity to therapy. In addition, tumor sensitivity to therapy can vary between and within tumor lesions. Heterogeneity of target expression is typically determined by (molecular) pathology, the gold standard for diagnosis, either obtained by tumor biopsies or from circulating tumor products in blood, such as proteins, miRNA or DNA [8]. PET using radiolabeled drugs could offer additional benefits to pathology, namely in overcoming some of the limitations associated with pathology. For example, obtaining high yields of representative tumor samples to establish the correct diagnosis is not always possible due to difficulties reaching the tumor [9]. A limitation associated with blood sampling markers is the fact that the obtained

data cannot be related to a specific lesion. Here, PET may help by providing (whole body) imaging that takes multiple tumor lesions as well as normal tissues into account. This bears an enormous potential for tailoring therapy to fit the patient's individual needs. In addition, this technique is *in vivo*, non-invasive and not prone to sampling errors.

However, there are limitations to PET imaging. Ideally, drugs are labeled with radionuclides by way of substitution. As this will not alter the parent molecule's configuration, the PK of the parent drug's unlabeled and labeled form remains identical. When substitution is not possible, the radionuclide will be attached to the parent drug. The molecular structure of the labeled form is then altered, whereby the PK of the tracer may not be fully representative of the parent drug anymore. Furthermore, large interpatient differences in terms of tracer metabolism can cause alterations in the signal-to-noise ratio and hamper a clear interpretation of the data. Other limitations are associated with the choice of the scanning protocol (see Figure 2). A dynamic protocol allows for accurate quantification of tracer uptake, however, is constrained to a single fixed field of view and does not allow whole body techniques. However, if the intention of the protocol is to scan the whole of the body, a static protocol will be used and quantification of uptake will be less accurate as compared to the dynamic scanning protocols. There may be infrastructural limitations such as the absence of a tracer production capacity. e.g. a cyclotron. Typically any very short-lived tracer like carbon-11 labeled TKI has to be produced immediately prior to injection and is not suited for shipping to remote centers.

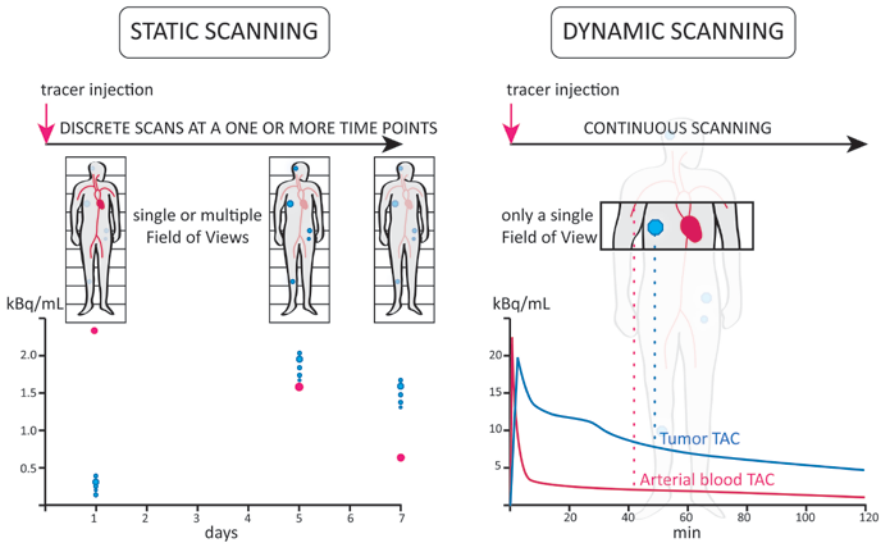

Fig. 2. Main differences between static and dynamic scanning procedures are shown schematically. Using a dynamic protocol, PET continuously scans a fixed single Field of View (FoV) of approximately 18 cm that contains the volume of interest (e.g. tumor = blue octagon) and an arterial blood pool (e.g. the left ventricle, aorta or large arteries = red cone and red lines). The post tracer injection time (radio)activity curves (TACs) of the tumor and arterial blood pool are plotted (typically for several minutes to several hours).An accurate uptake measure can be calculated using these TACs. This protocol is typically used for tracers with a rapid PK profile. In static scanning, a single FoV is scanned for a relatively short period of time (usually several minutes), allowing for multiple FoVs to be scanned (e.g. when multiple tumor lesions are present = blue octagons). Typically, static scans are performed using tracers that reach a steady state in their tumor TAC (or tumor-to-blood ratio) or using tracers with a slow PK (e.g. radiolabeled mAbs). The latter scenario allows for multiple scans after a single injection, as depicted above. The plotted (radio)activity concentration in the tumor lesions (blue octagons) is the highest at day 5 post injection, while the tumor-to-blood ratio is the highest on day 7, as the blood pool activity (red dots) continuously decreases.

3. Immuno-PET

The current antibody therapies are shown in Table 1 (see also Figure 3). Radiolabeled mAbs that have been investigated in immuno-PET studies are shown in Table 2.

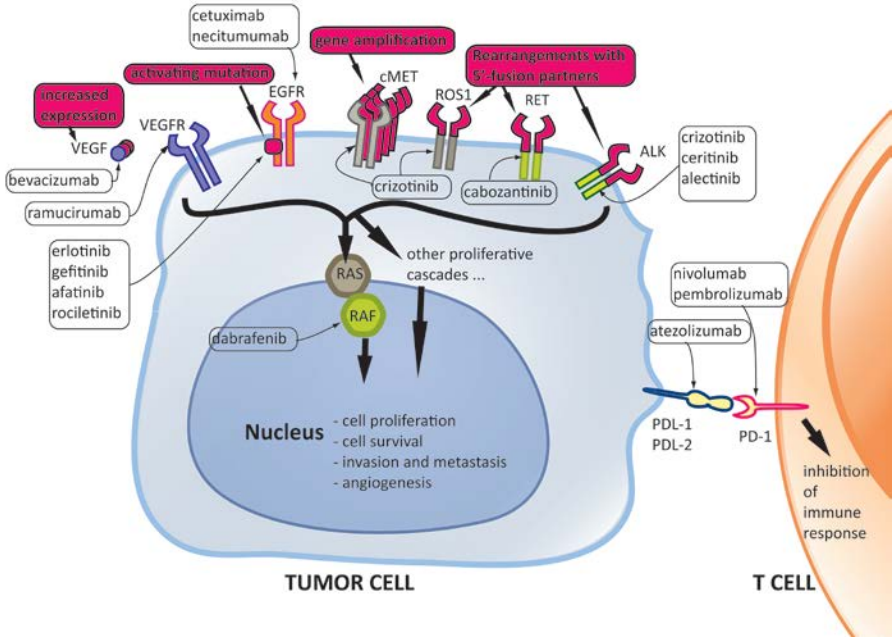

Fig. 3. *A simplified overview of the targets and mechanisms of action of the targeting drugs used in NSCLC is depicted.*

Table 2. Immuno-PET trials.

Drug target	Year Ref	Tracer (injected dose)	Design - scanned population	Xenograft cell line	Scanning protocol - Timing[a] - uptake parameter	Results[b]

EGFR	2009 [10]	^{64}Cu-DOTA-panitumumab (7 - 8 MBq)	athymic nude mice with subcutaneous xenografts	SQB20 SAS UM-SCC-22B	4 to 48 h %ID/g	Tracer uptake was lowest in the cell line with highest EGFR expression. However, this cell line demonstrated the lowest vessel density and vascular permeability, which may have caused this effect.
EGFR	2010 [11]	^{86}Y-CHX-A''-DTPA-panitumumab (1.8 – 2.0 MBq)	athymic nude mice with subcutaneous xenografts	LS-174T PC-3 A431	0.5 to 3 days %ID/cc	The highest tracer uptake was seen in the highest EGFR-expressing cell line, and uptake increased from day 1 through 3. Adding cold panitumumab uptake blocked tracer uptake.
EGFR	2011 [12]	^{86}Y- CHX-A''-DTPA-panitumumab ^{86}Y- CHX-A''-DTPA-cetuximab (1.7 – 1.9 MBq)	athymic nude mice with subcutaneous xenografts	NCI-H226 NCI-H2052 MSTO-211H	0.5 to 3 days %ID/cc	Both tracers showed comparable high tumor uptake in EGFR-expressing xenografts. Uptake was blocked by cold mAb. Blood clearance of ^{86}Y-cetuximab was faster than ^{86}Y-

						panitumumab. Tumor-to-liver ratio was higher in ^{86}Y-panitumumab than ^{86}Y-cetuximab.
EGFR	2012 [13]	[^{89}Zr]panitumumab (1.7 – 1.9 MBq)	athymic nude mice with subcutaneous, intraperitoneal and pulmonary xenografts	LS-174T A431 A375	1 to 7 days %ID/g	Tracer uptake was higher in EGFR expressing cell lines. Uptake was blocked by adding cold panitumumab. The highest uptake was seen in peritoneal tumors, then thoracic and then subcutaneous tumors of EGFR expressing cell lines.
EGFR	2013 [14]	[^{89}Zr]panitumumab (10.18 ± 1.24 MBq)	athymic nude mice with subcutaneous xenografts	BT-474, MDA-MB-231 MDA-MB-468	1 to 6 days %ID/g	High tracer uptake was seen in high EGFR expressing cell lines, uptake was highly correlated with EGFR expression levels.

EGFR	2005 [15]	[^{89}Zr]cetuximab (0.32 - 0.5 MBq)	athymic nude mice with subcutaneous xenografts	A431	1 to 6 days %ID/g	High tracer uptake was seen in the EGFR-expressing tumor.
EGFR	2007 [16]	^{64}Cu-DOTA-cetuximab (5 – 10 MBq)	athymic nude mice with subcutaneous (MDA-MB-435 in mammary fat pad) xenografts	U87MG PC-3 CT-26 HCT-8 HCT-116 SW620 MDA-MB-435	1 to 48 h %ID/g	Linear correlation between tracer uptake and EGFR expression in tumors. Uptake reaching a plateau after 24 hours.
EGFR	2008 [17]	^{64}Cu-DOTA-cetuximab (5.6 and 7.8 MBq)	athymic nude mice with subcutaneous (MDA-MB-435 in mammary fat pad) xenografts	A431 MDA-MB-435	4 to 46 h SUV	High tracer uptake was only seen in the high EGFR expressing cell line. Tracer uptake was blocked by adding cold cetuximab.
EGFR	2008 [18]	^{64}Cu-DOTA-cetuximab (7.4 MBq)	athymic nude mice with subcutaneous xenografts	CaSki	At 24 h p.i. SUV	High tracer uptake was seen in the high EGFR-expressing tumor.
EGFR	2009	[^{89}Zr]cetuximab	athymic nude mice with	A-431 T-47D	1 to 96 h	Tracer uptake was higher in intermediate

	[19]	(3.75 ± 0.14 MBq)	subcutaneous xenografts	U-373 HT-29	%ID/cc	EGFR-expressing cell lines than high expressing cell line, the uptake was the lowest in the low EGFR-expressing cell line. Possible explanations for the mismatch may include inadequate vasculature and perfusion, resulting in a heterogeneous and limited tracer uptake.
EGFR	2010 [20]	^{86}Y-CHX-A''-DTPA-cetuximab (3.8 – 4.0 MBq)	athymic nude mice with subcutaneous xenografts	LS-174T HT29 PC-3 DU145 SKOV3 SHAW	1 to 3 days %ID/cc	High EGFR expressing cell lines had the highest tracer uptake, which could be blocked dose-dependently by adding cold cetuximab.
EGFR	2010 [21]	^{64}Cu-DOTA-cetuximab (7 – 8 MBq)	athymic nude mice with subcutaneous xenografts	UM-SCC-22B SCC1	4 to 48 h % ID/g	The highest tracer uptake was seen in the low EGFR expressing tumor, which also seemed to grow on cetuximab. This was ascribed to decreased vessel density and vascular

						permeability.
EGFR	2013 [22]	[^{89}Zr]cetuximab (step 1: 2x60MBq; Step 2: 120MBq)	9 patients (6 NSCLC and 3 HNC) were co-injected with [^{89}Zr]cetuximab and cold cetuximab prior to scanning; prim objective was safety, secondary objective was tumor imaging		Step 1: at days 4, 5, 6 p.i. (patient 1 was also scanned at day 12 p.i.) Step 2: at days 5, 6, 7 p.i. TBR	No toxicity was observed in both steps. Heterogeneous uptake was seen in tumors. Best timing for TBR may be at late time points (up to 12 days p.i.)
EGFR	2015 [23]	[^{89}Zr]cetuximab (37 ± 1 MBq)	10 KRASwt mCRC patients were co-injected with [^{89}Zr]cetuximab and cold cetuximab		1 h to 10 days SUV	Six patients had hotspots, 4 out of 6 had clinical benefit, while 3 out of 4 patients without hotspots had progressive disease.
VEGF-A	2007 [24]	[^{89}Zr]bevacizumab (3.5 ± 0.5 MBq)	athymic nude mice with subcutaneous xenografts	SKOV-3	1 to 7 days %ID/g	Increased tumor uptake was seen from 3 days onward.
VEGF-A	2010 [25	[^{89}Zr]bevacizumab (6 ± 0.27	In xenografted athymic nude mice,	A2780 CP70	At days 1 and 6 p.i.	The untreated high VEGF-A expressing tumor showed

	]	MBq)	PET was performed before and after HSP90 inhibition therapy (for 2 weeks)		%ID/g	high uptake, which decreased after therapy together with VEGF expression, vessel density, and proliferation rate.
VEGF-A	2011 [26]	[^{64}Cu]bevacizumab (5 – 8 MBq)	nude mice with subcutaneous xenografts	HT29	1 to 48 h %ID/g	Tumor tracer uptake was increased, correlating with tumor EGFR expression. Tracer uptake was blocked by adding cold bevacizumab.
VEGF-A	2011 [27]	^{86}Y-CHX-A"-DTPA-bevacizumab (1.8 – 2.0 MBq)	athymic nude mice with subcutaneous xenografts	LS-174T SKOV-3 MSTO-211H	1 to 3 days %ID/cc	Tracer uptake was highest in the 2 high VEGF expressing tumors. Tracer uptake was blocked by adding cold bevacizumab.
VEGF-A	2012 [28]	^{64}Cu-NOTA-bevacizumab-800CW (a dual labeled bevacizumab with 800CW (i.e. a NIRF dye) and ^{64}Cu-NOTA	athymic nude mice with subcutaneous xenografts	U87MG	4 to 72 h % ID/g	Tumor uptake was visible, this was correlated to ex vivo NIRF imaging. Uptake was blocked by adding cold bevacizumab.

		(i.e. a PET label)) (5 - 10 MBq)				
VEGF-A	2012 [29]	[^{89}Zr]bevacizumab (5 MBq)	In xenografted nude mice, PET was performed before and at day 9 of everolimus therapy (for 2 weeks)	A2780	At day 6 p.i. SUVmean	Tracer uptake decreased with everolimus therapy, correlating with decreased VEGF-A in tumor lysates.
VEGF-A	2013 [30]	[^{64}Cu]bevacizumab (2.96 – 3.7 MBq)	athymic nude mice with subcutaneous xenografts underwent PET before and after everolimus therapy (for 7 days)	786-O	At 24 h p.i. SUV	High tracer uptake was seen in the tumor, which decreased with everolimus therapy together with VEGF secretion, VEGFR activation, and growth arrest.
VEGF-A	2013 [31]	[^{89}Zr]bevacizumab (37 MBq)	23 breast cancer patients underwent a PET scan prior to surgery		At 4 days p.i. SUVmax	Tracer uptake could be visualized in 25 out of 26 tumors and tracer uptake correlated with tumor VEGF-A levels.
VEGF-A	2014 [32	[^{89}Zr]bevacizumab (36.4 ± 0.9	7 NSCLC patients were scanned		At day 4 and 7 p.i.	Tracer uptake of [^{89}Zr]bevacizumab was visible in all patients and

	]	MBq)	prior to treatment with bevacizumab combined with carboplatin-paclitaxel		SUVpeak	showed a positive trend between tracer uptake and PFS and OS.
VEGF-A	2014 [33]	[^{89}Zr]bevacizumab (37 MBq)	14 NET patients underwent PET scans at baseline and 2 and 12 weeks after start of everolimus therapy		At day 4 p.i. SUVmax and SUVmean	In 4 patients no uptake was seen. In 10 patients, 19% of tumor lesions above 1cm were visualized. SUVmax decreased by 7% at 2 weeks and 35% at 12 weeks. Decrease during therapy was correlated to RECIST response at 6 months.
VEGF-A	2015 [34]	[^{89}Zr]bevacizumab (37 MBq)	22 mRCC patients were scanned at baseline and 2 and 6 weeks after start of therapy using bevacizumab with either IFN-α or		At day 4 p.i. SUVmax and SUVmean	Intrapatient and interpatient heterogeneity was seen in tracer uptake. SUVmax decreased at 2 and 6 weeks on bevacizumab/IFN-α therapy, however, with bevacizumab/sunitinib a slight

			sunitinib			initial decrease at 2 weeks followed by an increase was seen. Baseline SUVmax > 10 was associated with improved PFS. No correlation was seen between SUVmax and blood VEGF-A levels.
VEGFR-2	2015 [35]	^{64}Cu-NOTA-ramucirumab (5 - 10 MBq)	athymic nude mice with subcutaneous xenografts	HCC4006 A549	3 to 48 h %ID/g	Uptake of ^{64}Cu-NOTA-ramucirumab was higher in VEGFR-2 positive tumors, uptake was blocked by adding cold ramucirumab.
PD1	2015 [36]	^{64}Cu-DOTA-(anti-mouse)PD1 (7 − 8 MBq)	xenografted nude transgenic Fox(p3+).LuciDTR4 mice, known to express PD-1 on their CD4(+) T-cells were scanned	B16-F10	1 to 48 h %ID/g	High tracer uptake was seen in lymphoid organs and tumors. BLI images of T-cells confirmed lymphocyte infiltration of tumors at the time of PET imaging. Tracer uptake decrease by adding

						unlabeled antibody.

Abbreviations: *%ID/g = percentage injected dose per gram; HNC = head and neck cancer; KRASwt = KRAS (Kirsten rat sarcoma viral oncogene homolog) wild type; mCRC = metastatic colorectal cancer; mRCC = metastasized renal cell carcinoma; NIRF = near-infrared fluorescence; NSCLC = non-small cell lung cancer; p.i. = post injection; RECIST = response evaluation criteria in solid tumours [37]; SUV = standardized uptake value; SUVmax = maximum SUV; SUVmean = average SUV per volume of interest; SUVpeak = average SUV within a 1cc sphere around the maximum SUV.*

Cell lines: *Colorectal adenocarcinoma (LS-174T, HT29, HCT-8, HCT-116, and SW620); Murine colorectal carcinoma (CT-26); Melanoma (A375, B16-F10); Breast cancer (BT-474, MDA-MB-231, MDA-MB-468, MDA-MB-435, and T-47D); Head and neck squamous cell carcinoma (SQB20, SAS, UM-SCC-22B, and SCC1); Prostate cancer (PC-3, DU145); Epidermoid cancer (A431); Malignant mesothelioma (NCI-H226, NCI-H2052, and MSTO-211H); Ovarian cancer (SKOV3, A2780, and CP70); Pancreatic cancer (SHAW); Glioblastoma (U-373 MG, U87MG); Cervical cancer (CaSki); Renal cell carcinoma (786-O); NSCLC (HCC4006, A549).*

*(**a**) Time interval from injection to scanning.*
*(**b**) Tracer uptake refers to tumor tracer uptake, unless stated otherwise.*

Monoclonal antibodies are large molecules of approximately 150 kD that are relatively easy to radiolabel in an inert way, i.e. that neither binding nor PK characteristic of the drug becomes altered [38]. As large molecules, mAbs are characterized by slow tissue penetration. Therefore, to image their PK behavior, mAbs need to be labeled with long-lived radionuclides such as zirconium-89 (see Table 3). Usually, radiolabeled mAbs do not allow for dynamic scanning because of their slow PK profile (see Figure 2). Rather, static whole body scanning protocols are performed. As radiolabeled mAbs fully bind to their targets only after a few days post injection (p.i.), static images using simplified uptake parameters, such as standardized uptake value (SUV), tumor-to-blood (TBR), and tumor-to-reference tissue ratios, are best suited.

Table 3. Typical differences between immuno-PET and TKI-PET.

	Immuno-PET	TKI-PET

Parent molecule	mAbs	TKIs	
Radionuclide (Decay half-life)	Copper-64 (12,7 h) Yttrium-86 (14,7 h) Bromine-76 (16,1 h) Zirconium-89 (78,4 h) Iodine-124 (4,2 days)	Carbon-11 (20,4 min) Fluorine-18 (109,8 min)	
Scanning Scanning protocol Injection to scanning time interval Uptake parameters	static up to several days simplified parameters: SUV (and its variants such as SUVmax and SUVpeak), TBR, TRR, etc.	static up to several hours simplified parameters: SUV and variants, TBR, TRR, etc	dynamic up to several hours dynamic: K1, Ki, V_T, etc
Advantages	whole body scans highly specific parent molecules stable inert labeling easy to process uptake parameters shippable for widespread use	whole body scans easy to process uptake parameters shippable for widespread use	PK modeling highly accurate uptake parameters
Limitations / caveats	radiation burden	accuracy of uptake parameters may be low depending on the PK modeling of the tracer	no whole body scans possible

***Abbreviations**: K1 = influx rate constant; Ki = net influx rate constant; mAbs = monoclonal antibodies; PK = pharmacokinetic; SUV = standardized uptake value; SUVmax = maximum SUV; SUVpeak = average SUV within a 1 mL sphere located around the pixel with maximum SUV; TBR = tumor-to-blood ratio; TKIs = tyrosine kinase inhibitors; TRR = target-to-reference tissue ratio; VT = volume of distribution.*

For optimizing the tumor uptake signal against the background noise, the choice of radionuclide is a key variable. After receptor binding, mAbs can become internalized by the target cells. Some long-lived radionuclides, such as bromine-76 and iodine-124 are then rapidly degraded and cleared from these cells. However, copper-64, yttrium-86 and zirconium-89 become captured intracellularly, causing a higher signal-to-noise ratio [38]. Also, some mAbs can show a sink effect, i.e. a large number of extra-tumoral receptor molecules has to be saturated before tumor receptor molecules can be imaged. In such cases, simultaneous injection of cold doses of mAbs with radiolabeled mAbs is needed to improve image quality [22, 23]. However, co-injection of cold mAbs also affects the quantification of tumor uptake as tumor target molecules become occupied with cold mAbs, thus decreasing accuracy of quantification. Imaging quality can also be determined by the timing between tracer injection and scanning, as scanning too early causes low signal-to-noise ratios, and scanning too late suffers from too much decay leading to poor statistics for image reconstruction and quantification. Typically, patients are scanned several days after injection of radiolabeled mAbs.

3.1 EGFR

Panitumumab and cetuximab are IgG2 and IgG1 antibodies directed against EGFR, respectively. In most xenograft PET studies, these radiolabeled anti-EGFR drugs showed increased uptake in EGFR-expressing tumors [11–14, 20]. Tracer uptake correlated with EGFR expression levels in some studies, but not in all [10, 21, 39]. The authors mentioned that decreased vessel density and vascular permeability may have caused this discrepancy. Other causes may have been variations in tumor size, injected dose, tumor interstitial pressure, and *ex vivo* assessment of EGFR expression. Uptake of both radiolabeled panitumumab and cetuximab could be blocked by adding nonlabeled drugs, indicating that there was specific binding. To our knowledge, 2 clinical immuno-PET studies were published, using an anti-EGFR mAb. Van Loon *et al*. performed a phase 1 study using [^{89}Zr]cetuximab, co-injected with cold cetuximab, in patients with NSCLC (N =6) and head and neck cancer (N=3) [22]. They found no toxicity associated with this tracer at a dose of 120MBq. Tumor

tracer uptake could be visualized as indicated by maximum TBR, which ranged from 0.9 to 14.8. These values were not correlated with EGFR expression in tumor samples. This study did not investigate the predictive value of tracer uptake. The other clinical study was performed by Menke *et al*. in 10 *KRAS* wild type colorectal cancer patients using a co-injection of [^{89}Zr]cetuximab and cold cetuximab [23]. Patients underwent 6 serial PET scans from 1 hr to 10 days post injection. Six out of 10 patients showed increased uptake, of whom 4 experienced benefit of the cetuximab therapy, while 3 out of 4 patients without increased uptake had progressive disease. These findings indicates that not only tumor [^{89}Zr]cetuximab binding can be visualized in patients, high tracer uptake may be associated with an increased response to cetuximab therapy.

3.2 VEGF/VEGFR

Bevacizumab and ramucirumab are IgG1 antibodies directed against VEGF-A and VEGFR2, respectively. All preclinical studies showed increased tumor uptake of radiolabeled bevacizumab in mice xenografted with VEGF-A expressing tumors as compared to non-VEGF expressing tumors [24, 27, 28]. Moreover, Chang et al. also showed that tumor uptake of [^{64}Cu]bevacizumab decreased after everolimus therapy, together with a decrease in VEGF-A secretion, VEGFR inactivity and growth arrest [30]. Similarly, tumor [^{89}Zr]bevacizumab uptake decreased after treatment with a HSP90 inhibitor, known to decrease VEGF-A expression [25]. Tumor tracer uptake was blocked by adding nonlabeled bevacizumab, supporting the notion that there is specific binding. These findings indicate that uptake [^{89}Zr]bevacizumab is correlated with varying levels of VEGF-A expression. This is very interesting, as VEGF-A is typically considered to be a soluble ligand. Possibly, tumor uptake may be caused by high paracrine expression and subsequent binding to extracellular matrix glycoproteins that act as non-signaling co-receptors, facilitating the binding of VEGF to VEGFR molecules [40]. To date, clinical PET studies using [^{89}Zr]bevacizumab were performed in patients with breast cancer, neuro-endocrine tumors (NET), renal cell carcinoma, and NSCLC. The concept of imaging the tumor VEGF-A expression using [^{89}Zr]bevacizumab was investigated in breast cancer patients by Gaykema et al. [31]. They showed that in 25 out of 26 tumors tracer uptake could be visualized, and that uptake was correlated to the tumor VEGF-A expression levels. Bahce et al. scanned 7 advanced NSCLC patients using [^{89}Zr]bevacizumab prior to treatment with bevacizumab combined with carboplatin and paclitaxel [32]. Using PET, tumors could be visualized in all patients (see Figure 4). Tracer uptake showed heterogeneity of uptake within tumor lesions and between lesions within the same patient. The level of tracer uptake was associated with improved progression free survival (PFS) and overall survival (OS). Comparable findings were done using this tracer in patients renal cell carcinoma and NET

treated with bevacizumab/IFN-a and everolimus, showing association of high baseline uptake with longer PFS and early change in uptake with tumor response, respectively [33, 34].

In mice with VEGFR-2 positive xenografts, [^{64}Cu]ramucirumab showed higher uptake as compared to target-negative xenografts. Also, tumor uptake was blocked by adding cold ramucirumab, again indicative of specific binding.

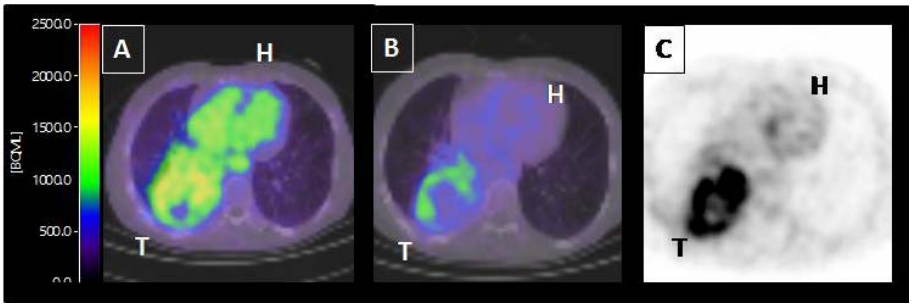

Fig. 4. *Axial CT-fused PET images in a NSCLC patient are shown, obtained after 5 (A) and 7 (B) days post injection (p.i.) of 37MBq [^{89}Zr]bevacizumab. Increased tracer accumulation is seen in the peripheral portions of the tumor mass (T), located in the right lower lobe. The central photopenic area correlates with central tumor necrosis as seen on the FDG images (C). Interestingly, at day 5 p.i. there is nearly similar activity in the blood pool, i.e. heart (H), as in the peripheral tumor parts. However, at day 7 p.i. the activity ratio in the blood pool is much lower than in the tumor, improving the tumor uptake signal. The color code indicates the radioactivity concentration (Bq/mL).*

3.3 Immune checkpoint inhibitors

Many cancers, including NSCLC, inhibit anti-tumor immune responses via the programmed death-1 (PD-1) pathway [41]. NSCLC patients treated with anti-PD-1 antibodies achieve tumor responses in approximately 20%. The presence of tumor infiltrating lymphocytes that express PD-1 may be predictive for response to anti-PD-1 therapy. Natarajan et al. used a radiolabeled anti-PD1 antibody, i.e. [^{64}Cu]-DOTA-(anti-mouse)PD1, in mice that express PD-1 on their T-cells [36]. These mice were xenografted with melanoma cells. High tracer uptake was seen in lymphoid organs and tumors. At the time of PET imaging, lymphocyte infiltration of tumors could be demonstrated by bioluminescence imaging. Also, by adding nonlabeled antibody the tumor tracer uptake decreased. These findings support the notion

that PD-1 target expression can be imaged using immuno-PET. No published preclinical studies using anti-PDL-1 or anti-CTLA4 antibodies could be found. Also, to the best of our knowledge, no clinical studies using anti-PD1 antibodies have been reported yet.

3.4 Clinical implication of immuno-PET in NSCLC

Preclinical immuno-PET studies have been performed using radiolabeled mAbs directed against nearly all currently actionable mAb targets in NSCLC, i.e. EGFR, VEGF-A, VEGFR2 and PD- 1. These studies have consistently shown that immuno-PET has the capacity for imaging target expression. However, only a very limited number of clinical studies have been published using radiolabeled mAbs that are of interest in the treatment of NSCLC. These pilot studies, all used [^{89}Zr]bevacizumab, and demonstrated that tumor uptake could be visualized and to a certain extent quantified. They also aimed to generate hypotheses about the predictive value of tumor tracer uptake. Although, different interesting correlations were found between tumor [^{89}Zr]bevacizumab uptake and clinical outcome, the predictive or prognostic value of imaging tumor VEGF-A with immuno-PET is still unclear. Larger trials are needed to evaluate whether [^{89}Zr]bevacizumab uptake is able to identify patients that will benefit from bevacizumab therapy.

More than a tool for research, immuno-PET imaging is potentially a future standard clinical assessment tool. Its many practical advantages, such as easy to produce stable and shippable tracers, and the possibility for whole body scanning protocols using simplified parameters for easy uptake measurement, will facilitate a broad application. However, its clinical success will depend on how tracer uptake will relate to target expression and will predict for therapy efficacy of the antibody that will be chosen as a tracer. This seems very promising for cancer immunotherapy. For example, the expression levels of PD1 and PD-L1 on tumor infiltrating T-cells or tumor cells, although not exclusionary, are indicative of an improved immunotherapy outcome in patients with non-squamous NSCLC. The use of the current pathology-based PD1 and PD-L1 expression markers, however, is hampered by unresolved issues such as varying immunohistochemistry antibodies, tissue preparation and processing variabilities, PD1/PD-L1 differences between primary versus metastatic biopsies, oncogenic versus induced PD-L1 expression levels that changes over time, and staining of tumor versus immune cells [41]. Immuno-PET could be used to overcome these limitations, as it provides a noninvasive means for repeated whole-body scanning, and to guide treatment decision management.

4. TKI-PET

In NSCLC, TKIs frequently target EGFR (10% of non-squamous NSCLC in Western population), ALK (5%), BRAF (2%), ROS1 (1-2%), RET (1-2%) and MET (2-4%) (see Figure 3) [42]. The main differences between TKI-PET and immuno-PET are shown in Table 3. Typically, TKIs are small molecules with a rapid PK profile that inhibit the kinase activity of various proliferation pathways. Tumor TKI accumulation depends not only on the presence of targeted kinase molecules, but also on their affinity. TKIs compete with ATP molecules for binding to the tyrosine kinase target. For example, erlotinib competes with ATP for the EGFR kinase domain. A 137-fold higher binding rate of erlotinib relative to ATP was seen in *ex vivo* tumors with EGFR exon 19 deletions, however, the presence of a secondary T790M mutation in EGFR exon 20 increased the affinity to ATP while decreasing for erlotinib [43]. Alterations in TKI affinity, i.e. the TKI/ATP-binding ratio, are critical in TKI therapy efficacy. For TKI-PET, adequate imaging of the changes in TKI affinity may play the most crucial role in successfully predicting therapy response.

Contrary to mAbs, TKIs are typically labeled with carbon-11 or fluorine-18, as the relatively short activity half-life of these radionuclides are best fitting with the biological half life of TKIs (see Table 1 and Table 4). Furthermore, TKI molecules usually have carbon and sometimes fluorine atoms that can be substituted with carbon-11 and fluorine-18 atoms, whereby their molecular configuration and PK characteristics can remain identical. After injection, radiolabeled TKIs are rapidly bound to their targets, and in case of reversible binders also rapidly released from their targets. Usually, TKIs undergo rapid renal or biliary clearance. In this setting, dynamic scanning is best used for pharmacokinetic modeling and quantitative tracer uptake analysis (see Figure 2). Although the analysis of a dynamic scan is more laborious than a static scan, the high accuracy of its results is clearly an advantage. Another advantage of using short-lived radionuclides is the short time period of decay, causing less radiation burden and patients can undergo a second PET scan relatively soon after the first one, in case of carbon-11 they can even undergo it on the same day.

Table 4. TKI-PET trials.

Drug target	Year Ref	Tracer (injected dose)	Design - scanned population	Xenograft cell line	Scanning protocol - Timing[a] - Uptake	Results[b]

					parameter	
EGFR	2007 [44]	[^{11}C]PD153035 (2.6 ± 0.7 MBq)	No PET scans were performed, only biodistribution analysis was performed in nude mice with subcutaneous xenografts	MDA-MB-468 A549 MDA-MB-231	Biodistribution measurements at 10, 30, and 60 min p.i. %ID/g	Higher tracer uptake was seen in high EGFR expressing tumors. Tracer uptake was blocked by cold PD153035.
EGFR	2011 [45]	[^{11}C]PD153035 (280.3 ± 113.6 MBq)	21 NSCLC patients (all histologies, EGFR mutational status unknown) underwent 3 PET scans (at baseline and 1 and 6 weeks after start of erlotinib therapy).		4 min at 20 min p.i. SUVmax	Tracer uptake showed a good correlation with OS and PFS on erlotinib therapy.
EGFR	2015 [46]	[^{11}C]PD153035 (? MBq)	nude mice with subcutaneous xenografts	HCC827 PC9 A549 H1975	30 min SUV and T/N	Sensitive cell lines showed higher tracer uptake and positive correlation with in vitro pEGFR

						expression.
EGFR	2013 [47]	[^{124}I]morpholino-IPQA (2.6 MBq)	NOD/SCID mice with subcutaneous xenografts were scanned before and 1 h after cold gefitinib.	H1299 cell lines transfected with L858R, E746-A750del, and wild type EGFR	60 min at 0 min p.i. and 30 min at 24 h p.i. %ID/g	Higher tracer uptake was seen in sensitive tumors. Tracer uptake decreased after pretreatment with gefitinib.
EGFR	2011 [48]	[^{18}F]F-PEG6-IPQA (7.4 MBq)	nude mice with subcutaneous xenografts	H3255 H441 PC 14 H1975	2 h dynamic scanning at 0 min p.i., followed by static scan at 3 h p.i. %ID/g and T/M	Tracer uptake was correlated to EGFR mutational status, the highest uptake was demonstrated in L858R harboring tumors.
EGFR	2008 [49]	[^{18}F]gefitinib (7.4 – 18.5 MBq)	xenografted SCID mice were used for [^{18}F]gefitinib PET scans and vervet monkeys for biodistribution analyses	U87 U87-EGFR H3255 H1975	2 h at 0 min p.i. SUV	No difference was seen in tracer uptake between tumors, due to high nonspecific uptake of [^{18}F]gefitinib.
EGFR	2009	[^{11}C]erlotinib	nude mice with subcutaneo	A549	90 min at 0 min p.i.	Tracer uptake was higher

	[50]	(10 - 15 MBq)	us xenografts	NCI358 HCC827	Bq/cc TAC	uptake in the sensitive cell line.
EGFR	2011 [51]	[^{11}C]erlotinib (500 ± 50 MBq)	13 NSCLC patients (all histologies, EGFR mutational status unknown) were scanned (using FDG and [^{11}C]erlotinib) prior to erlotinib therapy and after 12 weeks (with FDG only)		90 min at 0 min p.i. Hotspots (i.e. tumor-to-background ratio)	Tracer uptake was associated with better clinical outcome to erlotinib therapy. Four out of 9 patients showed increased tracer uptake, amongst which 1 died prior to response evaluation and 3 responded to erlotinib therapy. Nine out of 13 patients had no tracer accumulation, of which 3 died prior to response evaluation,

						2 had a stable disease, and 4 had progressive disease on erlotinib therapy.
EGFR	2011 [52]	[^{11}C]erlotinib (433 MBq)	1 NSCLC patient with an EGFR exon 19del and brain metastases was scanned prior to first line erlotinib therapy		60 min at 0 min p.i. tumor-to-cortex ratio	Brain metastases showed high tracer uptake and a radiologic response to erlotinib therapy.
EGFR	2013 [53]	[^{11}C]erlotinib (0.16 ± 0.12 mCi)	athymic nude mice with subcutaneous xenografts	PC9 HCC827 U87 U87-EGFR SW620	2 h at 0 min p.i. SUV	Higher tracer uptake was seen in sensitive tumors, uptake was blocked by adding cold erlotinib.
EGFR	2013 [54]	[^{11}C]erlotinib (256 ± 53 MBq)	10 NSCLC patients (5 EGFRmut vs. 5 EGFRwt)		60 min at 0 min p.i.	Tracer uptake showed good test retest

			underwent a $[^{15}O]H_2O$ PET scan followed by 2 $[^{11}C]$erlotinib scans (as test and retest)		V_T	repeatability. Also, higher uptake was seen in EGFRmut patients, which was independent of blood perfusion as measured by $[^{15}O]H_2O$ influx.
EGFR	2015 [55]	$[^{11}C]$erlotinib (16.4 ± 0.6 MBq)	athymic nude mice with subcutaneous xenografts	HCC827 QG56 H3255 H1975	60 min at 0 min p.i. SUV	Tracer uptake was higher in sensitive cell lines, namely EGFR exon 19del had the highest uptake.
EGFR	2016 [56]	$[^{11}C]$erlotinib (349 ± 46 MBq)	10 patients (EGFRmut) underwent a $[^{15}O]H_2O$ followed by a $[^{11}C]$erlotinib scan, both on and off erlotinib therapy		60 min at 0 min p.i V_T and TBR	Tracer uptake was decreased in all patients during erlotinib therapy, supporting the notion that $[^{11}C]$erlotinib exhibits specific binding in

						tumors, while tumor perfusion did not change.
EGFR, ERBB2	2015 [57]	[^{11}C]erlotinib (8 to 10 MBq) [^{18}F]afatinib (4 to 6 MBq)	athymic nude mice with subcutaneous xenografts	HCC827 A549 H1975	[^{11}C]erlotinib: 90 min at 0 min p.i. [^{18}F]afatinib: 120 min at 0 min p.i. %ID/g and tumor-to-background ratio	Both tracers showed higher uptake in the sensitive tumors. [^{18}F]afatinib demonstrated better tumor retention in all xenograft models.

Abbreviations: *%ID/g = percentage injected dose per gram; Bq/cc TAC = activity as determined by becquerels per volume of interest plotted in a time activity curve; EGFRmut = activating EGFR mutations; EGFRwt = wild type EGFR; p.i. = post injection; SUV = standardized uptake value; TBR = tumor-to-blood ratio; T/N = tumor tissue vs. non-tumor tissue uptake ratios; T/M = tumor to muscle ratio; V_T = volume of distribution.*

Cell lines: *NSCLC, EGFR exon 19 deletion (HCC827, PC9), EGFR exon 21 L858R (H3255), EGFR dual mutations L858R/T790M (H1975), EGFR wild type (A549 (moderate EGFR expression), QG56, NCI358, H441, and PC14); Breast cancer, EGFR wild type (MDA-MB-468 (high EGFR expression), MDA-MB-231 (low EGFR expression)); Glioblastoma, EGFR wild type (U87 (low EGFR expression), U87-EGFR (transfected with EGFR gene to highly express EGFR)); Colon cancer, EGFR wild type (SW620 (very low EGFR expression)).*

*(**a**) Scanning time.*
*(**b**) Tracer uptake refers to tumor tracer uptake, unless stated otherwise.*

4.1 EGFR TKI (not in clinical use)

[^{11}C]PD153035, i.e. ^{11}C-labeled 4-N-(3-bromoanilino)-6,7-dimethoxyquinazoline, is a PET tracer that is based on a reversible EGFR TKI. In xenografted mice, [^{11}C]PD153035 showed higher uptake in EGFR TKI sensitive NSCLC tumors as compared to insensitive tumors [44, 46]. Also, the uptake correlated positively with the level of EGFR expression, however, this was only seen in the sensitive tumors. When unlabeled PD153035 was added prior to tracer infusion, the uptake of [^{11}C]PD153035 in tumors was blocked, indicating that there was specific binding. Meng *et al.* studied the potential of this tracer for predicting clinical outcome of erlotinib therapy in 21 advanced NSCLC patients (EGFR status unknown) who had disease progression after chemotherapy [45]. The study showed that enhanced [^{11}C]PD153035 tumor uptake, as measured using SUVmax prior to or within 1-2 weeks after start of erlotinib treatment, correlated strongly with a better OS and longer PFS (HR = 0.40, P = 0.002, and HR = 0.044, P , 0.001, resp). Patients with high SUVmax (≥median) survived more than twice as long as patients with a low SUVmax (median OS = 11.4 vs. 4.6 mo, P = 0.002; PFS = 4.4 vs. 1.8 mo, P < 0.001). The authors also reported that this correlation was independent of histology. They proposed that this could be an added value of [^{11}C]PD153035, as EGFR-activating mutations are uncommon in squamous carcinoma NSCLC tumors.

Unlike [^{11}C]PD153035, many 4-anilinoquinazoline derivatives that were proposed as EGFR imaging tracers showed inferior *in vivo* stability, high non-specific binding and rapid dissociation rates. To deal with the latter problem irreversible EGFR TKIs, such as [^{124}I]morpholino-IPQA and [^{18}F]F-PEG6-IPQA [47, 48], were developed. These tracers showed higher accumulation in EGFR mutated NSCLC tumors than in EGFR wild type tumors. [^{18}F]F-PEG6-IPQA demonstrated superior PK characteristics, such as better water solubility, renal clearance, and lower background noise than [^{124}I]morpholino-IPQA. Moreover, the main metabolite of [^{18}F]F-PEG6-IPQA, i.e. [^{18}F]F-PEG6, was unable to cross cell membranes, indicating that the measured tumor activity originated from the parent tracer. A clinical trial using [^{18}F]F-PEG6-IPQA is now ongoing (NCT01320059).

4.2 Gefitinib

The potential use of [^{18}F]gefitinib as a PET tracer for predicting EGFR expression and mutational status in NSCLC xenografts was assessed by Su et al [49]. No difference was seen in uptake of [^{18}F]gefitinib in xenografts with low and high EGFR expression, and no difference was seen between sensitive and resistant cell lines. These findings were ascribed to a high degree of non-specific binding, resulting from gefitinib's high lipophilicity. Besides fluorine-18, the synthesis of carbon-11 labeled gefitinib has also been published [59]. However, to our best knowledge, no clinical or preclinical studies of [^{11}C]gefitinib in NSCLC have been reported.

4.3 Erlotinib

Erlotinib labeled with carbon-11, i.e. [^{11}C]erlotinib, was used in several preclinical studies in mice, xenografted with NSCLC tumors [50, 53, 55, 57]. All studies reported increased uptake of [^{11}C]erlotinib in sensitive tumors. Also, by adding nonlabeled erlotinib, the uptake was blocked, indicating this tracer's specific binding capacity. The first clinical study using [11C]erlotinib, by Memon et al., investigated 13 NSCLC patients that were planned to receive erlotinib therapy [51]. A [11C]erlotinib PET was performed prior to erlotinib therapy, patients also underwent an FDG PET scan prior to therapy and 12 weeks after start of therapy. EGFR mutational status was not evaluated. In 4 patients, the [11C]erlotinib scan showed increased uptake in tumors and malignant lymph nodes. Out of these 4 patients, 3 showed a stable disease to erlotinib therapy, the remaining patient died before evaluation. Out of the remaining 9 patients without increased uptake, 3 died before evaluation, 2 had a stable disease, and 4 patients had disease progression at 12 weeks. The authors also reported that in some cases [^{11}C]erlotinib PET could identify lesions that had not been visualized using FDG PET, however, these lesions were not confirmed by pathology. The same investigators published a case report of a NSCLC patient with an activating EGFR exon 19 deletion and brain metastases [52]. The [^{11}C]erlotinib PET showed accumulation in the brain metastases. Post-treatment MRI and CT demonstrated regression of both the brain metastases and primary lung tumor. Next, Bahce et al. performed a quantitative study using a dynamic scanning protocol with continuous arterial sampling in 10 NSCLC patients [54]. Full tracer pharmacokinetic analysis determined that the 2-tissue reversible compartment model using volume of distribution (V_T) as uptake parameter fitted the PET data best. By using V_T, tracer uptake could be assessed more accurately than by SUV. This study demonstrated that [^{11}C]erlotinib V_T was higher in patients with an activating EGFR exon 19 deletion than in patients with wild type EGFR tumors. This difference was statistically significant and was not determined by differences in EGFR expression levels or tumor perfusion, which was assessed by quantitative PET studies using radiolabeled water ([^{15}O]H_2O). In a follow up clinical study, 10 patients were scanned on and off erlotinib therapy [56]. Tumor tracer uptake decreased in all patients during erlotinib therapy, supporting the notion that [^{11}C]erlotinib exhibits specific binding, while tumor perfusion as measured by [^{15}O]H_2O remained unchanged during therapy. In addition, Yaqub et al. showed that the simplified uptake parameter that best represented tumor [^{11}C]erlotinib uptake was TBR in the postinjection interval between 40 and 60 minutes. TBR was more accurate than SUV, however, was less accurate than V_T [59]. A clinical trials using this tracer is ongoing (Dutch trial register NTR3670).

4.4 Afatinib

Another EGFR TKI that is approved for the treatment of EGFR mutated NSCLC is afatinib, which is a second generation irreversible EGFR TKI. In contrast to gefitinib and erlotinib that inhibit only EGFR, afatinib inhibits EGFR as well as ERBB2 and ERBB4. Afatinib has been radiolabeled with fluorine-18, i.e. [^{18}F]afatinib. The first preclinical study was performed by Slobbe *et al.* using xenografted mice [57]. Tumors with activating EGFR showed a higher [^{18}F]afatinib uptake as compared to wild type EGFR tumors. Adding nonlabeled afatinib blocked tumor [^{18}F]afatinib uptake. Analysis of [^{18}F]afatinib metabolism and biodistribution in tumor-bearing mice demonstrated high stability of the tracer in plasma (>80% of intact [18F]afatinib at 45 min p.i.), rapid clearance from both blood and muscle tissue and rapid tumor accumulation (after 10 min p.i.). Tumor retention of [^{18}F]afatinib was shown to be relatively stable from 5 min until 120 min post injection. When compared to [^{11}C]erlotinib, higher tumor-to-background ratios were seen with [^{18}F]afatinib in EGFR wild type and EGFR exon 19del (1.0 vs 1.5 and 1.9 vs 2.3, respectively) tumors, no difference was seen in tumors harboring a T790M secondary mutation. A clinical trial using [^{18}F]afatinib is ongoing at our center (Dutch trial register NTR5203) (see Figure 5).

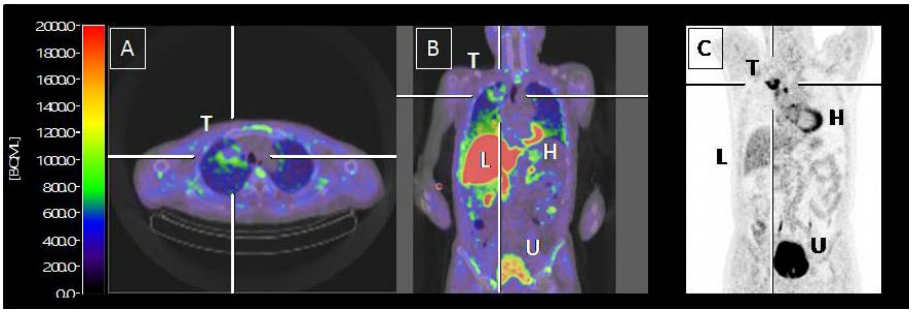

Fig. 5. *Axial (A) and coronal (B) CT-fused [18F]afatinib PET images are shown of a NSCLC patient, harboring an EGFR exon 19 deletion. Increased activity is seen in the rims of the tumor (T), located in the right upper lobe. The central photopenic area correlates with central tumor necrosis as seen on the FDG images (C). Also, the liver (L) and urinary bladder (U) show increased activity, probably due to clearance of the tracer and its metabolites. The color code indicates the radioactivity concentration (Bq/mL). These static[18F]afatinib PET images were obtained at 90 min post injection of 75 MBq [18F]afatinib, and were part of a series of whole body scans, performed for dosimetric purposes.*

4.5 Clinical implications of TKI-PET in NSCLC

To our best knowledge, only EGFR TKI were used in the published TKI-PET studies in NSCLC. [^{11}C]PD153035 and [^{11}C]erlotinib were studied the most and have consistently demonstrated to achieve higher uptake in tumors with activating EGFR mutations, indicating that TKI-PET can image increased EGFR affinity to TKI. In clinical pilot studies, not only tumor uptake of both tracers could be visualized, significant correlations were found between high tracer uptake and better erlotinib therapy outcome. However, these tracers are not suitable for widespread clinical use due to the short half-life of their carbon-11 label. To circumvent this limitation, fluorine-18 labeled next generation irreversible EGFR TKI, e.g.[^{18}F]F-PEG6-IPQA and [^{18}F]afatinib, were studied. These tracers are expected to be better suited for clinical use as the fluorine-18 label allows for their shipment to other PET centers. Moreover, in preclinical studies, these tracers did show better tumor-to-background ratios as compared to [^{11}C]PD153035 and [^{11}C]erlotinib, respectively. However, these next generation tracers are expected to bind irreversibly, meaning that the uptake of these tracers will be strongly dependent on the delivery to the target receptor, i.e. on tumor perfusion, which may impede correct quantification of uptake.

Overall, TKI-PET is a great research tool for pharmacokinetic studies, however, for TKI-PET tracers to become a standard clinical assessment tool across numerous countries and hospitals, some practical conveniences should be provided, for example the ability for assessing all tumor lesions by whole body imaging and the use of stable and shippable tracers. TKI-PET tracers, fulfilling these conditions are potentially applicable in the routine clinical practice because this technique has the unique ability to image the affinity and therefore the sensitivity of a receptor for the studied TKI. This was already demonstrated for EGFR, but besides EGFR, future TKI-PET studies should investigate TKIs directed against ALK, BRAF, ROS1, RET, and MET. For example, crizotinib, a multi-target TKI used in the treatment of ALK rearranged NSCLC, has also activity against ROS1 and MET. Theoretically, in these patients, radiolabeled crizotinib and PET may predict therapy response irrespective of the sensitizing DNA aberration that was found in the tumor. This could lead to a whole new way of personalizing therapy without necessarily performing tumor molecular analysis.

5. In summary

In the last decade, the number of mAbs and TKI used in the treatment of NSCLC rapidly increased as a result of the identification of ever more critical tumor

targets. PET using radiolabeled targeting mAbs and TKIs can provide an imaging biomarker for personalizing therapy.

In this review, we discussed that preclinical immuno-PET and TKI-PET studies have consistently shown their capacity for imaging target expression. At present, the results obtained in clinical studies, mostly designed as pilot studies, suggest promising correlations between tumor tracer uptake and clinical outcome, although not conclusive and needing validation by future larger studies. Nonetheless, taking into account their pioneering work and the complexity of the experimental setting in which they are performed, these studies pave the way towards better understanding the mechanisms behind imaging targeted drugs and their potential to predict tumor sensitivity to therapy.

6. References

1. Ferlay J, Soerjomataram I, Ervik M, Dikshit R, Eser S, Mathers C, et al. GLOBOCAN 2012 v1. 0, Cancer Incidence and Mortality Worldwide: IARC CancerBase No. 11. International Agency for Research on Cancer, Lyon, France. 2013. globocan iarc fr. 2015.

2. Mok TS, Wu YL, Thongprasert S, Yang CH, Chu DT, Saijo N, et al. Gefitinib or carboplatin-paclitaxel in pulmonary adenocarcinoma. New England Journal of Medicine. 2009, 361: 947–957.

3. Boolell V, Alamgeer M, Watkins DN, Ganju V. The evolution of therapies in Non-small cell lung cancer. Cancers. 2015, 7: 1815–1846.

4. Varnäs K, Varrone A, Farde L. Modeling of PET data in CNS drug discovery and development. Journal of pharmacokinetics and pharmacodynamics. 2013, 40: 267–279.

5. Van Tinteren H. The implementation of PET in non-small-cell lung cancer in the Netherlands. Clinical Oncology. 2006, 18: 156–157.

6. Van Tinteren H, Hoekstra OS, Smit EF, van den Bergh JH, Schreurs AJ, Stallaert RA, et al. Effectiveness of positron emission tomography in the preoperative assessment of patients with suspected non-small-cell lung cancer: the PLUS multicentre randomised trial. The Lancet. 2002, 359: 1388–1392.

7. Bahce I, Vos C, Dickhoff C, Hartemink K, Dahele M, Smit E, et al. Metabolic activity measured by FDG PET predicts pathological response in locally advanced superior sulcus NSCLC. Lung Cancer. 2014, 85: 205–212.

8. Rolfo C, Fanale D, S Hong D, M Tsimberidou A, A Piha-Paul S, Pauwels P, et al. Impact of microRNAs in resistance to chemotherapy and novel targeted agents in non-small cell lung cancer. Current pharmaceutical biotechnology. 2014, 15: 475–485.

9. Cobo M, Isla D, Massuti B, Montes A, Sanchez JM, Provencio M, et al. Customizing cisplatin based on quantitative excision repair cross-complementing 1 mRNA expression: a phase III trial in non-small-cell lung cancer. J Clin Oncol. 2007, 25: 2747–54.

10. Niu G, Li Z, Xie J, Le Q-T, Chen X. PET of EGFR antibody distribution in head and neck squamous cell carcinoma models. J Nucl Med. 2009, 50: 1116–23.

11. Nayak TK, Garmestani K, Baidoo KE, Milenic DE, Brechbiel MW. Preparation, biological evaluation, and pharmacokinetics of the human anti-HER1

monoclonal antibody panitumumab labeled with 86Y for quantitative PET of carcinoma. Journal of Nuclear Medicine. 2010, 51: 942–950.

12. Nayak TK, Garmestani K, Milenic DE, Baidoo KE, Brechbiel MW. HER1-targeted 86 Y-panitumumab possesses superior targeting characteristics than 86 Y-cetuximab for PET imaging of human malignant mesothelioma tumors xenografts. PLoS One. 2011, 6: e18198.

13. Nayak TK, Garmestani K, Milenic DE, Brechbiel MW. PET and MRI of metastatic peritoneal and pulmonary colorectal cancer in mice with human epidermal growth factor receptor 1-targeted 89Zr-labeled panitumumab. J Nucl Med. 2012, 53: 113–20.

14. Bhattacharyya S, Kurdziel K, Wei L, Riffle L, Kaur G, Hill GC, et al. Zirconium-89 labeled panitumumab: a potential immuno-PET probe for HER1-expressing carcinomas. Nuclear medicine and biology. 2013, 40: 451–457.

15. Perk LR, Visser GW, Vosjan MJ, Stigter-van Walsum M, Tijink BM, Leemans CR, et al. 89Zr as a PET surrogate radioisotope for scouting biodistribution of the therapeutic radiometals 90Y and 177Lu in tumor-bearing nude mice after coupling to the internalizing antibody cetuximab. Journal of Nuclear Medicine. 2005, 46: 1898–1906.

16. Cai W, Chen K, He L, Cao Q, Koong A, Chen X. Quantitative PET of EGFR expression in xenograft-bearing mice using 64Cu-labeled cetuximab, a chimeric anti-EGFR monoclonal antibody. European journal of nuclear medicine and molecular imaging. 2007, 34: 850–858.

17. Ping Li W, Meyer LA, Capretto DA, Sherman CD, Anderson CJ. Receptor-binding, biodistribution, and metabolism studies of 64Cu-DOTA-cetuximab, a PET-imaging agent for epidermal growth-factor receptor-positive tumors. Cancer biotherapy \& radiopharmaceuticals. 2008, 23: 158–171.

18. Eiblmaier M, Meyer LA, Watson MA, Fracasso PM, Pike LJ, Anderson CJ. Correlating EGFR expression with receptor-binding properties and internalization of 64Cu-DOTA-cetuximab in 5 cervical cancer cell lines. Journal of Nuclear Medicine. 2008, 49: 1472–1479.

19. Aerts HJWL, Dubois L, Perk L, Vermaelen P, van Dongen GAMS, Wouters BG, et al. Disparity between in vivo EGFR expression and 89Zr-labeled cetuximab uptake assessed with PET. J Nucl Med. 2009, 50: 123–31.

20. Nayak TK, Regino CAS, Wong KJ, Milenic DE, Garmestani K, Baidoo KE, et al. PET imaging of HER1-expressing xenografts in mice with 86Y-CHX-A''-DTPA-cetuximab. Eur J Nucl Med Mol Imaging. 2010, 37: 1368–76.

21. Niu G, Sun X, Cao Q, Courter D, Koong A, Le Q-T, et al. Cetuximab-based immunotherapy and radioimmunotherapy of head and neck squamous cell carcinoma. Clin Cancer Res. 2010, 16: 2095–105.

22. Van Loon J, Hoebers F, Lalisang R, Dingemans A, Zeegers K, Wang S, et al. OC-020: Non Invasive PET Imaging of Cetuximab-Zirconium-89 Biodistribution: A Phase i Trial. Radiotherapy and Oncology. 2013, S7.

23. Menke-van der Houven van O, Gootjes EC, Huisman MC, Vugts DJ, Roth C, Luik AM, et al. 89Zr-cetuximab PET imaging in patients with advanced colorectal cancer. Oncotarget. 2015, 6: 30384–30393.

24. Nagengast WB, de Vries EG, Hospers GA, Mulder NH, de Jong JR, Hollema H, et al. In vivo VEGF imaging with radiolabeled bevacizumab in a human ovarian tumor xenograft. J Nucl Med. 2007, 48: 1313–9.

25. Nagengast WB, de Korte MA, Oude Munnink TH, Timmer-Bosscha H, den Dunnen WF, Hollema H, et al. 89Zr-bevacizumab PET of early antiangiogenic tumor response to treatment with HSP90 inhibitor NVP-AUY922. J Nucl Med. 2010, 51: 761–7.

26. Paudyal B, Paudyal P, Oriuchi N, Hanaoka H, Tominaga H, Endo K. Positron emission tomography imaging and biodistribution of vascular endothelial growth factor with 64Cu-labeled bevacizumab in colorectal cancer xenografts. Cancer science. 2011, 102: 117–121.

27. Nayak TK, Garmestani K, Baidoo KE, Milenic DE, Brechbiel MW. PET imaging of tumor angiogenesis in mice with VEGF-A-targeted 86Y-CHX-A ″-DTPA-bevacizumab. International Journal of Cancer. 2011, 128: 920–926.

28. Zhang Y, Hong H, Engle JW, Yang Y, Barnhart TE, Cai W. Positron emission tomography and near-infrared fluorescence imaging of vascular endothelial growth factor with dual-labeled bevacizumab. American journal of nuclear medicine and molecular imaging. 2012, 2: 1.

29. Van der Bilt ARM, Terwisscha van Scheltinga AGT, Timmer-Bosscha H, Schröder CP, Pot L, Kosterink JGW, et al. Measurement of tumor VEGF-A levels with 89Zr-bevacizumab PET as an early biomarker for the antiangiogenic effect of everolimus treatment in an ovarian cancer xenograft model. Clin Cancer Res. 2012, 18: 6306–14.

30. Chang AJ, Sohn R, Lu ZH, Arbeit JM, Lapi SE. Detection of rapalog-mediated therapeutic response in renal cancer xenografts using 64 Cu-bevacizumab immunoPET. PloS one. 2013, 8: e58949.

31. Gaykema SBM, Brouwers AH, Lub-de Hooge MN, Pleijhuis RG, Timmer-Bosscha H, Pot L, et al. 89Zr-bevacizumab PET imaging in primary breast cancer. J Nucl Med. 2013, 54: 1014–8.

32. Bahce I, Huisman MC, Verwer EE, Ooijevaar R, Boutkourt F, Vugts DJ, et al. Pilot study of 89Zr-bevacizumab positron emission tomography in patients with advanced non-small cell lung cancer. EJNMMI Research. 2014, 4: 35.

33. Van Asselt SJ, Oosting SF, Brouwers AH, Bongaerts AH, de Jong JR, Lub-de Hooge MN, et al. Everolimus reduces 89Zr-bevacizumab tumor uptake in patients with neuroendocrine tumors. Journal of Nuclear Medicine. 2014, 55: 1087–1092.

34. Oosting SF, Brouwers AH, van Es SC, Nagengast WB, Munnink THO, Lub-de Hooge MN, et al. 89Zr-Bevacizumab PET Visualizes Heterogeneous Tracer Accumulation in Tumor Lesions of Renal Cell Carcinoma Patients and Differential Effects of Antiangiogenic Treatment. Journal of Nuclear Medicine. 2015, 56: 63–69.

35. Luo H, England CG, Graves SA, Sun H, Liu G, Nickles RJ, et al. PET Imaging of VEGFR-2 Expression in Lung Cancer with 64Cu-labeled Ramucirumab. Journal of Nuclear Medicine. 2015, jnumed–115.

36. Natarajan A, Mayer AT, Xu L, Reeves RE, Gano J, Gambhir SS. Novel Radiotracer for ImmunoPET Imaging of PD-1 Checkpoint Expression on Tumor Infiltrating Lymphocytes. Bioconjugate chemistry. 2015, 26: 2062–2069.

37. Eisenhauer E, Therasse P, Bogaerts J, Schwartz L, Sargent D, Ford R, et al. New response evaluation criteria in solid tumours: revised RECIST guideline (version 1.1). European Journal of Cancer. 2009, 45: 228–247.

38. Van Dongen GAMS, Poot AJ, Vugts DJ. PET imaging with radiolabeled antibodies and tyrosine kinase inhibitors: immuno-PET and TKI-PET. Tumor Biology. 2012, 1–9.

39. Aerts HJ, van Baardwijk AA, Petit SF, Offermann C, van Loon J, Houben R, et al. Identification of residual metabolic-active areas within individual NSCLC tumours using a pre-radiotherapy 18 Fluorodeoxyglucose-PET-CT scan. Radiotherapy and Oncology. 2009, 91: 386–392.

40. Wu FTH, Stefanini MO, Mac Gabhann F, Kontos CD, Annex BH, Popel AS. A systems biology perspective on sVEGFR1: its biological function, pathogenic role and therapeutic use. J Cell Mol Med. 2010, 14: 528–52.

41. Gandini S, Massi D, Mandalà M. PD-L1 expression in cancer patients receiving anti PD-1/PD-L1 antibodies: A systematic review and meta-analysis. Critical Reviews in Oncology/Hematology. 2016,.

42. Shea M, Costa DB, Rangachari D. Management of advanced non-small cell lung cancers with known mutations or rearrangements: latest evidence and treatment approaches. Therapeutic advances in respiratory disease. 2015, 1753465815617871.

43. Carey KD, Garton AJ, Romero MS, Kahler J, Thomson S, Ross S, et al. Kinetic analysis of epidermal growth factor receptor somatic mutant proteins shows increased sensitivity to the epidermal growth factor receptor tyrosine kinase inhibitor, erlotinib. Cancer Res. 2006, 66: 8163–71.

44. Wang H, Yu J, Yang G, Song X, Sun X, Zhao S, et al. Assessment of 11C-labeled-4-N-(3-bromoanilino)-6, 7-dimethoxyquinazoline as a positron emission tomography agent to monitor epidermal growth factor receptor expression. Cancer science. 2007, 98: 1413–1416.

45. Meng X, Loo BW, Ma L, Murphy JD, Sun X, Yu J. Molecular imaging with 11C-PD153035 PET/CT predicts survival in non-small cell lung cancer treated with EGFR-TKI: a pilot study. J Nucl Med. 2011, 52: 1573–9.

46. Dai D, Li X-F, Wang J, Liu J-J, Zhu Y-J, Zhang Y, et al. Predictive efficacy of 11C-PD153035 PET imaging for EGFR-tyrosine kinase inhibitor sensitivity in non-small cell lung cancer patients. International Journal of Cancer. 2015,.

47. Yeh SH-H, Lin C-F, Kong F-L, Wang H-E, Hsieh Y-J, Gelovani JG, et al. Molecular imaging of nonsmall cell lung carcinomas expressing active mutant EGFR kinase using PET with [(124)i]-morpholino-IPQA. Biomed Res Int. 2013, 2013: 549359.

48. Yeh HH, Ogawa K, Balatoni J, Mukhapadhyay U, Pal A, Gonzalez-Lepera C, et al. Molecular imaging of active mutant L858R EGF receptor (EGFR) kinase-expressing nonsmall cell lung carcinomas using PET/CT Supporting Information. Proceedings of the National Academy of Sciences. 2011, 108: 1603–1608.

49. Su H, Seimbille Y, Ferl GZ, Bodenstein C, Fueger B, Kim KJ, et al. Evaluation of [18 F] gefitinib as a molecular imaging probe for the assessment of the epidermal growth factor receptor status in malignant tumors. European journal of nuclear medicine and molecular imaging. 2008, 35: 1089–1099.

50. Memon AA, Jakobsen S, Dagnaes-Hansen F, Sorensen BS, Keiding S, Nexo E. Positron emission tomography (PET) imaging with [11C]-labeled erlotinib: a micro-PET study on mice with lung tumor xenografts. Cancer Res. 2009, 69: 873–8.

51. Memon AA, Weber B, Winterdahl M, Jakobsen S, Meldgaard P, Madsen HHT, et al. PET imaging of patients with non-small cell lung cancer employing an EGF receptor targeting drug as tracer. Br J Cancer. 2011, 105: 1850–5.

52. Weber B, Winterdahl M, Memon A, Sorensen BS, Keiding S, Sorensen L, et al. Erlotinib accumulation in brain metastases from non-small cell lung cancer: visualization by positron emission tomography in a patient harboring a mutation in the epidermal growth factor receptor. Journal of Thoracic Oncology. 2011, 6: 1287–1289.

53. Petrulli JR, Sullivan JM, Zheng M-Q, Bennett DC, Charest J, Huang Y, et al. Quantitative analysis of [11C]-erlotinib PET demonstrates specific binding for activating mutations of the EGFR kinase domain. Neoplasia. 2013, 15: 1347–53.

54. Bahce I, Smit EF, Lubberink M, van der Veldt AAM, Yaqub M, Windhorst AD, et al. Development of [(11)C]erlotinib positron emission tomography for in vivo evaluation of EGF receptor mutational status. Clin Cancer Res. 2013, 19: 183–93.

55. Abourbeh G, Itamar B, Salnikov O, Beltsov S, Mishani E. Identifying erlotinib-sensitive non-small cell lung carcinoma tumors in mice using [11C] erlotinib PET. EJNMMI research. 2015, 5:

56. Bahce I, Yaqub M, Errami H, Schuit RC, Schober P, Thunnissen E, et al. Effects of erlotinib therapy on [11C] erlotinib uptake in EGFR mutated, advanced NSCLC. EJNMMI research. 2016, 6: 1–13.

57. Slobbe P, Windhorst AD, Stigter-van Walsum M, Smit EF, Niessen HG, Solca F, et al. A comparative PET imaging study with the reversible and irreversible EGFR tyrosine kinase inhibitors [11C] erlotinib and [18F] afatinib in lung cancer-bearing mice. EJNMMI research. 2015, 5:

58. Zhang M-R, Kumata K, Hatori A, Takai N, Toyohara J, Yamasaki T, et al. [11C] Gefitinib ([11c] Iressa): radiosynthesis, in vitro uptake, and in vivo imaging of intact murine fibrosarcoma. Molecular Imaging and Biology. 2010, 12: 181–191.

59. Yaqub M, Bahce I, Voorhoeve C, Schuit RC, Windhorst AD, Hoekstra OS, et al. Quantitative and simplified analysis of 11C-erlotinib studies. Journal of Nuclear Medicine. 2016, jnumed–115.

Chapter 3

Development of [^{11}C]erlotinib Positron Emission Tomography for *in vivo* evaluation of Epidermal Growth Factor Receptor mutational status

Idris Bahce

Egbert F. Smit

Mark Lubberink

Astrid A. M. van der Veldt

Maqsood Yaqub

Albert D. Windhorst

Robert C. Schuit

Erik Thunnissen

Daniëlle A. M. Heideman

Pieter E. Postmus

Adriaan A. Lammertsma

N. Harry Hendrikse

Clin Cancer Res. 2013 Jan 1;19(1):183-93.

Abstract

PURPOSE: To evaluate whether, in patients with non-small cell lung carcinoma (NSCLC), tumor uptake of [11C]erlotinib can be quantified and imaged using positron emission tomography, and to assess whether the level of tracer uptake corresponds with the presence of activating tumor epidermal growth factor receptor (EGFR) mutations.

PATIENTS AND METHODS: Ten NSCLC patients, 5 with an EGFR exon 19 deletion and 5 without, were scanned twice (test-retest) on the same day with an interval of at least 4 hours. Each scanning procedure included a low-dose CT scan, a 10 min dynamic [^{15}O]H_2O scan, and a 1 h dynamic [^{11}C]erlotinib scan. Data were analyzed using full tracer kinetic modeling. EGFR expression was evaluated using immunohistochemistry.

RESULTS: The quantitative measure of [^{11}C]erlotinib uptake, i.e. volume of distribution (V_T), was significantly higher in tumors with activating mutations, i.e. all with exon 19 deletions, (median V_T = 1.76, range 1.25 – 2.93) than in those without activating mutations (median V_T = 1.06, range 0.67 – 1.22) for both test and retest data (P = 0.014 and P = 0.009, respectively). Good reproducibility of [^{11}C]erlotinib V_T was seen (intraclass correlation coefficient = 0.88). Intergroup differences in [^{11}C]erlotinib uptake were not correlated with EGFR expression levels nor tumor blood flow.

CONCLUSION: [^{11}C]erlotinib V_T was significantly higher in NSCLC tumors with EGFR exon 19 deletions.

Introduction

In the Western population, approximately 10% of patients with non-small cell lung carcinoma (NSCLC) harbor an activating mutation in their tumor epidermal growth factor receptor (EGFR) genes. The most common activating EGFR mutations are exon 19 deletions (particularly delE746–A750) and exon 21 point mutations (particularly L858R) (1; 2). Proper identification of these patients, usually presenting with advanced stage disease, is of clinical importance, as recent trials have shown that treatment with EGFR tyrosine kinase inhibitors (TKI), such as erlotinib or gefitinib, results in a high response rate and significantly longer progression free survival (PFS) than treatment with classical cytotoxic chemotherapy (3–5).

Identifying patients with activating mutations, however, remains a major clinical challenge. Obtaining representative tumor tissue samples for mutation analysis is often limited by practical issues, such as inability to reach the tumor site, low yields of malignant cells or tumor heterogeneity. Indeed, results of recent clinical trials have shown that tissue procurement may not be possible in over one-fifth of patients (6). A non-invasive technique may overcome the obstacles associated with tumor tissue sampling. For this, positron emission tomography (PET), which allows for *in vivo* imaging of physiologic processes, seems to be best suited.

Compared to NSCLC tumors with wild type EGFR, those with activating EGFR mutations have higher TKI binding affinity (7). Therefore, uptake of radiolabeled TKI may be higher in tumors with activating EGFR mutations. In the present study, [11C]erlotinib, chemically identical to erlotinib itself, was used. Imaging of TKI sensitive tumor xenografts has already been demonstrated in an *in vivo* model using this tracer (8).

Although [11C]erlotinib has been used to image NSCLC tumors in a limited number of patients, no quantitative analysis has been described (9),(10). Quantification, however, is essential for an objective comparison of uptake in different tumors. Therefore the aims of the present study were to develop the optimal tracer kinetic model and its corresponding measure for quantification of [11C]erlotinib uptake in NSCLC, to determine its reproducibility, and to assess whether tumor uptake of [11C]erlotinib correlates with EGFR mutational status.

Materials and Methods

Study design

This study consisted of a number of distinct steps. Patients with and without an activating EGFR mutation underwent two dynamic [^{11}C]erlotinib PET scans with continuous arterial blood sampling on the same day. Each [^{11}C]erlotinib scan was preceded by a [^{15}O]H_2O scan to assess tumor blood perfusion. First, [^{11}C]erlotinib data from all patients, including test-retest information, were used to determine the optimal model for describing erlotinib kinetics. This model was used to assess whether there were changes between tumors with and without activating EGFR mutations. Finally, validity of a non-invasive image derived input function was evaluated in an attempt to simplify the protocol for routine clinical applications

Patients

Ten patients with NSCLC were included, 5 with and 5 without an activating mutation. Inclusion criteria were: histological diagnosis of NSCLC, EGFR mutational status as assessed by high resolution melting (HRM) and sequencing of tumor biopsies (11; 12), EGFR expression as determined by immunohistochemistry (IHC), an age of 18 years or older, a life expectancy of at least 12 weeks, presence of a malignant lesion within the chest of at least 1.5 cm diameter as measured by computed tomography (CT), and written informed consent. Exclusion criteria were: claustrophobia, pregnancy, lactation, metal implants in the thorax, and use of concurrent or previous treatment with experimental drugs within 30 days prior to scanning. The study was approved by the Medical Ethics Review Committee of the VU University Medical Center.

Synthesis of [11C]erlotinib

[^{11}C]erlotinib was synthesized under GMP conditions according to the EU directive on radiopharmaceuticals, EudraLex - Volume 4. The precursor was custom synthesized at Syncom (Groningen, The Netherlands). The carbon-11 label was introduced at the 7-methoxyethoxy position of the precursor, 6-O-desmethyl-erlotinib (OSI 420), using [^{11}C]methyl iodide (Supplementary Figure 1). [^{11}C]methyl iodide was synthesized from [^{11}C]CO_2 according to standard procedures and subsequently distilled in a solution of the precursor in acetonitrile and tetra-n-butylammonium hydroxide. The maximum yield was obtained after 5 minutes at 80°C. After cooling down and dilution with 0.75 mL of water, the mixture was injected onto a Waters SymmetryPrep C18 7µm 300x7.8 mm HPLC column, which was eluted with 70/30 25 mM phosphate buffer pH 3.5 / acetonitrile mixture. The product, [^{11}C]erlotinib, eluted at 9.5 minutes. This fraction was collected in 20 mL of water for injection. The total solution was passed over a preconditioned (10 mL of sterile ethanol 96% and subsequently 10 mL of water for injection) Waters Sep-Pak tC18 cartridge. This cartridge was washed with 20 mL of water for injection and

subsequently the product was eluted from the cartridge with 1.0 mL of sterile ethanol (96%) and 14 mL of a sterile and pyrogen free solution of 7.1 mM NaH_2PO_4 saline. The final mixture was passed over a Millex GV 0.22 µm filter, yielding a sterile, isotonic and pyrogen free solution of 2183-3476 MBq of [^{11}C]erlotinib with a (radio)chemical purity > 98% and a specific activity of 184-587 GBq·µmol^{-1} at end of synthesis (N=20). The product was analyzed using HPLC with a Phenomenex LUNA C18 5µm 250x4.6 mm column which was eluted with 55/45 acetonitrile/saline.

PET-CT SCANNING

All patients underwent two scanning sessions on the same day, with an interval of at least 4 hours to allow for radioactive decay of carbon-11. Scans were performed on a Gemini TF-64 PET/CT scanner (Philips Medical Systems, Best, the Netherlands). PET data were normalized and all appropriate corrections were applied for dead time, decay, randoms, scatter and attenuation. Reconstruction of PET data was performed using the 3D RAMLA algorithm with CT based attenuation correction, resulting in a final voxel size of 4x4x4 mm and a spatial resolution of 5-7 mm full width at half maximum. Prior to scanning, all patients were asked to fast from midnight, but a light breakfast before 8:00 a.m. was allowed. First, a low dose CT scan (50 mAs, without iv or oral contrast) was performed. In order to assess tumor perfusion, 370 ± 37 MBq (mean ± standard deviation) [^{15}O]H_2O was injected intravenously, simultaneously starting a 10 min emission scan in 3D acquisition mode. Subsequently 256 ± 53 MBq (mean ± standard deviation) [^{11}C]erlotinib (corresponding to a non-pharmacological dose of 2.2 ± 0.46 µg erlotinib) was injected intravenously, simultaneously starting a 60 min emission scan in 3D acquisition mode. [^{15}O]H_2O and [^{11}C]erlotinib emission scans were acquired in list mode and, prior to reconstruction, sorted into 26 (1x10, 8x5, 4x10, 2x15, 3x20, 2x30 and 6x60 s) and 36 (1x10, 8x5, 4x10, 2x15, 3x20, 2x30, 6x60, 4x150, 4x300 and 2x600 s) frames with increasing frame duration, respectively. No corrections for patient motion and/or respiratory motion were applied.

ARTERIAL BLOOD SAMPLING

An indwelling cannula was inserted in the radial artery for arterial blood sampling. No blood was withdrawn during [^{15}O]H_2O PET scans, as it has previously been demonstrated that these scans can be quantified using an image derived input function (13). During the [^{11}C]erlotinib PET scans, arterial blood was withdrawn continuously at a rate of 5 mL·min^{-1} for the first 5 minutes followed by 1 mL·min^{-1} for an additional 35 minutes. This was monitored using an on-line detection system (Veenstra Instruments, Joure, the Netherlands), cross-calibrated against the PET scanner (14). In addition, manual arterial samples (7 mL) were taken at 2.5, 5, 10, 15, 20, 30, 40 and 60 minutes after injection of [^{11}C]erlotinib. These discrete

samples were used for calibration of the on-line arterial curve, and for measuring plasma to whole blood ratios and radiolabeled plasma parent and metabolite fractions as function of time.

METABOLITE ANALYSIS

Manual blood samples were analyzed for blood and plasma radioactivity concentrations and for radiolabeled fractions (i.e. parent and both polar and nonpolar metabolites) of [^{11}C]erlotinib. Whole blood (0.5 mL) was weighted in duplicate and after centrifuging (5 minutes; 7°C; 4000 r.p.m.), plasma was harvested and 0.5 mL plasma was weighted in duplicate. A well-counter, cross-calibrated against the PET scanner, was used to determine activity concentrations in whole blood and plasma.

To determine the fractions of [^{11}C]erlotinib and its labeled metabolites in each sample, solid phase extraction (SPE) and high performance liquid chromatography (HPLC) were used. 1 mL of plasma was diluted with 2 mL of water and loaded onto an activated Waters Sep-Pak tC2 SPE column. To separate the parent compound from its metabolites, an HPLC system was used. The eluate was injected onto a Phenomenex Gemini 5µ 250x10mm with a flow of 3 mL·min^{-1}. The gradient system was a mixture of acetonitrile (A) and 10 mM ammoniumacetate (B), and was programmed as following: t=0 min 90% B, t=15 min 30% B, t=20 min 30% B, t=21 min 90% B, t=25 min 90% B. Fractions were collected and measured for radioactivity with a gamma-counter to generate an HPLC profile.

REGION OF INTEREST (ROI) DEFINITION

First, images were converted to ECAT7 format. Regions of interest (ROI) were drawn manually within (i.e. smaller than) tumor contours on the CT images, avoiding blood vessels and necrosis as much as possible, using CAPP software (CTI/Siemens, Knoxville, TN, USA), and subsequently projected onto the corresponding PET images. CAPP software was also used to generate tumor time-activity curves (TAC) for all tumor ROI of both [^{15}O]H_2O and [^{11}C]erlotinib scans.

PHARMACOKINETIC ANALYSIS OF [11C]ERLOTINIB DATA

Pharmacokinetic modeling was performed using in-house software, developed within the Matlab (The MathWorks Inc., Natick, MA, USA) environment. First, using standard nonlinear regression techniques, tumor [^{11}C]erlotinib TAC were fitted to different (i.e. 1-tissue, irreversible 2-tissue and reversible 2-tissue) compartment models (15) using the measured metabolite corrected plasma time-activity curve as input function. The optimal model was selected based on both Akaike Information and Schwarz Criteria (16; 17). For the 1-tissue compartment model the outcome

measure of tracer uptake is the volume of distribution VT, and for the irreversible 2-tissue compartment model it is the influx rate constant Ki. In case of the reversible 2-tissue compartment model, both VT and the non-displaceable binding potential (BP_{ND}) can be used as outcome parameters. The most appropriate parameter was chosen depending on test-retest variability. When fitting to the different compartment models, a blood volume parameter was included to correct for the intravascular contribution to the signal.

IMAGE DERIVED INPUT FUNCTION (IDIF)

A less invasive alternative to using continuous arterial blood sampling in [^{11}C]erlotinib kinetic analyses is the use of an image derived input function (IDIF), however, results obtained with IDIF need to be validated against full arterial sampling. IDIF reflects the activity concentration in plasma over time, and is derived from dynamic PET data of the arterial blood pool. To generate IDIF, ROI were drawn within the ascending aorta of early [^{11}C]erlotinib frames (typically 30 to 35 s after injection) in 10 successive slices, resulting in an approximate volume of 6.3 mm^3. By multiplying the arterial whole blood TAC derived from the aorta ROI with a multi-exponential function, derived from the best fit to the plasma-to-whole blood radioactivity ratios of the discrete arterial samples, a plasma TAC was obtained. Then, the plasma TAC was corrected for metabolites using a sigmoid function derived from the best fit to the measured parent fractions of the arterial samples. Finally, this metabolite corrected plasma TAC was used as IDIF (18).

ANALYSIS OF TUMOR PERFUSION

Using nonlinear regression, tumor [^{15}O]H_2O TAC were processed according to the standard single tissue compartment model with IDIF as input function, as described previously (13). This analysis generated blood flow (F) values, reflecting tumor perfusion ($mL \cdot cm^{-3} \cdot min^{-1}$).

MUTATION ANALYSIS

Mutation analysis of EGFR was performed using high resolution melting (HRM) and sequencing, as described previously (11; 12).

IMMUNOHISTOCHEMISTRY

EGFR protein expression intensity was determined using immunohistochemistry (IHC) and scored visually, i.e. semi-quantitatively, as described previously (19).

TUMOR RESPONSE EVALUATION

Response during erlotinib treatment was measured using RECIST criteria (20).

STATISTICAL ANALYSIS

Statistical analysis was performed using SPSS software (SPSS for Windows 15.0, SPSS, Inc.) Level of agreement between test and retest scans was determined using the intraclass correlation coefficient (ICC) with a 2-way random effects model. Values for the ICC range from 0 to 1. Values close to 0 indicate poor agreement between test and retest scans, whereas values close to 1 indicate high agreement. ICC values above 0.70 are considered to have good reproducibility. In addition, the Mann–Whitney test was used to compare V_T and tumor perfusion (F) values between patient groups with and without activating EGFR mutations. Correlations were explored using the Spearman's correlation coefficient (r_s). A two-tailed probability value of $P < 0.05$ was considered significant.

Results

Patients characteristics

Baseline characteristics of all patients are shown in Table 1. Patients were divided into 2 groups. Group 1 consisted of NSCLC patients without activating EGFR mutations. Patient 5 in this group was diagnosed with an adenocarcinoma, harboring only an exon 20 insertion (D770–N771 (ins GG) + N771T). This is a rare primary oncogenic mutation, insensitive to erlotinib, not considered to be an activating EGFR mutation, and thus classified in group 1 (21). All other patients in this group had a wild type tumor EGFR. All patients in group 2 had an exon 19 deletion. High EGFR expression in all tumor cells, as assessed by IHC, was reported for 4 out of 5 tumors in group 1, and for all tumors in group 2. Examples are shown in Figure 1.

Except for one, all patients underwent two scan sessions for a total of 19 [^{11}C]erlotinib scans. Patient 9 in group 2 missed the first [^{11}C]erlotinib scan due to technical problems with the arterial cannula.

Table 1. Patient and treatment characteristics.

Group	Patient number	Patient characteristics Age Sex	Stage (TNM)	Biopsy Time until PET scan Histology	Erlotinib therapy TKI prior to PET scan[a]

		Smoking status Ethnicity		IHC EGFR DNA sequencing	TKI after PET scan[b]
1	1	61 male former smoker Caucasian	IIIb (cT4Nx-2M0)	20 days ASC +++ Wild type	NA NA
1	2	57 male former smoker Caucasian	IIIb (cT4Nx-2M0)	4 months after PET scan SCC +++ Wild type	NA NA
1	3	59 female former smoker Caucasian	IV (cT4N2M1a)	20 months AC +++ Wild type	2 months / PD / 3 months NA
1	4	46 female never smoker African	IV (cT4N2M1a)	16 months AC ++ Wild type	4 months / PD / 41 months NA

1	5	65 male former smoker Caucasian	IV (rT2aN1M1a)	28 months AC +++ Exon 19 wild type; Exon 20 insertion (D770–N771 (ins GG) + N771T)	NA NA
2	6	46 female never smoker Asian	IIIb (cT4N3M0)	13 days AC +++ Exon 19 deletion (del E746–A750)	NA 18 months / PR / 1 day
2	7	47 male never smoker Asian	IV (cT3N0M1a)	1 month AC +++ Exon 19 deletion (del L747–T751)	19 months / PR / 4 months 20 months[c] / PR / 3 weeks
2	8	51 female	IV (T2aN3M1b)	6 days ASC	1st episode[d]: 11 months /

		never smoker Caucasian		+++ Exon 19 deletion (del E746–A750)	PR 2nd episode: 3 months / PD / 3 weeks NA
2	9	37 female never smoker Caucasian	IIa (rT1N1M0)	10 months AC +++ Exon 19 deletion (del E746–A750)	NA NA[e]
2	10	54 female never smoker Caucasian	IV (T4N0M1a)	12 months AC +++ Exon 19 deletion (del E746–A750)	18 months / PR / 11 months 4 months / PR / 1 day

***Abbreviations**: AC= adenocarcinoma, ASC= adenosquamous carcinoma, SCC= squamous cell carcinoma, NA= not applicable, PD= progressive disease, PR= partial response.*

Patients were categorized into 2 groups, according to the presence of activating mutations. Disease stage is indicated using the IASLC classification, 7th edition (25). Using IHC, EGFR protein expression was visually scored as high (+++), moderate (++) or low (+) (19). EGFR mutational status was assessed by DNA sequencing on tumor biopsies (11; 12).

(a) *Erlotinib therapy duration, best response, and TKI free period for patients treated prior to scanning are shown.*
(b) *Treatment duration, best response and start date of erlotinib for patients treated after scanning are shown. Best response to TKI therapy prior and after scanning was scored according to RECIST criteria (20).*
(c) *Patient 7 is progression free to date, i.e. 22 months and ongoing.*
(d) *Patient 8 was treated twice with erlotinib: in a first episode she achieved partial response, but treatment was discontinued after 11 months due to disease progression. Six months after discontinuation she was retreated with erlotinib, this time she did not achieve tumor response.*
(e) *Patient 9 was treated with chemoradiation, not with TKI, as this patient had only local disease.*

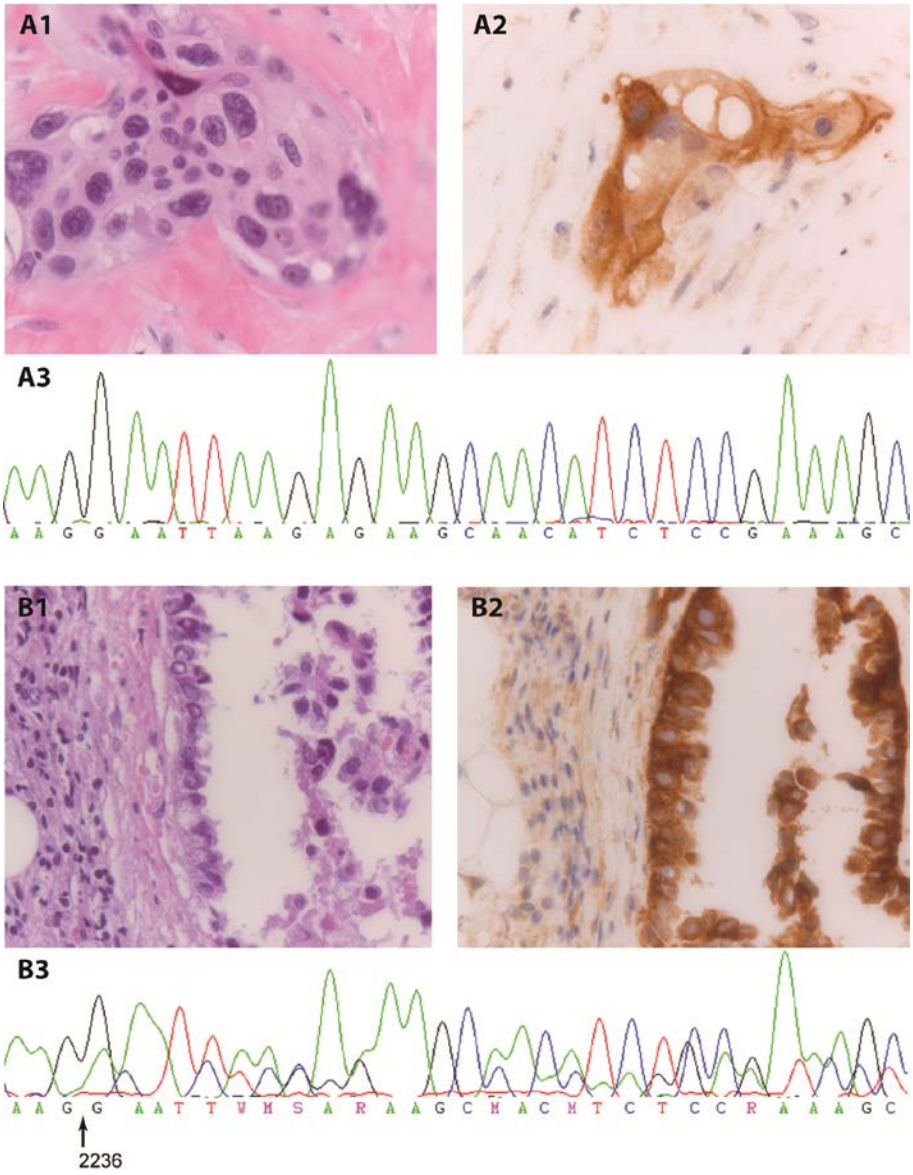

***Fig 1**. Images obtained from tumor biopsy (at 40x objective) of patient 2, stained with (A1) hematoxylin and eosin (H&E) and (A2) EGFR IHC (19) and of patient 6, stained with (B1) H&E and (B2) EGFR IHC. EGFR DNA sequences c.2233 through c.2264 are shown from the above mentioned patients with respectively (A3) wild type EGFR and (B3) an exon 19 deletion (c.2236_2250del15; p.del E746–A750; start of the deletion is indicated by ↑). The nucleic acid coordinates used to name the EGFR mutations are based on RefSeq sequence NM_005228.3.*

Treatment characteristics

Prior to this study, 5 patients had been treated with TKI. In group 1, patients 3 and 4 had received TKI as second line therapy without experiencing any tumor response. In group 2, patients 7 and 10 initially had achieved a partial response on TKI, but treatment was discontinued due to drug toxicity and disease progression, respectively. Patient 8 achieved an initial partial response on TKI for almost a year. Upon first disease progression, she was treated with cytotoxic chemotherapy showing a partial response. After a second progression, she restarted TKI therapy, this time without tumor response (see Table 1).

After the [^{11}C]erlotinib study, none of the patients in group 1 and 3 patients in group 2 started treatment with TKI. Patient 6 was treated with TKI for the first time, whilst patients 7 and 10 were treated again. All achieved a partial response. Patients 6 and 10 maintained this partial response for 18 and 4 months, respectively. To date, 20 months after start of treatment, patient 7 still has a partial response (see Table 1).

Pharmacokinetic analysis of [^{11}C]erlotinib data

Tumor sizes ranged from approximately 5 to 100 mm^3, with tumor ROI, drawn inside the tumor contours, varying between 2.4 to 91.4 mm^3. Analysis of tumor TAC, using both Akaike and Schwarz criteria, showed that the reversible 2-tissue model provided the best fits in 15 out of 19 scans. Therefore, further analyses were performed using this model only. Figure 2 shows fits to a typical tumor TAC using the three plasma input models investigated. Fits for all different compartment models were corrected for intravascular activity by including a blood volume parameter. These blood volume fractions were non-zero in most patients (median 0.06; range 0 – 0.40) for the defined ROI.

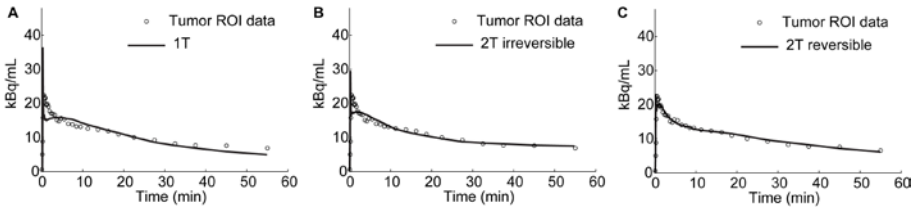

Fig 2. *Tumor [^{11}C]erlotinib TAC (open circles) with best fits according to **(A)** 1-tissue, **(B)** irreversible 2-tissue, and **(C)** reversible 2-tissue compartment models. The latter fit describes the measured PET data best.*

***Abbreviations**: ROI= region of interest.*

This model provides two potential parameters of interest, VT and BP_{ND}. VT was selected as outcome measure, because of its superior test-retest variability (ICC for V_T and BP_{ND} were 0.88 (95% CI 0.55-0.97) and -0.02 (95% CI -0.64-0.62), respectively). V_T results are shown in Table 2.

V_T of [11C]erlotinib was higher in tumors with EGFR exon 19 deletions than in tumors without activating EGFR mutations. This result was found both for test and retest scans (*P* = 0.014 and *P* = 0.009, respectively; Table 2). Patient 9 in group 2 had a higher fitting error, which was probably due to the presence of lymphoid tissue in the tumor ROI. Representative parametric [11C]erlotinib images, using Logan analysis over the interval 20 to 60 min (22), of NSCLC patients with wild type and mutated EGFR are shown in Figure 3.

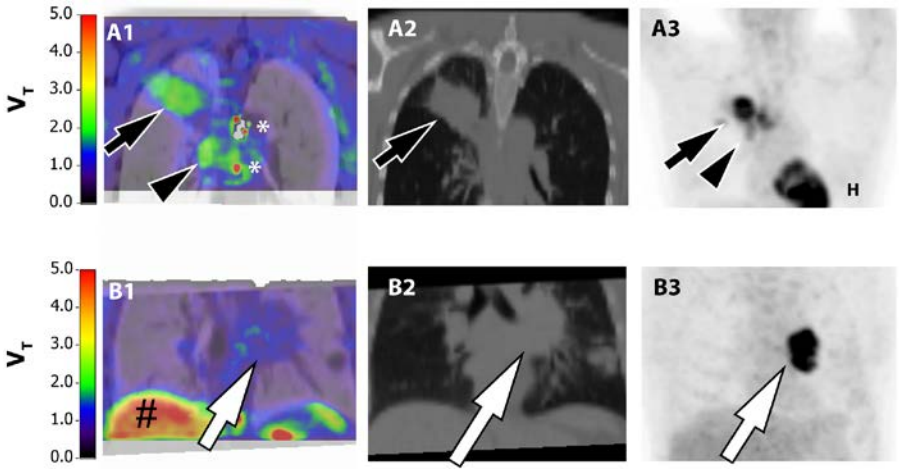

Fig 3. *Representative images of 2 different NSCLC patients:*

*(**A**) Patient 6 with an EGFR exon 19 deletion, tumor in the right upper lobe (black arrow) and mediastinal lymph nodes (black arrowhead). (**B**) Patient 2 with wild type EGFR, tumor located at the left hilum (white arrow).*

*Patient 6 (with mean tumor V_T of 1.30) shows higher tumor uptake than patient 2 (with mean tumor V_T of 0.67) as indicated by the color code. The liver (**#**) shows physiological uptake of metabolized and non-metabolized [11C]erlotinib. (*****) Notice high V_T artifacts caused by mediastinal blood vessels.*

*Coronal images are shown of (**A1, B1**) CT fused parametric [^{11}C]erlotinib V_T, (**A2, B2**) CT, and (**A3, B3**) [^{18}F]FDG uptake. (H) High FDG uptake is seen in the heart.*

Table 2. Fitted VT of [11C]erlotinib and perfusion values with associated standard errors (of the fit).

Nr	EGFR	V_T of [^{11}C]erlotinib ± SE (unitless)				Perfusion ± SE (mL·cm^{-3}·min^{-1})	
		Sampler[a]		IDIF[b]			
		Scan 1	Scan 2	Scan 1	Scan 2	Scan 1	Scan 2
1	WT	1.12 ± 0.20	0.90 ± 0.01	0.99 ± 0.11	0.90 ± 0.04	0.36 ± 0.02	0.30 ± 0.04
2	WT	0.67 ± 0.01	0.67 ± 0.04	0.69 ± 0.01	0.69 ± 0.02	0.34 ± 0.02	NA
3	WT	1.22 ± 0.37	1.17 ± 0.12	1.31 ± 0.36	1.27 ± 0.14	0.33 ± 0.02	0.33 ± 0.02
4	WT	1.09 ± 0.02	1.18 ± 0.02	1.11 ± 0.02	1.17 ± 0.02	0.65 ± 0.03	0.67 ± 0.03
5	Ins Ex20	0.90 ± 0.04	1.03 ± 0.04	0.89 ± 0.04	1.20 ± 0.26	0.43 ± 0.04	0.42 ± 0.03
6	Ex19del	1.30 ± 0.02	1.76 ± 0.02	1.33 ± 0.03	1.90 ± 0.04	0.48 ± 0.01	0.57 ± 0.02
7	Ex19del	1.84 ± 0.07	2.16 ± 0.10	1.90 ± 0.10	2.20 ± 0.12	0.56 ± 0.02	0.46 ± 0.01
8	Ex19del	1.27 ± 0.07	1.25 ± 0.05	1.33 ± 0.07	1.42 ± 0.07	0.57 ± 0.05	0.65 ± 0.04
9	Ex19del	NA	2.93 ± 0.94	NA	2.35 ± 0.50	NA	0.31 ± 0.04

10	Ex19del	1.57 ± 0.06	1.77 ± 0.06	2.22 ± 1.50	1.85 ± 0.07	1.29 ± 0.09	2.07 ± 0.17
Test vs. Retest		ICC = 0.88 (95% CI 0.55-0.97), *P* < 0.001		ICC = 0.85 (95% CI 0.46-0.96), *P* = 0.001		ICC = 0.81 (95% CI 0.32-0.96), *P* = 0.004	
Mutated vs. Non-mutated		Mann-Whitney. two-tailed Scan 1 *P* = 0.014 Scan 2 *P* = 0.009		Mann-Whitney. two-tailed Scan 1 *P* = 0.014 Scan 2 *P* = 0.009		Mann-Whitney. two-tailed Scan 1 *P* = 0.111 Scan 2 *P* = 0.413	

***Abbreviations**: SE= standard error, WT= wild type EGFR, NA= not applicable, CI= confidence interval.*

Scans 1 and 2 refer to test and retest scans.

***(a)** Plasma input based on continuous arterial blood sampling (standard method).*
***(b)** IDIF input based on limited blood sampling (less invasive method).*

V_T values obtained with metabolite corrected IDIF (Table 2) correlated well with those obtained with full arterial sampling(r_s = 0.96 , P < 0.001), considered to be gold standard, as indicated in Figure 4. Using IDIF data, tumors with EGFR exon 19 deletions also had significantly higher V_T values than those without for both test and retest scans (*P* = 0.014 and *P* = 0.009, respectively). The test-retest variability (ICC = 0.85, 95% CI 0.46-0.96) was similar as obtained with full arterial sampling.

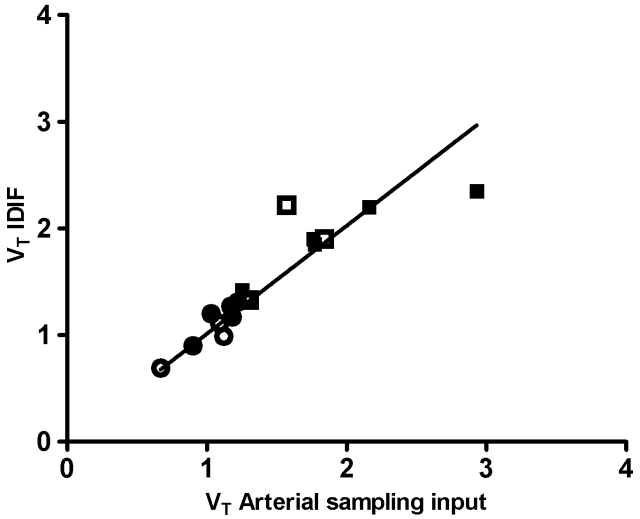

Fig 4. *Correlation between V_T values derived from IDIF and those obtained using full arterial sampling. Test (n= 9) and retest (n= 10) data were pooled. Spearman correlation coefficient = 0.92, P < 0.01 (Table 2).*

Plasma analysis

The parent fraction in groups 1 and 2, indicating unchanged [^{11}C]erlotinib in plasma, steadily decreased to 54 ± 2 % and 43 ± 7 % (mean ± standard deviation) at 60 minutes after injection, whilst polar radiolabeled metabolites steadily increased over 60 minutes to 31 ± 21 % and 33 ± 17 %, respectively. The fraction of nonpolar metabolites, as assessed by HPLC, was too small to be quantified reliably. Therefore, use of SPE only (i.e. measuring polar metabolites) was sufficient. Results for wild type and mutated EGFR patients are shown in Supplementary Figure 2. The fractions do not add up to 100%, because not all blood samples could be measured in all subjects.

Perfusion

Due to technical problems, only one [^{15}O]H_2O scan was performed in patients 2 and 9. There was no difference in tumor blood flow between both groups, with *P* values of 0.111 and 0.413 for test (n= 9) and retest (n= 9) scans, respectively. There was good test-retest variability (ICC = 0.81, Table 2). Average [^{11}C]erlotinib K1 values for wild type and mutated EGFR were not significantly different (*P* = 0.372) with 0.30 (SD = 0.29) and 0.44 (SD = 0.13), respectively. Correlation between K1 and flow was good (r_s = 0.70, *P* = 0.031).

Discussion

Pharmacokinetic modeling using arterial sampling

The aim of this study was to develop a method to quantify [11C]erlotinib uptake in NSCLC tumors, which could be used as an *in vivo* tool for detecting activating EGFR mutations. For quantification of PET tracer studies, the gold standard is kinetic modeling using a measured metabolite corrected arterial plasma curve as input function. Using this approach, best fits were obtained with the reversible 2-tissue compartment model, providing volume of distribution (V_T) as a measure of [11C]erlotinib uptake. The test-retest design of the present study showed that [11C]erlotinib V_T values were reproducible (Table 2). This model was used in all further analyses.

Pharmacokinetic modeling using IDIF

[11C]erlotinib V_T values obtained using IDIF correlated well with V_T obtained using arterial sampling (Figure 4). Reproducibility of IDIF based [11C]erlotinib V_T values was also good for all patients (Table 2). These findings validate the use of IDIF in future studies, making this technique better suitable for routine clinical use. Although continuous arterial sampling can now be omitted, image derived whole blood curves still need to be corrected for both plasma-to-whole blood radioactivity ratios and the fraction of radiolabeled metabolites. Even though this needs to be confirmed for [11C]erlotinib, these measurements may be obtained from a number of discrete venous rather than arterial samples, as shown in studies using other tracers (23).

EGFR mutational status

Unintentionally only patients with exon 19 deletions, and no patients with other activating mutations, such as L858R, were included in group 2. VT of [11C]erlotinib, as determined using both arterial sampling and IDIF, was significantly higher in group 2 than in group 1, for both test and retest scans. Although many factors contribute to tumor [11C]erlotinib accumulation in PET, the differences in V_T may be caused by differences in affinity to erlotinib. Erlotinib competes with ATP to bind at the ATP-binding site of the EGFR kinase domain. Kinase assay studies have found values for the erlotinib dissociation constant (K_i) of 3.3, 6.3 and 17.5 nM, and Michaelis-Menten constant (K_M) values for ATP of 129.0, 10.9 and 5.0 µM for exon 19 deletions, exon 21 point mutations and wild type EGFR, respectively (7). This means that erlotinib affinity is higher for EGFR with activating mutations than for wild type EGFR, while ATP affinity is lower. Compared with wild type EGFR, exon 19 deletions and exon 21 mutations exhibit 137-fold and 6-fold higher binding to erlotinib relative to ATP (i.e. K_i / K_M ratios), respectively (7).

Contributing factors

Although high affinity of erlotinib for EGFR represents a favorable parameter for [^{11}C]erlotinib as a PET tracer, differences in K_i / K_M ratios between wild type and mutated EGFR (i.e. more than 100-fold for exon 19 deletions) are not reflected in the same magnitude in V_T values (i.e. almost 2-fold). Clearly, *in vitro* studies occur in more simplified circumstances than *in vivo* studies, lacking complex interactions, such as non-specific binding and the presence of radiolabeled metabolites that cause underestimation of V_T differences. In addition, *in vitro* conditions may deviate from normal physiological conditions. For example, differences in ATP affinity between wild type EGFR and mutated EGFR are seen at low ATP concentrations, but at higher, near physiological ATP concentrations, these differences become less significant (7; 24). Other *in vivo* factors may also contribute to the observed differences in tumor [^{11}C]erlotinib uptake, such as EGFR protein expression and blood flow. However, both tumor EGFR protein expression and tumor blood flow were comparable between tumors with and without an EGFR exon 19 deletion.

Erlotinib therapy

In this study 6 out of 10 patients received erlotinib therapy, either prior or post scanning. In group 1, only 2 patients were treated with erlotinib. This was prior to scanning, and none of the two low V_T patients achieved tumor response. Three patients in group 2 were treated with erlotinib after scanning. These 3 high V_T patients achieved a partial response. The remaining patient in group 2 (patient 8) developed resistance to erlotinib, which was diagnosed 3 weeks prior to her [^{11}C]erlotinib PET. Interestingly, her V_T was higher than in the non-mutated group, but the lowest observed in the mutated group, which could be in accordance with her clinically diminished TKI sensitivity. Although the sample size in this study is too small to draw any definite conclusions, these findings support the hypothesis that increased [^{11}C]erlotinib V_T correlates with tumor response to erlotinib. Clearly, these findings need to be confirmed in larger trials.

Recently, results of a qualitative study on 13 patients undergoing [^{11}C]erlotinib scanning were reported (9). Four patients died before response evaluation. Of the 9 patients who were evaluable for tumor response to erlotinib therapy, all 3 patients with high [^{11}C]erlotinib accumulation showed stable disease, whereas 4 out of 6 patients with lower accumulation had progressive disease, and the remaining 2 had stable disease. Unfortunately, EGFR mutational status was not measured in this study. Nevertheless, these results also indicate that [^{11}C]erlotinib uptake may predict tumor sensitivity to erlotinib therapy.

Clinical response to TKI depends on EGFR affinity to TKI and ATP, but also on oncogene addiction of tumor cells. As, in clinical practice, up to 80% of patients harboring activating EGFR mutations respond to TKI, it could be hypothesized that responders have EGFR driven growth and non-responders may have other mechanisms that activate proliferation. Whether tumor growth in a patient is fully driven by the EGFR pathway cannot be measured using [11C]erlotinib PET.

Study limitations

This study has a number of limitations. Firstly, being a proof-of-concept study, only a limited number of patients were included. According to the inclusion criteria, all activating EGFR mutations, including exon 19 deletions and exon 21 point mutations were allowed to enter group 2. Unintentionally, only patients with exon 19 deletions were included. The fact that patients with exon 21 point mutations (L858R) were not included possibly avoided confounding effects caused by differences in TKI affinity between both mutations. Cell based studies have shown that EGFR with exon 19 deletions are more sensitive to TKI than L858R EGFR (7; 24). On the other hand, clinical trials have shown highly comparable response rates in both mutations. This suggests that TKI have sufficient affinity to provoke similar initial tumor responses in both types of mutations. [11C]erlotinib uptake in patients with exon 21 point mutations is unknown and should be investigated in future studies.

Full kinetic modeling and arterial blood sampling were used to derive the volume of distribution of [11C]erlotinib. This approach provides the most accurate assessment of erlotinib uptake, which is important in the present proof of concept study. It is, however, less suitable for routine clinical studies and further studies are needed to assess simplified analytical methods, such as the standardized uptake value (SUV). Preliminary data indicate that a SUV analysis provides a poorer discrimination between both patients groups. On the other hand, tumor-to-blood ratios appear to be more promising. A full comparison is in progress. Simplified methods are also relevant for whole body scans, enabling the study of interlesional heterogeneity.

Differences in V_T between both patient groups could potentially be due to differences in non-specific binding. The non-specific component of V_T given by K_1/k_2, however, did not significantly differ between groups. Ideally, this should be confirmed in an independent measurement. One possibility would be to measure V_T after a blocking dose with cold erlotinib. This is, however, not possible in patients and needs to be performed in future animal studies.

V_T differences between groups appear modest, when compared to the differences in K_i / K_M ratios between mutated and wild type EGFR. However, V_T values between groups are clearly distinct, with excellent test-retest repeatability, justifying further validation studies with larger numbers of patients, to answer the question whether V_T can be used to effectively distinguish between patients who will and will not benefit from TKI treatment.

In this study, using SPE followed by HPLC, the radioactive parent compound fraction was discriminated from the radioactive metabolite fractions in arterial plasma samples. Clearly, metabolite fractions in tumors were not determined. Previous pharmacology studies have shown that the main metabolite of erlotinib is OSI-420, the precursor to which the C-11 label is introduced in the synthesis of [^{11}C]erlotinib. After losing the C-11 label at the 7-methoxyethoxy position, OSI-420 becomes nonradioactive, and does not show up on the PET scan. This metabolism does result in small polar radiolabeled metabolites like C-11 formaldehyde, C-11 formic acid and/or C-11 carbonmonoxide. These metabolites could cause some bias, i.e. an underestimation, of V_T differences between groups.

Biopsies were not taken at the time of scanning, as indicated in Table 1. No biopsies were taken for the purpose of the present study. This is a relevant limitation, especially for patients with exon 19 deletions who were treated with TKI (i.e. patients 7, 8 and 10) prior to scanning, as they may have developed secondary mutations, e.g. T790M, that could decrease the affinity of EGFR for [^{11}C]erlotinib. In patient 7, no secondary mutations were found in biopsies taken 1 month prior to scanning. This biopsy was considered representative. In addition, to date (i.e. 22 months) this patient has maintained a partial response to erlotinib. Patient 8 and 10 underwent an additional biopsy, revealing the presence of T790M, 6 and 12 months after scanning, respectively, indicating that disease progression was probably due to this secondary mutation. It is believed that T790M mutations are already present in tumor cells with activating mutations, and that during TKI therapy a clonal selection takes place. This means that both patients 8 and 10 could have had T790M bearing tumor cells during scanning, but to which extent and how this changed [^{11}C]erlotinib uptake is unclear.

Future perspectives

More studies are needed to validate and substantiate the present findings. In future research, the use of simplified parameters such as SUV should be investigated. In addition, future research needs to focus on heterogeneity in tumor [^{11}C]erlotinib V_T, especially after initiation of TKI therapy and after disease progression occurs. In case of emerging resistance to TKI, [^{11}C]erlotinib PET may

reveal residual TKI sensitive tumor sites, which could justify continuation of TKI within a more complex treatment protocol. As all TKI treated patients develop resistance, this is an important clinical issue. Furthermore, the use of static whole body [^{11}C]erlotinib scans could provide a means to evaluate distant metastatic lesions and their TKI sensitivity. The present study with [^{11}C]erlotinib can serve as a template for other studies using radiolabeled TKI that target different tyrosine kinases and activate proliferative pathways in a variety of other malignancies.

In conclusion, the present study shows that measuring [^{11}C]erlotinib uptake by V_T using PET is feasible. [^{11}C]erlotinib V_T is higher in NSCLC patients with EGFR exon 19 deletions. Therefore, this non-invasive *in vivo* method shows promise as a tool for individualizing therapy by identifying those patients, who may benefit from TKI therapy.

References

1. Pao W, Miller V, Zakowski M, Doherty J, Politi K, Sarkaria I, et al. EGF receptor gene mutations are common in lung cancers from “never smokers” and are associated with sensitivity of tumors to gefitinib and erlotinib. Proceedings of the National Academy of Sciences of the United States of America. 2004;101(36):13306.

2. Lynch TJ, Bell DW, Sordella R, Gurubhagavatula S, Okimoto RA, Brannigan BW, et al. Activating mutations in the epidermal growth factor receptor underlying responsiveness of non-small-cell lung cancer to gefitinib. New England Journal of Medicine. 2004;350(21):2129-2139.

3. Maemondo M, Inoue A, Kobayashi K, Sugawara S, Oizumi S, Isobe H, et al. Gefitinib or chemotherapy for non-small-cell lung cancer with mutated EGFR. New England Journal of Medicine. 2010;362(25):2380-2388.

4. Mitsudomi T, Morita S, Yatabe Y, Negoro S, Okamoto I, Tsurutani J, et al. Gefitinib versus cisplatin plus docetaxel in patients with non-small-cell lung cancer harbouring mutations of the epidermal growth factor receptor (WJTOG3405): an open label, randomised phase 3 trial. The lancet oncology. 2010;11(2):121-128.

5. Mok TS, Wu YL, Thongprasert S, Yang CH, Chu DT, Saijo N, et al. Gefitinib or carboplatin-paclitaxel in pulmonary adenocarcinoma. New England Journal of Medicine. 2009;361(10):947-957.

6. Cobo M, Isla D, Massuti B, Montes A, Sanchez JM, Provencio M, et al. Customizing cisplatin based on quantitative excision repair cross-complementing 1 mRNA expression: a phase III trial in non-small-cell lung cancer. Journal of clinical oncology : official journal of the American Society of Clinical Oncology. 2007;25(19):2747-54.

7. Carey KD, Garton AJ, Romero MS, Kahler J, Thomson S, Ross S, et al. Kinetic analysis of epidermal growth factor receptor somatic mutant proteins shows increased sensitivity to the epidermal growth factor receptor tyrosine kinase inhibitor, erlotinib. Cancer research. 2006;66(16):8163-71.

8. Memon AA, Jakobsen S, Dagnaes-Hansen F, Sorensen BS, Keiding S, Nexo E. Positron emission tomography (PET) imaging with [11C]-labeled erlotinib: a micro-PET study on mice with lung tumor xenografts. Cancer research. 2009;69(3):873-8.

9. Memon AA, Weber B, Winterdahl M, Jakobsen S, Meldgaard P, Madsen HHT, et al. PET imaging of patients with non-small cell lung cancer employing an

EGF receptor targeting drug as tracer. British journal of cancer. 2011;105(12):1850-5.

10. Weber B, Winterdahl M, Memon A, Sorensen BS, Keiding S, Sorensen L, et al. Erlotinib accumulation in brain metastases from non-small cell lung cancer: visualization by positron emission tomography in a patient harboring a mutation in the epidermal growth factor receptor. Journal of Thoracic Oncology. 2011;6(7):1287.

11. Heideman D, Thunnissen F, Doeleman M, Kramer D, Verheul H, Smit E, et al. A panel of high resolution melting (HRM) technology-based assays with direct sequencing possibility for effective mutation screening of EGFR and K-ras genes. Analytical Cellular Pathology. 2009;31(5):329-333.

12. Kramer D, Thunnissen F, Gallegos-Ruiz M, Smit E, Postmus P, Meijer C, et al. A fast, sensitive and accurate high resolution melting (HRM) technology-based assay to screen for common K-ras mutations. Analytical Cellular Pathology. 2009;31(3):161-167.

13. van der Veldt AAM, Hendrikse NH, Harms HJ, Comans EFI, Postmus PE, Smit EF, et al. Quantitative Parametric Perfusion Images Using 15O-Labeled Water and a Clinical PET/CT Scanner: Test-Retest Variability in Lung Cancer. Journal of Nuclear Medicine. 2010;51(11):1684.

14. Boellaard R, van Lingen A, van Balen SCM, Hoving BG, Lammertsma AA. Characteristics of a new fully programmable blood sampling device for monitoring blood radioactivity during PET. European Journal of Nuclear Medicine and Molecular Imaging. 2001;28(1):81-89.

15. Lammertsma AA, Bench CJ, Hume SP, Osman S, Gunn K, Brooks DJ, et al. Comparison of methods for analysis of clinical [11C]raclopride studies. Journal of cerebral blood flow and metabolism : official journal of the International Society of Cerebral Blood Flow and Metabolism. 1996;16(1):42-52.

16. Schwarz G. Estimating the dimension of a model. The annals of statistics. 1978;6(2):461-464.

17. Akaike. A new look at the statistical model identification. I E E E Trans Autom Control. 1974;19716–23.

18. Yaqub M, Boellaard R, Kropholler MA, Lammertsma AA. Optimization algorithms and weighting factors for analysis of dynamic PET studies. Physics in medicine and biology. 2006;514217.

19. Ruiz MIG, Floor K, Steinberg S, Grünberg K, Thunnissen FBJM, Belien JAM, et al. Combined assessment of EGFR pathway-related molecular markers and prognosis of NSCLC patients. British journal of cancer. 2008;100(1):145-152.

20. Eisenhauer E, Therasse P, Bogaerts J, Schwartz L, Sargent D, Ford R, et al. New response evaluation criteria in solid tumours: revised RECIST guideline (version 1.1). European Journal of Cancer. 2009;45(2):228-247.

21. Greulich H, Chen T-H, Feng W, Jänne PA, Alvarez JV, Zappaterra M, et al. Oncogenic transformation by inhibitor-sensitive and -resistant EGFR mutants. PLoS medicine. 2005;2(11):e313.

22. Logan J, Fowler JS, Volkow ND, Wolf AP, Dewey SL, Schlyer DJ, et al. Graphical analysis of reversible radioligand binding from time-activity measurements applied to [N-11C-methyl]-(-)-cocaine PET studies in human subjects. Journal of Cerebral Blood Flow & Metabolism. 1990;10(5):740-747.

23. Visvikis D, Francis D, Mulligan R, Costa D, Croasdale I, Luthra S, et al. Comparison of methodologies for the in vivo assessment of 18 FLT utilisation in colorectal cancer. European Journal of Nuclear Medicine and Molecular Imaging. 2004;31(2):169-178.

24. Mulloy R, Ferrand A, Kim Y, Sordella R, Bell DW, Haber DA, et al. Epidermal growth factor receptor mutants from human lung cancers exhibit enhanced catalytic activity and increased sensitivity to gefitinib. Cancer research. 2007;67(5):2325-30.

25. Goldstraw P, Cancer IA for the S of L. Staging manual in thoracic oncology. Editorial Rx Press; 2009.

Chapter 4

Quantitative and Simplified Analysis of ^{11}C-Erlotinib Studies

Maqsood Yaqub

Idris Bahce

Charlotte Voorhoeve

Robert C. Schuit

Albert D. Windhorst

Otto S. Hoekstra

Ronald Boellaard

N. Harry Hendrikse

Egbert F. Smit

Adriaan A. Lammertsma

J Nucl Med 2016; 57:861–866

Abstract

PURPOSE: Quantitative assessment of ^{11}C-erlotinib uptake may be useful in selecting non–small cell lung cancer (NSCLC) patients for erlotinib therapy. The purpose of this study was to find the optimal pharmacokinetic model for quantification of uptake and to evaluate various simplified methods for routine analysis of ^{11}C-erlotinib uptake in NSCLC patients.

METHODS: Dynamic ^{15}O-H_2O and ^{11}C-erlotinib scans were obtained in 17 NSCLC patients, 8 with and 9 without an activating epidermal growth factor receptor mutation (exon 19 deletion or exon 21-point mutation). Ten of these subjects also underwent a retest scan on the same day. ^{11}C-erlotinib data were analyzed using single-tissue and 2-tissue-irreversible and -reversible (2T4k) plasma input models. In addition, several advanced models that account for uptake of radiolabeled metabolites were evaluated, including a variation of the 2T4k model without correcting for metabolite fractions in plasma (2T4k-WP). Finally, simplified methods were evaluated—that is, SUVs and tumor-to-blood ratios (TBR)—for several scan intervals.

RESULTS: Tumor kinetics were best described using the 2T4k-WP model yielding optimal fits to the data (Akaike preference, 43.6%), acceptable test–retest variability (12%), no dependence on perfusion changes, and the expected clinical group separation ($P < 0.016$). Volume of distribution estimated using 2T4k-WP and 2T4k were highly correlated ($R^2 = 0.94$). Similar test–retest variabilities and clinical group separations were found. The 2T4k model did not perform better than an uncorrected model (2T4k-WP), probably because of uncertainty in the estimation of true metabolite fractions. Investigation of simplified approaches showed that SUV curves normalized to patient weight, and injected tracer dose did not reach equilibrium within the time of the scan. In contrast, TBR normalized to whole blood (TBR-WB) appeared to be a useful outcome measure for quantitative assessment of ^{11}C-erlotinib scans acquired 40–60 min after injection.

CONCLUSION: The optimal model for quantitative assessment of ^{11}C-erlotinib uptake in NSCLC was the 2T4k-WB model. The preferred simplified method was TBR-WB (40–60 min after injection) normalized using several whole-blood samples.

Introduction

PET is the method of choice for in vivo visualizing and quantifying molecular pathways and interactions in the human body. PET may be useful for predicting and monitoring response to treatment in non–small cell lung cancer (NSCLC) patients, potentially providing an in vivo method to optimize treatment strategies.

At present, treatment of NSCLC patients includes surgery, radiotherapy, and chemotherapy. Next to cytotoxic chemotherapy, various forms of targeted therapy are in use, such as treatment with epidermal growth factor receptor (EGFR) tyrosine kinase inhibitors (TKIs). In NSCLC tumors, these TKIs show a higher efficacy if an activating EGFR mutation is present (1–3). Identification of patients with activating EGFR mutations remains a challenge, because tumor sampling for DNA sequencing is not always possible (4).

Recently, the TKI erlotinib was labeled with ^{11}C, thereby enabling in vivo studies of its kinetic behavior using PET. In an initial study in humans, a method to quantify ^{11}C-erlotinib uptake was reported (5). This method required a dynamic scan protocol of up to 60 min to characterize ^{11}C-erlotinib kinetics in tumor tissue. In addition, although it was shown that an image-derived input function (IDIF) could be used for quantification of ^{11}C-erlotinib uptake in drug-naïve patients, several arterial blood samples were still required to calibrate this IDIF and to estimate parent ^{11}C-erlotinib fractions. This initial study did not, however, investigate pharmacokinetic models that allow for tumor uptake of labeled metabolites of ^{11}C-erlotinib.

The main objective of the present study was to identify the optimal pharmacokinetic model for quantification of tumor ^{11}C-erlotinib kinetics in NSCLC patients, including models that account for uptake of labeled metabolites of ^{11}C-erlotinib. The second objective was to investigate simplified methods that could be used in combination with whole-body scans, enabling the assessment of multiple lesions in the same patient.

Materials and methods

Scanning Protocol

Data were derived from an ongoing clinical study, approved by the Medical Ethics Review Committee of VU University Medical Center, consisting of 17 subjects: 8 with an activating EGFR mutation (exon 19 deletion or exon 21-point mutation, MT)

and 9 without EGFR mutation/wild-type. The EGFR exon 19 deletions and exon 21-point mutation (L858R) confer to TKI sensitivity (6). EGFR exon 20 insertions (D770-N771 and V769-D770) are known to be insensitive to EGFR TKI (7). Each subject gave written informed consent before inclusion in the study.

Each subject was scanned on a Gemini TF-64 PET/CT scanner (Philips). The scan protocol consisted of a low-dose CT for attenuation correction followed by dynamic ^{15}O-H_2O and ^{11}C-erlotinib PET scans. These scans were obtained after intravenous bolus injections of 370 ± 37 and 256 ± 53 MBq of ^{15}O-H_2O and ^{11}C-erlotinib, respectively. No significant differences in either injected activity or specific activities were seen between the groups. Ten patients underwent the full protocol twice on the same day to assess test–retest variability.

Acquired list-mode data were reconstructed into 26 (1 x 10, 8 x 5, 4 x 10, 2 x 15, 3 x 20, 2 x 30, and 6 x 60 s) and 36 (1 x 10, 8 x 5, 4 x 10, 2 x 15, 3 x 20, 2 x 30, 6 x 60, 4 x 150, 4 x 300, and 2 x 600 s) frames for ^{15}O-H_2O and ^{11}C-erlotinib scans, respectively. Data were reconstructed using 3-dimensional row-action maximum-likelihood algorithm (8) in combination with CT-based attenuation correction, providing images with a final voxel size of 4 x 4 x 4 mm^3 and a spatial resolution of 5–7 mm in full width at half maximum. Reconstructions included all usual corrections, such as detector normalization, and decay, dead time, attenuation, randoms, and scatter corrections.

During the ^{11}C-erlotinib scans, up to 8 manual arterial samples were taken at discrete times (~2.5, 5, 10, 15, 20, 30, 40, and 60 min after injection) (9). These samples were used to adjust the IDIF for calibration offsets and plasma–to–whole-blood ratios and to correct for labeled metabolites.

Region-of-Interest Definition

Using the CT images, we manually drew volumes of interest within the tumor boundaries, avoiding blood vessels and necrosis as much as possible. Subsequently, these regions of interest were projected onto the corresponding ^{15}O-H_2O or ^{11}C-erlotinib dynamic PET image sequences to extract regional tumor time–activity curves. Finally, IDIF volumes of interest were generated by defining circular regions of interest inside the descending aorta using a summed image of the early dynamic PET frames (typically 30–35 s after injection) in 10 successive slices, resulting in an approximate volume of 6.3 mm^3. Although, in general, use of the ascending aorta is to be preferred, in this study the descending aorta was used, as it was within the field of view for all patients. In addition, IDIF volumes of interest were placed as far away from the liver as possible to avoid spill-over.

Kinetic Analysis Using Plasma Input Models

All time–activity curves were analyzed using plasma input-based pharmacokinetic models (10). ^{15}O-H_2O time–activity curves were analyzed using an IDIF and the standard single-tissue-compartment model (1T2k) with an additional parameter for fractional arterial blood volume (11). Analysis of ^{11}C-erlotinib time–activity curves was performed using 3 conventional pharmacokinetic plasma input models (10), all with an additional parameter for fractional blood volume: 1T2k; 2T3k, irreversible 2-tissue-compartment model; and 2T4k, reversible 2-tissue-compartment model.

Standard pharmacokinetic models assume various simplifications that do not have to apply in the case of tumors. For example, metabolites could enter the tumor tissue, and this is not considered in the standard models. Therefore, 3 additional nonconventional models were developed and evaluated: 1T2k-x2, 2 parallel 1T2k plasma input models, one for parent ^{11}C-erlotinib and the other for labeled metabolites to assess whether labeled metabolites enter tumor tissue; 2T4k_1T2k, 2 parallel plasma input models, a 2T4k model for parent ^{11}C-erlotinib and a 1T2k model for labeled metabolites, again assessing whether labeled metabolites enter tumor tissue; and 2T4k-WP, a pragmatically modified 2T4k model using whole blood as an input function rather than parent plasma to assess whether a metabolite-corrected input function is indeed necessary.

Fit quality was assessed visually, and the Akaike criterion (12) was used to assess the goodness of fit for the various models. The best models were used to derive various kinetic parameters such as binding potential (BP_{ND}) and volume of distribution (V_T). Parameter estimates from these models were compared with each other using the Pearson product moment correlation coefficients. In addition, test– retest analyses were performed to assess parameter variability, and each parameter was evaluated for its capacity to differentiate between the 2 clinical groups. Next, dependency of the kinetic parameters on perfusion was assessed by deriving the Pearson correlation coefficients with ^{15}O-H_2O–derived blood flow (F) values. Finally, to understand the effects of metabolites on model preferences, individual metabolite profiles and time–activity curves were plotted with curves color-coded according to the preferred model. As a level of metabolism, the metabolite fraction measured at 60 min after injection was used.

Simplified (Static) Analyses

The accuracies of several simplified static approaches were evaluated. SUVs, normalized for patient weight and injected dose, were evaluated for 4 different time intervals (20–30, 30–40, 40–50, and 50–60 min). In addition, tumor-to-blood ratios (TBRs) were evaluated using both arterial whole blood (TBR-WB) and

metabolite corrected plasma (TBR-PP) activity concentrations. The same 4 time intervals (20–30, 30–40, 40–50, and 50–60 min) were used for this analysis.

For all simplified measures, the equilibration time was derived from normalized time–activity curves. Next, simplified parameters for the optimal time interval were compared with parameter estimates derived from the optimal kinetic models using the Pearson correlation coefficients. In addition, test–retest analysis, clinical group separation, and dependency on perfusion were determined to assess possible usefulness in clinical practice.

Results

Patient Characteristics

Patient characteristics are given in Table 1. This table also lists missing ^{11}C-erlotinib and ^{15}O-H_2O scans due to technical reasons (radiosynthesis failure or patient movement) or because a full test– retest study was not performed. In addition, all scans from 2 subjects were excluded because of nonquantifiable uptake in the tumor. One of these patients showed lymph node relapse (subject 15) and the other heterogeneous tumor uptake due to a mixture of atelectasis and tumor (subject 8). In patient 6, an EGFR exon 20- point mutation (G779S), a rare mutation of unknown significance, was seen together with a driver mutation of Kras exon 1 and was therefore considered resistant to EGFR TKI (7,13). In patient 14, both an EGFR exon 19 deletion and an EGFR exon 20 (T790M) was seen. These mutations confer to TKI sensitivity and TKI resistance, respectively.

Table 1 Patient characteristics and overview of scans performed

Group	Patient no.	Age (y) / sex	Tumor EGFR mutational status	^{11}C-erlotinib Scan 1 / Scan 2	^{15}O-H_2O Scan 1 / Scan 2
1	1	61 / Male	Wild type	Yes / Yes	Yes / Yes
1	2	57 / Male	Wild-type	Yes / Yes	Yes / Failed

1	3	59 / Female	Wild-type	Yes / Yes	Yes / Yes
1	4	48 / Female	Wild-type	Yes / Yes	Yes / Yes
1	5	65 / Male	Exon 20 ins (D770-N771(ins GG) + N771T)	Yes / Yes	Yes / Yes
1	6	64 / Female	Exon 20 (G779S) + Kras exon1 (c.37 G>T, pG13C)	Yes / No	Yes / No
1	7	69 / Female	Wild-type	Yes / No	Yes / No
1	8	47 / Female	Wild-type	Yes / Yes	Yes / Yes
1	9	79 / Female	Exon 20 ins (V769-D770 (ins ASV))	Moved / No	Moved / No
1	10	74 / Male	Wild-type	Yes / No	Yes / No
2	11	48 / Female	Exon 21 point mutation (L858R)	Yes / No	Yes / No
2	12	46 / Female	Exon 19 deletion (delE746-A750)	Yes / Yes	Yes / Yes
2	13	47 / Male	Exon 19 deletion (delL747-T751)	Yes / Yes	Yes / Yes
2	14	51 / Female	Exon 19 deletion (delE746-A750) + exon 20 (T790M)	Yes / Yes	Yes / Yes
2	15	37 / Female	Exon 19 deletion (delE746-A750)	No / Yes	No / Yes
2	16	54 / Female	Exon 19 deletion (delE746-A750)	Yes / Yes	Yes / Yes

2	17	68 / Female	Exon 19 deletion (delE746-S752)	Yes / No	Yes / No

Input Data

Figure 1 summarizes measurements of all blood sample data. Only polar metabolite fractions could be measured, because activity levels were too low to measure nonpolar metabolites reliably. A relatively low level of metabolites was seen in most subjects with an average (±SD) of 29% ± 21% at 60 min. The variability in tracer metabolism within patients was maximally 20%, but the differences between the patients were much larger because of the differences in liver function between NSCLC patients (Fig. 1C). Several initial measurements (n = 10) of nonpolar metabolites showed that their overall contribution was small, making it difficult, if not impossible given the short half-life of ^{11}C, to measure the minor nonpolar metabolite fraction with any degree of accuracy. Therefore, input functions were not corrected for nonpolar metabolites but only for polar metabolites.

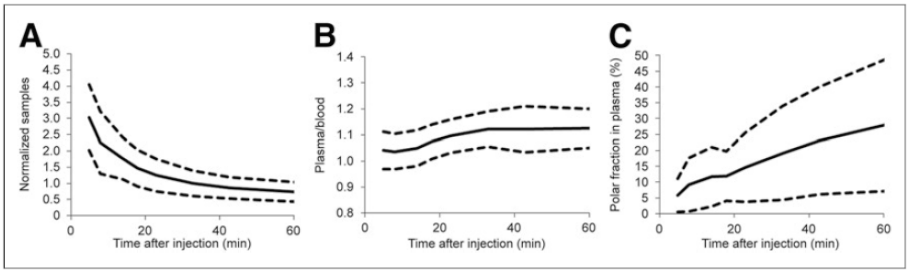

Fig 1. *Data from manual blood samples with whole-blood concentrations normalized to injected dose and patient weight (A), plasma–to–whole-blood ratios (B), and polar metabolite fractions in plasma (C) as function of time. Solid lines represent average values, and dashed lines represent values with 1 SD difference.*

Optimal Kinetic Model for ^{11}C-Erlotinib

Visual assessment of ^{11}C-erlotinib tumor fits showed that the 1T2k model was unable to fit the time–activity curves properly (Fig. 2). This was in concordance with results from the Akaike information criterion, which showed that, among the standard models, ^{11}C-erlotinib data were best fitted to the reversible 2-tissue

model (96% preference), followed by the 2T3k model (4% preference), with no preference for the 1T2k model.

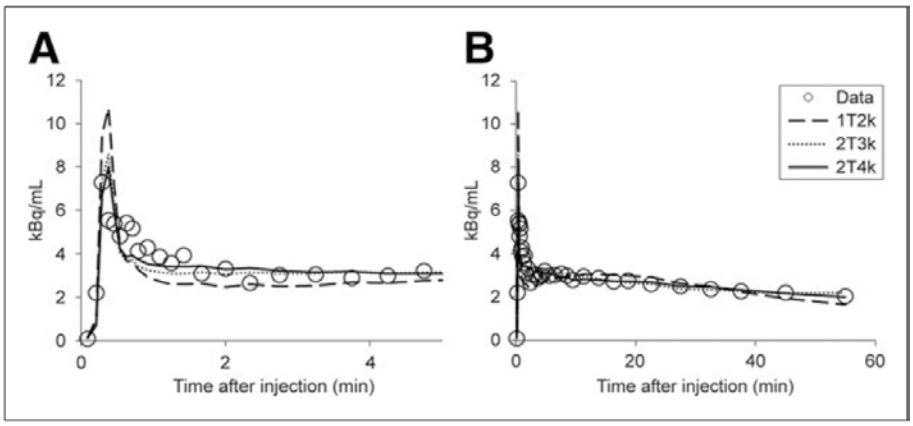

Fig 2. *Typical ^{11}C-erlotinib tumor time–activity curve fitted to conventional plasma input models. (A) Initial part (0–5 min) of time–activity curve. (B) Full time–activity curve (0–60 min).*

When the nonconventional models were included, the Akaike criterion showed preference for the 2T4k-WP model (43.6%), followed by conventional 2T4k (21.7%) and 2T4k-1T2k (21.7%) models. The 1T2k-x2 model was preferred in only 13% of the cases. Therefore, the 2T4k-WP was selected for further comparisons with the conventional 2T4k model.

Relating Akaike model preference to metabolite curves (Fig. 3A) indicated that the standard metabolite-corrected plasma input model (2T4k) was preferred only in the case of relatively low levels of metabolite fractions. However, visually, for these data the Akaike model preference did not seem to be related to the shape of the time–activity curve (Fig. 3B).

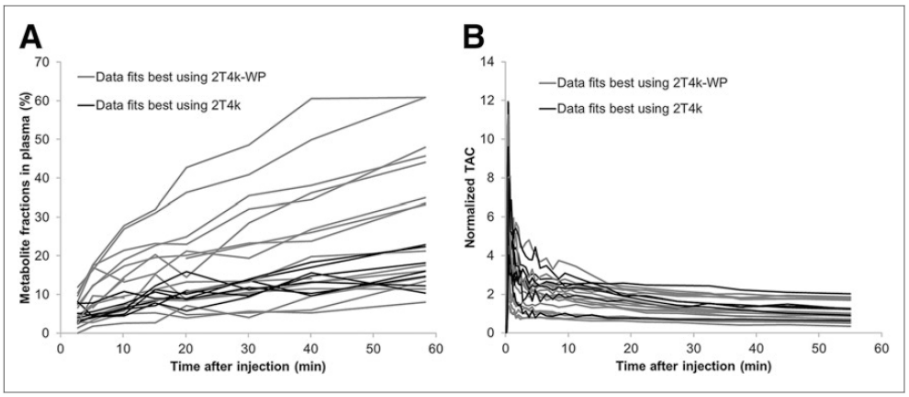

Fig 3. *Effect of metabolism on Akaike model preference measured metabolite fractions in plasma as function of time (A) and normalized tumor time–activity curves (TAC) (B). In both figures, curves are color-coded according to Akaike preferred model.*

Corresponding kinetic parameters from both models (2T4k and 2T4k-WP) correlated well, and V_T was found to be the most accurate measure for assessing ^{11}C-erlotinib uptake in tumors. For example, V_T values of 2T4k and 2T4k-WP models were highly correlated (R_2 = 0.94), giving only a small underestimation of 2T4k-WP values as compared with those obtained using 2T4k (1.7%). Furthermore, test–retest variability of all kinetic parameters (K1, V_T, BP_{ND}) and level of metabolism were not significantly different between groups. As for both models, variability averaged over the entire group was acceptable for V_T (12%) but high for BP_{ND} (53%) using both models. Therefore, BP_{ND} was not assessed any further. Both models demonstrated a significant group difference of the average V_T between the 2 clinical groups ($P < 0.016$, Fig. 4). In addition, both 2T4k and 2T4k-WP models showed expected relationships with ^{15}O-H_2O–derived blood flow (F) values—that is, good correlation between ^{11}C-erlotinib K1 and F (R^2 = 0.80 for both 2T4k and 2T4k- WP models) and no correlation between ^{11}C-erlotinib V_T and F (R^2 = 0.11 and 0.17 for 2T4k and 2T4k-WP models, respectively).

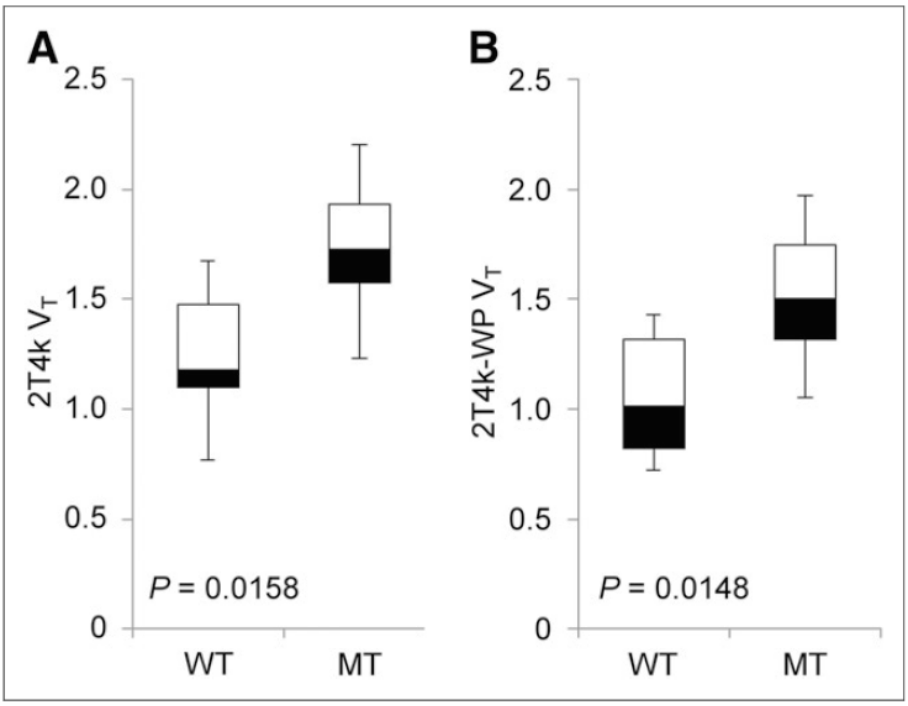

Fig 4. *Box plots showing group differences for 2T4k V_T (A) and 2T4k-WP V_T (B). MT = subjects with an activating EGFR mutation; WT = wild type/without EGFR mutation.*

Simplifications

Time–activity curves did not show an equilibration uptake within the duration of the scan (Fig. 5), as they were constantly declining until the end of the scan time. Therefore, use of SUV to quantify ^{11}C-erlotinib uptake is time dependent and thus suboptimal for imaging this reversible ligand. In contrast, TBR showed equilibration after 40 min, although somewhat better for TBR-WB than for TBR-PP (Fig. 5).

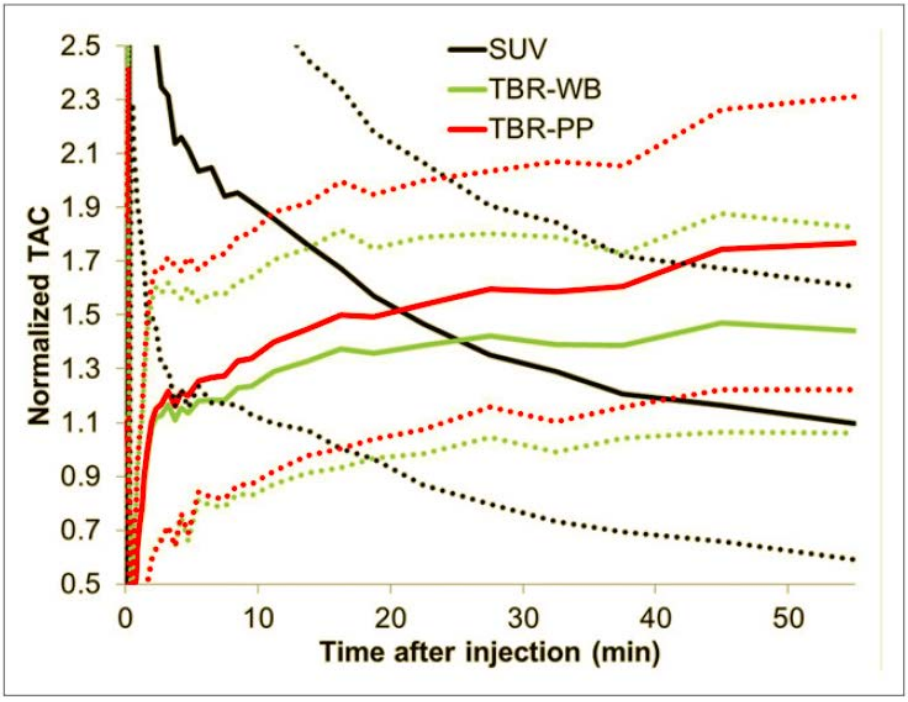

Fig 5. *Average time–activity curves (TAC) (solid lines) normalized to patient weight and injected dose (SUV) and to blood data with (TBR_PP) and without metabolite correction (TBR_WB). Dotted lines represent 1 SD from mean.*

In addition, TBR-WB showed a better correlation with 2T4k-WP–derived V_T than TBR-PP for both the intervals 40–50 (Fig. 6A) and 50–60 (Fig. 6B) min. The correlation with 2T4k-WP V_T, however, was interval dependent and for TBR-WB changed by 7% between the 2 intervals, with a larger change for TBR-PP (Fig. 6).

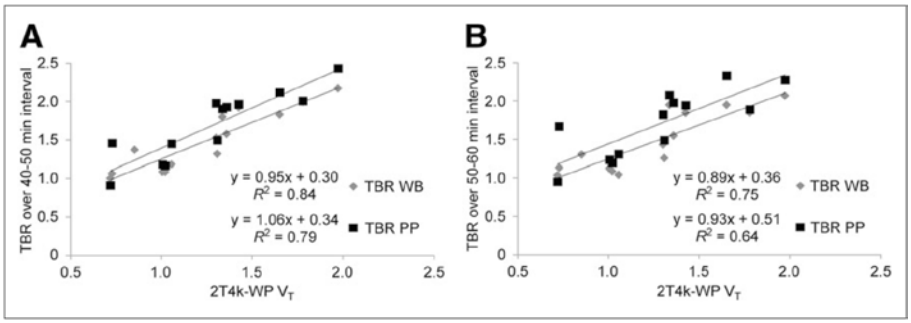

Fig 6. *Correlations of TBR-WB and TBR-PP with 2T4k-WP–derived V_T for intervals of 40–50 (A) and 50–60 min (B).*

TBR-WB seems to be a more stable parameter than TBR-PP, and further evaluations were therefore restricted to TBR-WB. TBR-WB showed no correlation with ^{15}O-H_2O–derived F (R^2 = 0.02). Test–retest analysis showed good variability for TBR-WB 40–50 min (8.2%) and acceptable variability for TBR-WB 50–60 min (13.7%). However, there was no significant difference between the 2 clinical groups for both intervals (40–50 min, P = 0.07, Fig. 7A; 50–60 min, P = 0.15, Fig. 7B).

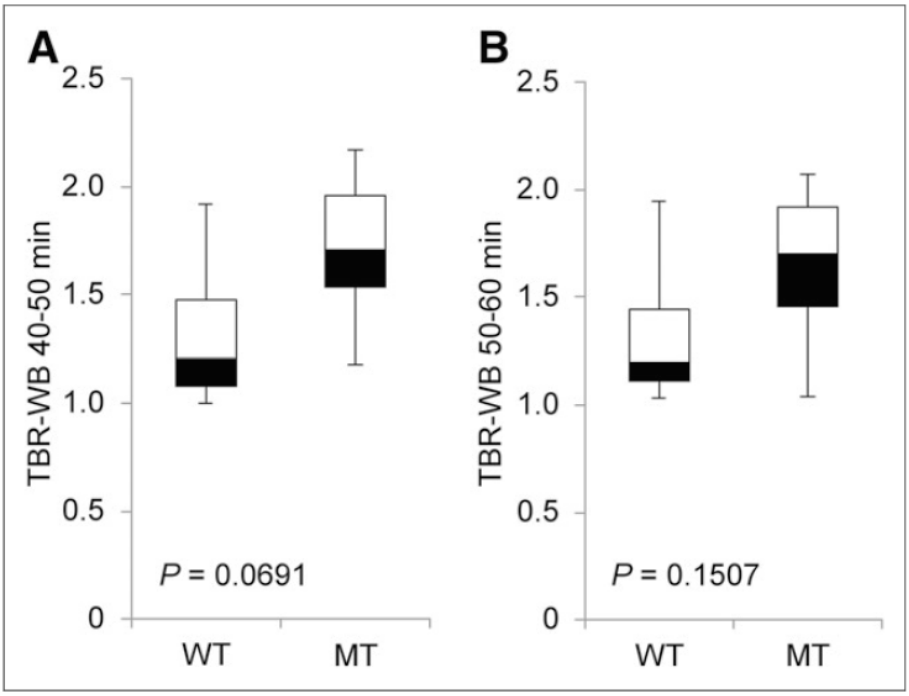

Fig 7. *Box plots showing group differences for TBR-WB (40–50 min) (A) and TBR-WB (50–60 min) (B). MT = subjects with an activating EGFR mutation; WT = wild type/without EGFR mutation.*

Discussion

In this study, various pharmacokinetic models for quantification of ^{11}C-erlotinib kinetics in NSCLC patients were evaluated, including several nonconventional models that account for uptake of labeled metabolites in tumor tissue. In addition, simplified methods were evaluated that would allow for whole-body scans without arterial sampling.

Optimal Kinetic Model

For all conventional models, metabolite-corrected plasma input functions are used, as they assume that there is no uptake of radiolabeled metabolites in tumor tissue. Metabolite correction requires accurate measurements of metabolite fractions in plasma.

In the present study, metabolite measurements were hampered by technical issues—that is, low counts within the sample measurement times. Therefore, it was not possible to measure the (very low) level of nonpolar metabolites, and consequently the metabolite correction was based only on measurement of polar metabolites. This approach can be justified by the fact that levels of nonpolar metabolites were low (<1%).

Among conventional models, the optimal model was the 2T4k model. This model showed, both visually (Fig. 2) and according to the Akaike information criterion, better fits than the 1T2k and 2T3k models. Furthermore, ^{11}C-erlotinib uptake (V_T) can be estimated reproducibly using the 2T4k model, with an acceptable test–retest variability of 12%. Finally, the 2T4k model provided V_T values that were significantly different between the 2 clinical groups ($P < 0.016$).

As mentioned above, conventional tracer kinetic models assume no uptake of metabolites in tumor tissue. Given the microvascular structure of tumors, it is important to also investigate alternative models that account for ^{11}C-labeled metabolites entering tumor tissue. Investigation of several of these nonconventional models showed that the metabolite input models (1T2k-x2 and 2T4k- 1T2k) showed a poorer performance than the 2T4k-WP model. In addition, the Akaike criterion indicated that the conventional 2T4k and nonconventional 2T4k-1T2k models performed equally well but poorer than the 2T4k-WP model. This suggests that either no metabolites enter the tumor or, more likely, the 1T2k-x2 and 2T4k-1T2k models do not provide reproducible results. This, in turn, could be due to the relatively slow uptake of metabolites, resulting in unreliable parameter estimates for the metabolite compartment. Therefore, it was decided to select the 2 most probable models (2T4k- WP and 2T4k) for further investigation.

When looking at the fitted kinetic parameters themselves, overall a slightly better performance was seen for the 2T4k-WP model than for the 2T4k model. Nevertheless, strong correlations were found between corresponding kinetic parameters from both models. Physiologically and clinically plausible outcome parameters were obtained for the 2T4k-WP model when test–retest variability, separation of the 2 clinical groups, and correlation with perfusion were considered. Interestingly, Akaike fit preference for 1 of the 2 models was not dependent on the shape of the tumor time–activity curves (Fig. 3B). However, preference for the conventional 2T4k model over the 2T4k-WP model was seen primarily in patients with a relatively low level of metabolism (Fig. 3A)—that is, in those cases in which the possible contribution of labeled metabolites to the signal would be small, thus favoring a model with less fit parameters. K1 from both models (2T4k and 2T4k-WP) was highly correlated with F, irrespective of the level of metabolism, because estimation of K1 primarily is based on fitting the initial part of the time–activity curve when the fraction of metabolites still is very low.

Future studies may be needed to improve metabolite measurements to accurately describe their true behavior. Findings from this study showed that quantification of dynamic ^{11}C-erlotinib data can be performed using the conventional 2T4k model, but in practice a simpler model not requiring metabolite correction at all (2T4k-WP) yields slightly better results and is, therefore, the preferred model.

Simplified Methods

Analysis of several simplified approaches showed that SUV curves normalized to patient weight and injected tracer dose did not reach equilibrium within the scan time, resulting in unstable outcomes (Fig. 5). Therefore, SUV cannot be used for reliable quantitative assessment of ^{11}C-erlotinib uptake up to 60 min after injection.

In contrast, TBR measures showed to be more useful for a simple semi-quantitative assessment of ^{11}C-erlotinib uptake, which could be used in combination with whole-body scans. TBR values, calculated over several time intervals after injection (40–60 min), were not correlated with perfusion (i.e., they were not flow dependent) and showed good correlation with 2T4k-WP V_T values (Fig. 6). Furthermore, performance was better for TBR-WB than for TBR-PP, which could be due to inaccuracies in estimation of metabolite fractions. However, TBR was less sensitive in distinguishing between the 2 clinical groups (i.e., EGFR-mutated vs. EGFR wild-type groups) compared with 2T4k-WP V_T. These groups showed significantly different V_T values ($P < 0.016$), but this was not the case for TBR-WB ($P < 0.15$). Contributing factors may be that TBR is a simplified measure and that the power of the present study is rather low (i.e., limited number of subjects).

Nevertheless, TBR-WB showed a trend toward a difference between patient groups, and, among the simplified measures, it provided the best correlation with 2T4k-WP–derived V_T. Although further studies are needed, at present, TBR-WB appears to be an attractive simplified method for analysis of (clinical) whole-body studies, which would be needed to assess potential interlesional heterogeneity in uptake of ^{11}C-erlotinib.

Conclusion

Analysis of dynamic ^{11}C-erlotinib studies can be performed using a reversible 2-tissue compartment model without metabolite correction (2T4k-WP), because it yields reproducible estimates of ^{11}C-erlotinib uptake (V_T) in tumors. A simplified method with potential is TBR-WB (40–60 min after injection). Results highly correlated with 2T4k-WP–derived V_T, and it would be suitable for assessing ^{11}C-erlotinib uptake in whole-body scans to asses multiple lesions at the same time.

References

1. Maemondo M, Inoue A, Kobayashi K, et al. Gefitinib or chemotherapy for non-small-cell lung cancer with mutated EGFR. N Engl J Med. 2010;362: 2380–2388.

2. Mitsudomi T, Morita S, Yatabe Y, et al. Gefitinib versus cisplatin plus docetaxel in patients with non-small-cell lung cancer harbouring mutations of the epidermal growth factor receptor (WJTOG3405): an open label, randomised phase 3 trial. Lancet Oncol. 2010;11:121–128.

3. Mok TS, Wu YL, Thongprasert S, et al. Gefitinib or carboplatin-paclitaxel in pulmonary adenocarcinoma. N Engl J Med. 2009;361:947–957.

4. Cobo M, Isla D, Massuti B, et al. Customizing cisplatin based on quantitative excision repair cross-complementing 1 mRNA expression: a phase III trial in non-small-cell lung cancer. J Clin Oncol. 2007;25:2747–2754.

5. Bahce I, Smit EF, Lubberink M, et al. Development of [^{11}C]erlotinib positron emission tomography for in vivo evaluation of EGF receptor mutational status. Clin Cancer Res. 2013;19:183–193.

6. Pao W, Chmielecki J. Rational, biologically based treatment of EGFR-mutant non-small-cell lung cancer. Nat Rev Cancer. 2010;10:760–774.

7. Wu JY, Wu SG, Yang CH, et al. Lung cancer with epidermal growth factor receptor exon 20 mutations is associated with poor gefitinib treatment response. Clin Cancer Res. 2008;14:4877–4882.

8. Matej S, Browne JA. Performance of a fast maximum likelihood algorithm for fully-3D PET reconstruction. In: Grangeat P, Amans J-L, eds. Three Dimensional Image Reconstruction in Radiology and Nuclear Medicine. Dordrecht, The Netherlands: Kluwer Academic Publishers; 1996:297–316.

9. Greuter HNJM, van Ophemert PLB, Luurtsema G, Franssen EJF, Boellaard R, Lammertsma AA. Validation of a multiwell gamma-counter for measuring highpressure liquid chromatography metabolite profiles. J Nucl Med Technol. 2004; 32:28–32.

10. Gunn RN, Gunn SR, Cunningham VJ. Positron emission tomography compartmental models. J Cereb Blood Flow Metab. 2001;21:635–652.

11. Hoekstra CJ, Stroobants SG. Hoekstra OS, Smit EF, Vansteenkiste JF, Lammertsma AA. Measurement of perfusion in stage IIIA-N2 non-small cell lung cancer using $H_2{}^{15}O$ and positron emission tomography. Clin Cancer Res. 2002; 8:2109–2115.

12. Akaike H. Fitting autoregressive models for prediction. Ann Inst Stat Math. 1969;21:243–247.

13. Smits AJ, Kummer JA, Hinrichs JW, et al. EGFR and KRAS mutations in lung carcinomas in the Dutch population: increased EGFR mutation frequency in malignant pleural effusion of lung adenocarcinoma. Cell Oncol (Dordr). 2012; 35:189–196.

Chapter 5

Effects of erlotinib therapy on [^{11}C]erlotinib uptake in EGFR mutated, advanced NSCLC

Idris Bahce

Maqsood Yaqub

Hanane Errami

Robert C. Schuit

Patrick Schober

Erik Thunnissen

Albert D. Windhorst

Adriaan A. Lammertsma

Egbert F. Smit

N. Harry Hendrikse

EJNMMI Res. 2016 Dec;6(1):10. doi: 10.1186/s13550-016-0169-8.

Abstract

INTRODUCTION: In non-small cell lung cancer (NSCLC) patients off erlotinib therapy, positron emission tomography (PET) using [^{11}C]erlotinib distinguished epidermal growth factor receptor (EGFR) mutations from wild type EGFR. However, tumor uptake of [^{11}C]erlotinib during erlotinib therapy is unknown. Therefore, the aims of this study were to evaluate tumor [^{11}C]erlotinib uptake in NSCLC patients both on and off erlotinib therapy, and to evaluate the effect of erlotinib therapy on tumor perfusion and its correlation to tumor [^{11}C]erlotinib uptake, and also, to investigate simplified uptake parameters using arterial and venous blood samples.

METHODS: Ten patients were to be scanned twice with a 1-2 weeks interval, i.e. on (E+) and off (E-) erlotinib therapy. Each procedure consisted of a Low Dose-CT scan, a 10-minutes dynamic [^{15}O]H_2O PET scan, and a 60-minutes dynamic [^{11}C]erlotinib PET scan with arterial and venous sampling at 6 time points. In patients(E+), the optimal compartment model was analyzed using Akaike's Information Criterion. In patients(E-), the uptake parameter was the volume of distribution (V_T), estimated by using metabolite-corrected plasma input curves based on image derived input functions and discrete arterial and venous blood samples. Tumor blood flow (TBF) was determined by K1 of [^{15}O]H_2O using the 1T2k model, and correlated with V_T and K1 values of [^{11}C]erlotinib. The investigated simplified parameters were SUV and tumor-to-blood ratio (TBR) at 40-60 min pi interval.

RESULTS: Of the 13 patients included, 10 were scanned twice. In patients(E+), [^{11}C]erlotinib best fitted the 2T4k model with V_T. In all patients, tumor V_T(E+) was lower than V_T(E-) (median V_T(E-) = 1.61, range 0.77-3.01; median V_T(E+) = 1.17, range 0.53-1.74; P = 0.004). Using [^{15}O]H_2O, 5 patients were scanned twice. TBF did not change with erlotinib therapy, TBF showed a positive trend towards correlation with [^{11}C]erlotinib K1, but not with V_T. TBR_{40-50} and TBR_{50-60}, using both arterial and venous sampling, correlated with V_T(E-)(all $r_s > 0.9$, $P < 0.001$), while SUV did not. In patients off and on therapy, venous TBR underestimated arterial TBR by 26%±12% and 9%±9%, respectively.

CONCLUSION: In patients on erlotinib in therapeutic dose, tumor V_T decreases with high variability, independent of tumor perfusion. For simplification of [^{11}C]erlotinib PET scanning protocols, both arterial and venous TBR 40-60 min post injection can be used, however, arterial and venous TBR values should not be interchanged as venous values underestimate arterial values.

Background

Non-small cell lung cancer (NSCLC) therapy has entered an era of precision medicine with an ever-increasing amount of therapeutic agents directed against specific tumor targets. Positron emission tomography (PET) is sometimes used to study the pharmacokinetic behavior of these new agents, and to identify patients that might be sensitive to these drugs [1]. For this, the molecularly targeting therapeutic agents are labeled with radionuclides to be used as PET tracers [2].

An important actionable target in NSCLC is the epidermal growth factor receptor (EGFR). EGFR tyrosine kinase inhibitors (TKI), such as erlotinib, inhibit growth in tumors that thrive mainly on the EGFR pathway, such as tumors with an activating EGFR mutation (EGFRmut) [3, 4]. PET using carbon-11 labeled erlotinib, [^{11}C]erlotinib, allowed to visualize and quantify tumor [^{11}C]erlotinib uptake in patients with EGFR mutated NSCLC [1, 5, 6]. Moreover, tumor [^{11}C]erlotinib uptake was shown to be higher in TKI-sensitive EGFRmut tumors as compared to tumors with a wild type EGFR, indicating that PET and [^{11}C]erlotinib may identify patients that are sensitive to erlotinib therapy [1].

Typically, EGFR TKI achieve a median progression-free survival of approximately 9-10 months in the first line setting [7]. Ultimately, all EGFRmut patients develop resistance to EGFR TKI during the course of treatment. Various patterns of disease progression may be observed. In many patients only a few tumor lesions will grow, while others remain unchanged. In such oligo-progressive cases, it is unclear whether EGFR TKI therapy should be discontinued [8]. Decision management could be guided by knowledge of the residual EGFR TKI sensitivity of the tumor lesions.

PET using [^{11}C]erlotinib may provide a means to determine residual TKI uptake after disease progression appears, and consequently may aid in deciding whether or not to discontinue EGFR TKI therapy. To answer this question, PET should preferably be performed during erlotinib treatment. However, thus far, [^{11}C]erlotinib PET scans were performed exclusively in the absence of erlotinib exposure [1, 5, 6]. To be able to interpret [^{11}C]erlotinib PET data of patients in this clinical setting, the effects caused by the presence of therapeutic concentrations of nonlabeled erlotinib on tumor [^{11}C]erlotinib uptake need to be investigated first. From a tracer pharmacokinetic perspective, studying the effects of erlotinib therapy on [^{11}C]erlotinib metabolism, plasma concentration, and tumor uptake can improve our understanding of the tracer uptake. These pharmacokinetic insights are needed for optimization of scanning protocols and design of future TKI PET studies. At present, the literature concerning this topic is limited, and to the best of our

knowledge no other clinical trial scanned patients with a radiolabeled EGFR TKI during treatment with the same EGFR TKI.

We performed a pilot study to assess the effect of pharmacological erlotinib concentrations on tumor [^{11}C]erlotinib uptake. The primary objective was to compare tumor tracer uptake using the gold standard measure for [^{11}C]erlotinib uptake V_T, i.e. volume of distribution, in the presence and absence of pharmacological concentrations of erlotinib. The secondary aim of this study was to assess the effects of erlotinib therapy on tumor blood flow and its correlation with tumor [^{11}C]erlotinib uptake. In addition, for simplification of future protocols, we also investigated simplified uptake parameters, i.e. standardized uptake values (SUV) and tumor-to-blood ratio (TBR). TBR was based on arterial samples, however, we also used venous samples. This was again important for simplification of future protocols, as arterial cannulation could be omitted if venous sampling was proven to be a valid substitute.

Methods

Patients

Patients with histologically proven EGFRmut NSCLC who were either planned to initiate erlotinib therapy or to stop erlotinib therapy due to disease progression while on erlotinib were asked to participate. Key inclusion criteria were: age above 18 years, life expectancy of at least 12 weeks, at least 1 tumor lesion with a diameter of at least 1.5 cm in the chest region as measured by CT, Karnofsky index >60%, and a written informed consent. Exclusion criteria were claustrophobia, pregnancy or lactating patients, metal implants in the thorax (e.g. pacemakers) that could interfere with PET/CT imaging, and concurrent treatment with experimental drugs. The study was approved by the Medical Ethics Review Committee of the VU University Medical Center. All patients provided written informed consent prior to inclusion.

Study design

The aim was to include 10 patients with EGFRmut NSCLC, who underwent 2 PET scan sessions. Patients who were on erlotinib therapy (E+) stopped therapy on the day of their first scan. Patients who were erlotinib naïve (E-) started therapy, immediately following the scanning procedure on day 1. For all patients, a second PET scan session was performed after 7 to 14 days. All PET scans were planned to start at the same time of the day, i.e. at 1.00 pm. Patients on erlotinib therapy were asked to take their last medication, i.e. erlotinib 150 mg, at 8.00 am.

PET/CT scanning procedure

One cannula was inserted into the radial artery for arterial blood sampling, and another one into a contralateral arm vein for tracer injection and venous blood sampling. Scans were performed on a Gemini TF-64 PET/CT scanner (Philips Medical Systems, Best, the Netherlands), which is a high performance, time-of-flight (TOF), fully 3-dimensional PET scanner combined with a 64-slice Brilliance CT scanner [9]. First, 370 MBq [^{15}O]H_2O was injected intravenously, simultaneously starting a 10 min emission scan. Next, a low dose CT scan (30 mAs, without contrast) was performed for attenuation correction. Subsequently, 349 ± 46 MBq of [^{11}C]erlotinib (synthesized as previously described and corresponding to a non-pharmacological dose of approximately 16.2 µg "cold" erlotinib with ≥ 18.5 GBq/micromol specific activity) was injected intravenously, simultaneously starting a 60 min emission scan [1]. [^{15}O]H_2O and [^{11}C]erlotinib emission scans were acquired in list-mode and reconstructed into 26 frames with progressive increase in frame duration (1x10, 8x5, 4x10, 2x15, 3x20, 2x30 and 6x60 s) and 36 frames (1x10, 8x5, 4x10, 2x15, 3x20, 2x30, 6x60, 4x150, 4x300 and 2x600 s), respectively. All appropriate corrections were applied for dead time, decay, randoms, scatter and attenuation. Reconstruction of PET data was performed using the 3D Row-Action Maximum-Likelihood Algorithm (RAMLA) with CT based attenuation correction. The final voxel size was 4x4x4 mm^3 and the spatial resolution 5-7 mm full width at half maximum. No corrections for patient motion were applied.

Arterial and venous samples (7 mL) were taken at 6 time points (i.e. at 5, 10, 20, 30, 40 and 60 minutes) after injection of [^{11}C]erlotinib. For both arterial and venous samples, plasma polar [^{11}C]erlotinib metabolites, and whole blood and plasma radioactivity concentrations were measured, as described previously [1].

Data analysis

For each patient, the primary tumor was identified on the low dose CT scan, and the tumor contours were delineated visually at the margins of the tumor on all planes where the primary tumor was visible, to generate a 3-dimensional tumor volume of interest (VOI). Large blood vessels and liver were avoided as much as possible. We did not delineate tumors on PET, as [^{11}C]erlotinib PET uptake depends strongly on tumor characteristics (e.g. EGFR mutation). CT-based contour delineation was performed using an in-house software, developed within the IDL (Interactive Data Language Virtual Machine 6.2, RSI Inc., Boulder, CO, USA) environment. Then, tumor VOIs were projected onto the dynamic [^{11}C]erlotinib PET scan to generate tumor [^{11}C]erlotinib time-activity curves (TACs). In addition, metabolite-corrected image-derived plasma input functions (IDIFs) were derived from VOIs drawn on 10 subsequent slices within the descending aorta

(approximately 7 mL). Then, this arterial whole blood TAC was calibrated by the whole-blood activity concentrations measured from the 6 manually drawn arterial blood samples. Next, the data was multiplied by the multi-exponential function that best fitted the plasma-to-whole blood ratios, again derived from the manual samples, to generate a plasma TAC. Then, the plasma TAC was corrected for metabolites using a sigmoid function derived from the best fit to the measured parent fractions of the arterial samples. Finally, a correction for delay was applied; this metabolite-corrected plasma TAC was used as IDIF [10–12].

A distinction was made in processing the kinetic data from patients on and off therapy. Previously, in patients off therapy the optimal model for tumor [^{11}C]erlotinib pharmacokinetics was found to be the reversible two-tissue model (2T4k) [1]. In patients off therapy, all tumor TACs were analyzed using this model. It was unknown, however, whether the same model was also valid for patients on erlotinib therapy. Therefore, in the latter patients, first the optimal model was identified by fitting tumor [^{11}C]erlotinib TACs to 3 conventional compartment models (i.e., single tissue, irreversible two-tissue, and reversible two-tissue) [10]. Subsequently, the optimal model was chosen on the basis of the Akaike Information Criterion [13]. After establishing the optimal model for patients on erlotinib therapy, all tumor TACs were analyzed using the corresponding preferred model. Pharmacokinetic analysis and modeling of tumor TACs and IDIF was performed using in-house software, developed within MATLAB (MathWorks, Inc).

In order to understand the effects of metabolism on V_T values under erlotinib therapy, the change in tumor V_T was correlated with the level of metabolism. As level of metabolism the parent fraction measured at 60 min post injection was used.

For [^{15}O]H_2O, same VOIs were drawn on the CT scans accompanying the [^{15}O]H_2O PET scans, and then projected onto the [^{15}O]H_2O data. All tumor TACs were analyzed with the standard single tissue compartment model (1T2k) for [^{15}O]H_2O [14], resulting in estimates of tumor blood flow (TBF) as calculated by K1 of [^{15}O]H_2O [15].

Simplified analyses

Accuracies of several simplified static approaches were evaluated. SUV, normalized for patient weight and injected dose, were evaluated in the interval 40-50 min and 50-60 min. In addition, TBR values were evaluated using both arterial and venous whole blood activity concentrations in the time interval 40-50 min and 50-60 min. These intervals were chosen, as unpublished analysis of previous scans showed

that TBR using whole blood activity between 40 and 60 min correlated best with V_T [1].

Statistical analysis

Statistical analysis was performed using SPSS software (SPSS for Windows 20.0, SPSS, Inc., Chicago, USA) and GraphPad (GraphPad Prism version 5.00 for Windows, GraphPad Software, San Diego, CA, USA). Spearman's correlation coefficient (r_s) and simple linear regression were used for correlations. A 2-tailed probability value of $P < 0.05$ was considered to be significant. Bland-Altman analysis was performed to assess agreement between venous TBR and arterial TBR, between TBR_{40-50} and TBR_{50-60}, and between venous and arterial tracer parent fractions. The Wilcoxon matched-pairs signed-rank test was used to test differences between scans with and without erlotinib therapy regarding V_T values, parent fraction values, whole blood SUV, and TBF values. This test was also used to assess differences between whole blood SUV obtained with arterial and venous samples.

Results

Patient characteristics

Patient characteristics are shown in Table 1. As 3 patients could only be scanned once, a total of 13 patients were recruited in order to obtain 10 patients who were scanned twice using [^{11}C]erlotinib. In 9 out of these 10 patients, both quantitative kinetic analyses could be obtained. In the remaining patient, this was not possible due to technical problems with blood sampling. In 7 out of 9 evaluable patients, the first [11C]erlotinib PET scan was without erlotinib therapy. In the remaining 2 out of 9 patients, the first scan was performed while receiving erlotinib therapy. In only 5 out of 9 evaluable patients, both [^{15}O]H_2O TBF(E-) and TBF(E+) could be derived. In the remaining patients, data from both [^{15}O]H_2O PET scans could not be performed or analyzed due to technical problems, as indicated in Table 1.

Table 1. Patient characteristics

Nr	Gender Age (yrs)	EGFR mutation (TKI sensitivit	Response to erlotinib* Change	[^{11}C]erlotinib PET scans Time interval to	Condition	Arterial sampling	Venous sampling	[^{15}O]H_2O PET scans	Remarks

		y)	in V_T #	second scan (days)					
1	F 60	exon19 (p.delE746-A750) and exon20 (T790M) (sensitive + resistant)	PD -	1st scan	E+	Yes	Yes	Yes	
				2nd scan 7	E-	NA	NA	NA	Synthesis of [^{11}C]erlotinib failed quality check
2	F 82	exon19 (p.delE746-A750) (sensitive)	CR -52%	1st scan	E-	Yes	Yes	Yes	
				2nd scan 14	E+	Yes	NA	Yes	No venous sampling due to clogging of the venous cannula
3	M 74	exon18 (p.G719S and p.E709A) (sensitive [24, 25])	PR -17%	1st scan	E-	Yes	Yes	Yes	
				2nd scan 13	E+	Yes	Yes	NA	Synthesis of [^{15}O]H_2O failed quality check
4	M 66	exon21 (p.P848L) (resistant	- -43%	1st scan	E-	Yes	Yes	Yes	
				2nd scan	E+	Yes	Yes	Yes	

		[26])		7					
5	F 61	exon19 (p.delE746-T751) (sensitive)	PD -	1st scan	E+	Yes	Yes	NA	Synthesis of [^{15}O]H_2O failed quality check
				2nd scan 7	NA	NA	NA	NA	Yield of [^{11}C]erlotinib synthesis too low
6	F 45	exon19 (p.delE746-A750) and exon20 (p.T790M) (sensitive + resistant)	Slow PD -47%	1st scan	E+	Yes	Yes	Yes	
				2nd scan 10	E-	Yes	Yes	Yes	
7	M 74	exon19 (p.E746-S752) and exon20 (p.T790M) (sensitive + resistant)	SD -	1st scan	E-	NA	NA	NA	Aberrant arterial and venous blood sample values Aberrant [^{15}O]H_2O PET data

				2nd scan 7	E+	Yes	Yes	Yes	
8	M 81	exon18 (p.G719S) and exon20 (p.S768I) (unclear [27–29])	SD -58%	1st scan	E-	Yes	Yes	Yes	
				2nd scan 7	E+	Yes	Yes	Yes	
9	F 55	exon19 (p.delE746-A750) (sensitive)	PR -29%	1st scan	E-	Yes	Yes	Yes	Aberrant $[^{15}O]H_2O$ PET data
				2nd scan 10	E+	Yes	Yes	Yes	
10	F 71	exon19 (p.delL747-S752 and p.P753Q) and exon20 (p.T790M) (sensitive + resistant)	Slow PD -25%	1st scan	E+	Yes	Yes	NA	No $[^{15}O]H_2O$ synthesis
				2nd scan 14	E-	Yes	Yes	NA	No $[^{15}O]H_2O$ synthesis
11	F 77	exon21 (p.L861Q) (sensitive [30])	SD -39%	1st scan	E-	Yes	Yes	Yes	
				2nd scan 7	E+	Yes	Yes	NA	No $[^{15}O]H_2O$ synthesis

12	M 70	exon19 (p.delE746 S752) (sensitive)	PR -	1st scan	E-	Yes	Yes	Yes	
				2nd scan 7	NA	NA	NA	NA	Yield of [11C]erlotinib synthesis too low
13	F 74	exon21 (p.L858R) and exon20 (p.T790M) (sensitive + resistant)	Slow PD -40%	1st scan	E-	Yes	Yes	Yes	
				2nd scan 7	E+	Yes	Yes	Yes	

***Abbreviations**: F = female, M = male, (E+) = with erlotinib therapy, (E-) = without erlotinib therapy, CR = complete response, PR = partial response, SD = stable disease, PD = progressive disease, NA = not available.*

**Tumor response to erlotinib as evaluated at the time of first scan (in patients stopping erlotinib), or tumor response to erlotinib after its initiation (in patients starting erlotinib therapy).*
#Change in VT as defined by (V_T(E+) - V_T(E-)) / V_T(E-)).

Effects of erlotinib therapy on plasma kinetics

Parent fractions of [11C]erlotinib, as measured in arterial plasma samples, were higher in patients on therapy at all time points (all $P < 0.05$, see Figure 1A). Change in tracer metabolism during erlotinib therapy did not correlate with changes in V_T ($r_s = 0.33$, $P = 0.385$), as shown in Figure 1B.

Arterial blood activity, normalized to injected dose and patient weight, was also higher in patients on therapy at all time points (all $P < 0.05$, Figure 1C). Detailed results are shown in Supplementary Table 1 and 2.

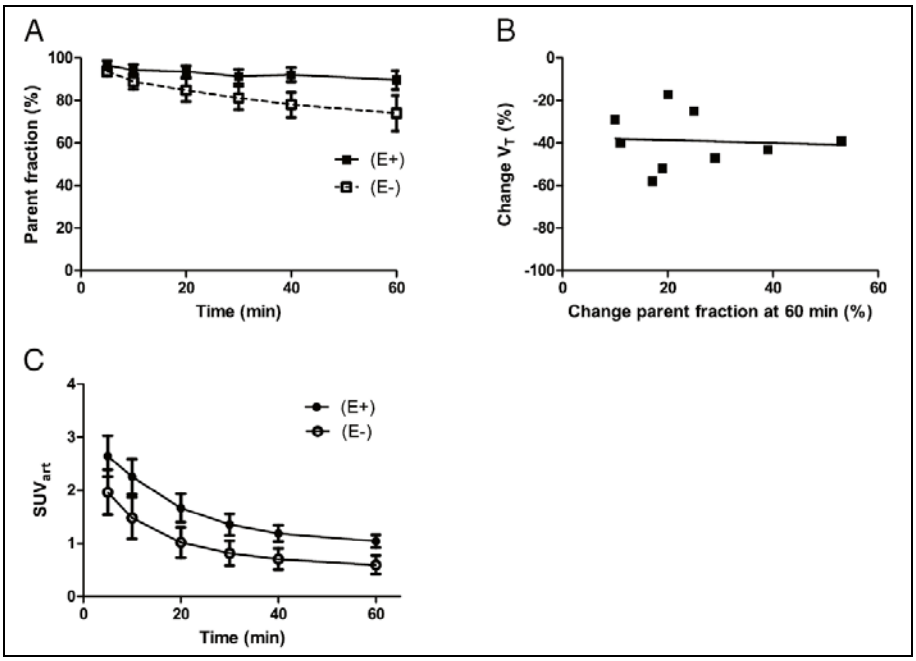

Fig. 1 *Effect of erlotinib therapy on parent fractions. Comparison of mean (±SD) arterial parent fractions of [^{11}C]erlotinib with and without erlotinib therapy (a). Correlation of VT change and arterial parent fractions change at 60 min post injection (b). Arterial blood SUV, i.e., activity normalized to injected dose and patient weight, in patients off and on therapy (c).*

***Abbreviations**: VT volume of distribution, SUV standardized uptake value, E− without erlotinib therapy, E+ with erlotinib therapy*

Effects of erlotinib therapy on kinetic modeling and tumor [^{11}C]erlotinib uptake

According to the Akaike Information Criterion, the reversible two-tissue compartment model (2T4k) was the preferred model in all patients(E+). This was also the case for patients(E-), confirming previous findings [1, 5, 6]. In all 9 evaluable patients, tumor [^{11}C]erlotinib V_T(E+) was significantly lower than V_T(E-) with a mean (±SD) intrapatient decrease of 38%±13% (median V_T(E-) = 1.61, range 0.77-3.01; median V_T(E+) = 1.17, range 0.53-1.74; P = 0.004; see Figure 2A). There was a good correlation between V_T(E+) and V_T(E-) (r_s = 0.82; P = 0.011), as shown in Figure 2B. See Supplementary Table 3 for detailed results.

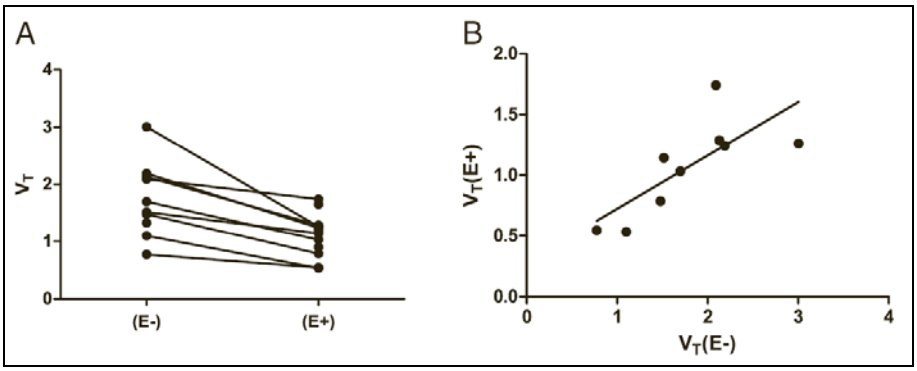

Fig. 2 *Tumor VT values. VT values of all patients without and with erlotinib therapy (a). Correlation between VT with and VT without erlotinib therapy (b).*

***Abbreviations**: VT volume of distribution, E− without erlotinib therapy, E+ with erlotinib therapy*

Effects of erlotinib therapy on tumor [^{15}O]H_2O perfusion

Tumor [^{15}O]H_2O perfusion did not change between patients on (N = 8) and off (N = 8) erlotinib therapy (with a mean±SD TBF of 0.475±0.194 mL/cm^3/min and 0.622±0.397 mL/cm^3/min, P =0.813, respectively, see Figure 3A). There was no correlation between TBF and [^{11}C]erlotinib V_T in patients(E-) and patients(E+) (r_s = -0.452, P = 0.268 and r_s = -0.167, P = 0.703, respectively, see Figure 3B). Tumor rate constant of [^{11}C]erlotinib influx, i.e. K1, showed a trend towards positive correlation with TBF(E-) and TBF(E+), however, this was not statistically significant (r_s = 0.714, P = 0.058 and r_s = 0.405, P = 0.327, respectively, see Figure 3C) (see Suppl Table 4 for detailed results).

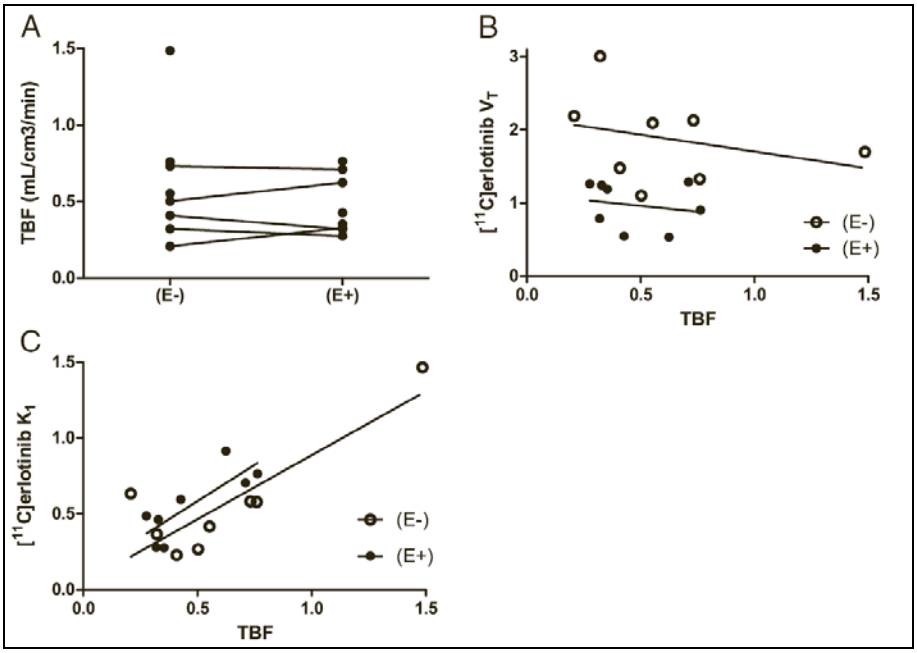

Fig. 3 *Tumor blood flow. TBF values of patients without (N = 8) and with (N = 8) erlotinib therapy (a). Correlation of tumor perfusion (TBF) with VT (b) and [11C]erlotinib K1 (c).*

Abbreviations*: TBF tumor blood flow, VT volume of distribution, E− without erlotinib therapy, E+ with erlotinib therapy, K1 influx rate constant*

Effects of erlotinib therapy on simplified uptake parameters

SUV did not correlate with V_T values, both on and off erlotinib therapy (r_s = 0.39, P = 0.260 and r_s = 0.30, P = 0.342, respectively). However, TBR_{40-50} values showed good correlation with V_T values, both on and off therapy (r_s = 0.97, P < 0.001 and r_s = 0.96, P < 0.001, respectively), as shown in Figure 4. TBR_{50-60} also showed good correlation (with r_s = 0.92, P < 0.001 and r_s = 0.99, P < 0.001, respectively). The mean (±SD) difference between TBR_{40-50} and TBR_{50-60} in patients off therapy was 4%±7%, and 1%±7% in patients on therapy.

Representative parametric [^{11}C]erlotinib images, using TBR_{50-60}, of a typical patient off and on erlotinib therapy are shown in Figure 5.

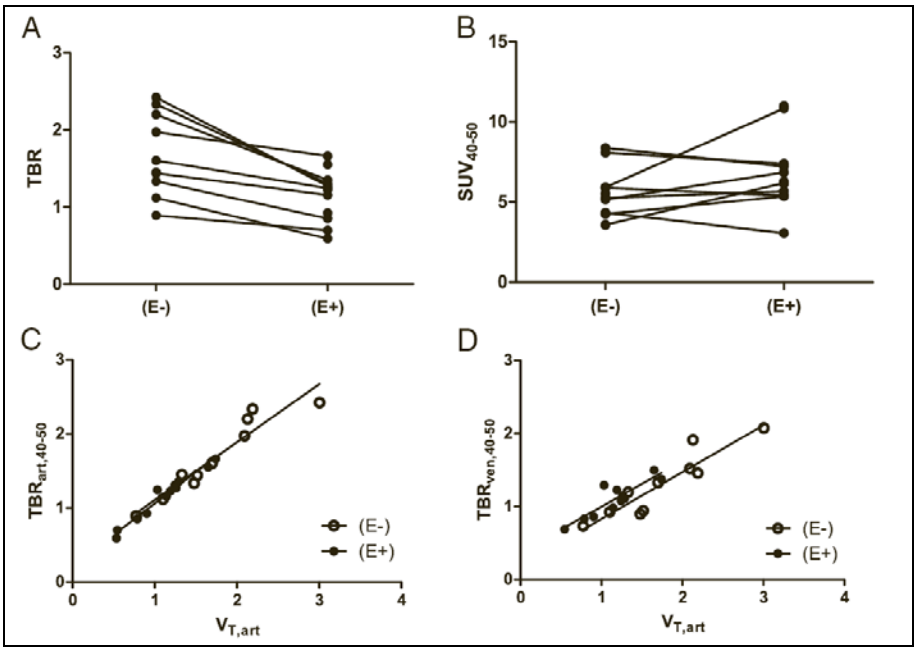

Fig. 4 *Simplified uptake parameters. TBR values from the 40–50-min post injection interval, using arterial samples (a) and SUVs from the 40–50-min post injection interval (b) in all patients off and on erlotinib therapy. Correlation between TBR values from the 40–50-min post injection interval, using arterial (c) and venous (d) samples, with V_T in all patients off and on erlotinib therapy.*

Abbreviations*: TBR tumor-to-blood ratio, SUV standardized uptake value, V_T volume of distribution, E− without erlotinib therapy, E+ with erlotinib therapy*

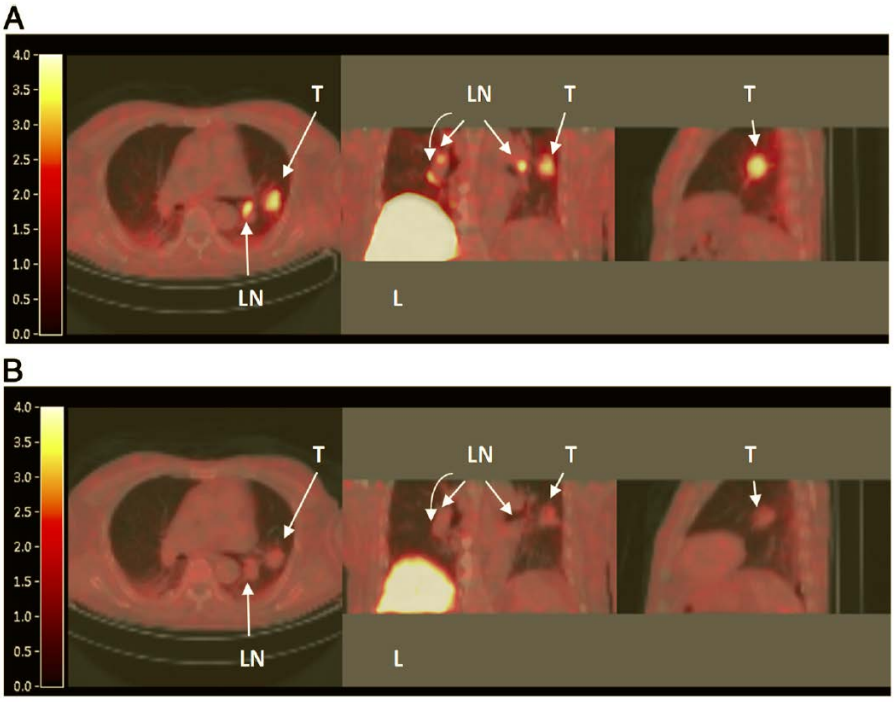

Fig. 5 *[^{11}C]Erlotinib PET images. PET images of a typical patient (Nr 8), who was scanned first off erlotinib therapy (a); he then started therapy and was scanned again after 7 days (b). Axial, coronal, and sagittal views are shown, obtained by CT-fused parametrically reconstructed [^{11}C]erlotinib $TBR_{art,50–60}$ PET images. The color scale indicates the $TBR_{art,50–60}$ value per pixel (unitless). The primary tumor lesion (T) and regional lymph nodes (LN) are clearly visible in the absence of erlotinib therapy. Also, high uptake is seen in the liver (L)*

Arterial versus venous whole blood activity

The mean venous blood activity values, normalized to injected dose and patient weight, were higher than the mean arterial values for all measured time points in patients(E-) ($P < 0.05$). In patients(E+) at 5 minutes post injection the venous values were significantly higher than arterial values, at the remaining time points no difference was observed. Figure 6A-6B illustrates the mean±SD whole blood SUV obtained from venous and arterial samples, in patients off and on erlotinib therapy.

Arterial versus venous metabolites

Metabolites analyses showed a good correlation between arterial and venous samples ($r_s = 0.91$, $P < 0.001$ and $r_s = 0.76$, $P < 0.001$) in patients(E-) and

patients(E+), respectively. There was a good agreement between arterial and venous parent fractions, both off and on erlotinib therapy (with an average (±SD) bias of -4.8%±4.6% and -0.7%±3.5%, respectively, see Figure 6C-6D).

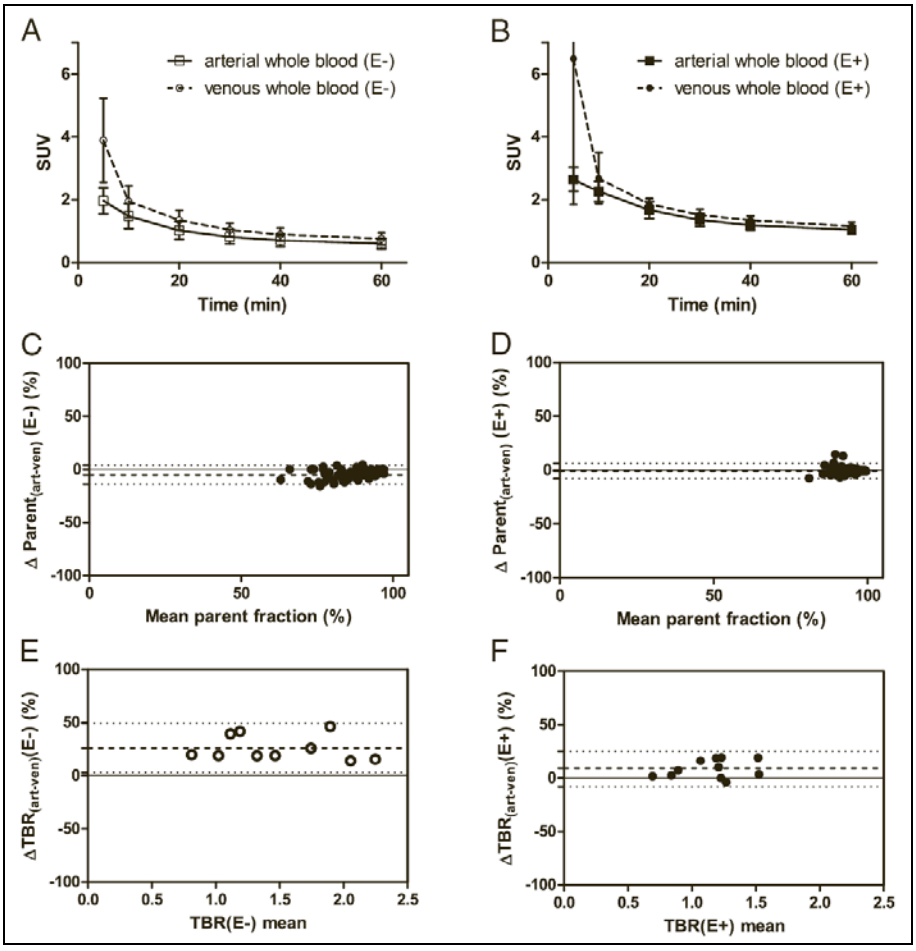

Fig. 6 *Arterial and venous sampling. Whole blood SUVs (mean ± SD) obtained from venous and arterial samples, in patients off (a) and on (b) erlotinib therapy. Bland-Altman plots demonstrating the arterial-venous parent fraction difference (%) per mean parent fraction value in patients off (c) and on (d) erlotinib therapy. In patients(E−) and patients(E+), a bias of −4.8 ± 4.6 and −0.7 ± 3.5 % was seen, respectively. Dotted lines indicate the mean bias and the 95 % limits of agreement. Next, Bland-Altman plots demonstrating the arterial-venous* $TBR_{40–50}$ *difference (%) per mean* V_T *value, in ten patients(E−) (e) and 11 patients(E+) (f) that had evaluable arterial and venous TBR values. The horizontal line indicates zero difference*

between arterial and venous $TBR_{40–50}$ measures, values above the zero difference line indicate lower venous $TBR_{40–50}$ values (i.e., an underestimation). In patients(E−) and patients(E+), a bias (i.e., average of the differences) of 26 ± 12 and 9 ± 9 % was seen, respectively. Dotted lines indicate the mean bias and the 95 % limits of agreement.

***Abbreviations**: TBR tumor-to-blood ratio, SUV standardized uptake value, E− without erlotinib therapy, E+ with erlotinib therapy*

Arterial versus venous TBR

Only 8 out of 9 evaluable patients had arterial and venous sampling in both conditions, i.e. with and without erlotinib therapy. TBR_{40-50} values obtained using arterial and venous blood samples showed good correlation with each other, both off (r_s = 0.95, P < 0.001) and on (r_s = 0.83, P = 0.002) erlotinib therapy. Similar results were obtained with TBR_{50-60} (with r_s(E-) = 0.89, P < 0.001 and r_s(E+) = 0.93, P < 0.001).

Venous sampling underestimated TBR_{40-50} as compared to arterial sampling in patients(E-) and patients(E+) by an average (±SD) of 26%±12% and 9%±9%, respectively (see Figure 6E-6F). However, venous TBR did have a good correlation with arterial V_T (r_s(E-) = 0.90, P < 0.001 and r_s(E+) = 0.79, P = 0.006), as shown in Figure 4D (see Suppl Table 5 for individual results).

Discussion

Effects of erlotinib therapy on tumor tracer uptake

The present study demonstrated that tumor [^{11}C]erlotinib V_T decreases significantly during erlotinib therapy.

To our best knowledge this is the first clinical study that investigated the change of radiolabeled EGFR TKI uptake in patients off and on treatment using the same EGFR TKI. In the presence of therapeutic concentrations of erlotinib, tumor [^{11}C]erlotinib uptake decreased. This was presumably caused by occupancy of EGF receptors by abundantly present non-labeled erlotinib, i.e. due to a decrease in available binding sites. Blocking studies in xenograft models provide support for this mechanism. Using [^{11}C]erlotinib, Petrulli et al. showed that NSCLC xenografts with activating EGFRmut (HCC827) in mice had lower tracer uptake when cold erlotinib was given along with the tracer [16]. In addition, Abourbeh et al. showed in mice bearing HCC827 xenografts more than 50% reduction in tumor [^{11}C]erlotinib uptake after

administration of excess non-labeled erlotinib [17]. Similar results were obtained with other radiolabeled TKI, such as [^{18}F]afatinib [18] and [^{11}C]PD153035 [19]. The fact that there was consistent decrease in [^{11}C]erlotinib uptake in the present study supports the notion that uptake of [^{11}C]erlotinib is, at least in part, due to specific binding. Furthermore, in the presence of therapeutic concentrations of erlotinib, obtained by taking a fixed oral dose of 150 mg erlotinib daily, there was still residual tumor tracer uptake. Interestingly, from a pharmacokinetic perspective, this may indicate that there may be room for increasing the therapeutic concentration of erlotinib, as at maximal concentration the specific binding would be absent.

Erlotinib therapy is known to induce metabolizing enzymes, such as CYP1A, CYP3A4 and CYP3A5 [20]. Also, *in vitro* data suggest that erlotinib stimulates the metabolism of midazolam in human microsomes, suggesting that erlotinib could induce its own metabolism and thus also increase the clearance of [^{11}C]erlotinib [21]. However, this was not observed in the present study. On the contrary, parent fractions at 60 minutes post injection were significantly higher during erlotinib therapy. Possibly, the presence of abundant non-labeled erlotinib also saturated the metabolizing enzymes, thereby slowing down metabolism of [^{11}C]erlotinib. Moreover, patients on therapy had higher blood activity concentrations, normalized to injected dose and patient weight. This may also be caused by higher concentrations of circulating parent tracer due to the blocking of receptors and enzymes by high concentrations of nonlabeled erlotinib.

Among the 9 evaluable patients, 2 were scanned first under erlotinib therapy and stopped therapy immediately thereafter. In these 2 patients, the abovementioned findings were also true, i.e. V_T(E+) was lower than V_T(E-) and metabolites(E+) were lower than metabolites(E-). This supports the notion that the presence of nonlabeled erlotinib determined these pharmacokinetic changes by the abovementioned mechanism.

High tumor sensitivity to erlotinib could potentially cause a large decrease in V_T. Namely, in the absence of cold erlotinib, EGFR TKI sensitive tumors are expected to have high [^{11}C]erlotinib V_T values as compared to resistant tumors [1]. Once cold erlotinib is added, EGF receptors become blocked causing V_T to drop. The results of this study confirmed that the patients with the largest decrease in V_T did have responsive tumors, however, there was no clear association between decrease in V_T and tumor response. To illustrate, 3 patients (patients 8, 2 and 6) had a large (i.e. approximately 50%) decrease in V_T. Patient 8 was treated with erlotinib therapy for a few weeks only. Erlotinib was stopped, as he refused to continue

therapy due to a pneumonia that he ascribed to erlotinib. He did have some tumor regression with erlotinib during these few weeks, however, not enough to be declared a partial response. Patient 2 had a complete response to erlotinib therapy after 3 months. Patient 6 had a slow disease progression prior to erlotinib scanning, she stopped erlotinib therapy after her first scan, but developed a severe flare of her disease within 1 week. Her second scan showed increased tumor volume and increased V_T, this illustrates that her tumor still had significant amount of sensitive clones. These cases demonstrate that high decrease in V_T can occur in sensitive tumors, however, there was no clear association, that is, responders did not exclusively show high decrease, as there were 2 other cases with partial tumor response to erlotinib therapy who showed moderate decrease in V_T of 29% and 17%. On the other hand, as a result of erlotinib therapy, changes can occur in the size of the tumor, its concentration of vital tumor cells and possibly its EGFR density. These changes can occur in a period as short as 7 to 14 days after initiation or discontinuation of therapy, and may also influence V_T. Therefore, any tumor response to erlotinib therapy may also influence the decrease of V_T during therapy. However, the limited number of patients scanned does not allow for extensive elaboration. Future studies including more patients should investigate the correlation between response and change in uptake.

The decrease in V_T varied between 17% and 58%. This high level of variability disqualifies V_T(E+) as substitute for V_T(E-). Any quantitative comparison between patients or between different time points in a single patient should be performed using V_T(E-). However, for intrapatient interlesional comparison at a single time point, V_T(E+) may still be considered. Whether tumor TKI sensitivity can be predicted by [^{11}C]erlotinib V_T(E+) remains to be investigated.

Effect of erlotinib therapy on tumor perfusion

Tumor perfusion was not changed by erlotinib treatment. Also, tumor perfusion showed no association with [^{11}C]erlotinib V_T(E-) nor with V_T(E+). However, there was a positive trend between tumor perfusion and the delivery of [^{11}C]erlotinib to the tumor, which is in accordance with the 2T4k model. These findings suggest that the extraction of [^{11}C]erlotinib remains unchanged during erlotinib therapy.

Simplified uptake parameters

For simplification of future scanning protocols, SUV was not found to be a suitable uptake parameter, as it did not correlate with V_T, both on and off therapy. SUV normalizes on basis of injected dose and patient weight, which is less accurate as compared to TBR that normalizes on basis of the blood pool activity itself. For example, during erlotinib therapy, the blood tracer concentrations were higher.

Due to this increased tracer availability, the absolute amount of tumor tracer binding may have changed in varying extent. Tumor SUV does not take this variable into account, whereas TBR does. Contrary to SUV, arterial and venous TBR showed an excellent correlation with arterial V_T, supporting the use of both arterial and venous TBR in the time interval of 40 to 60 minutes post injection in future whole body static scanning protocols.

Interestingly, venous TBR values were lower than the arterial TBR values, especially in patients off therapy. This was due to higher plasma activity in venous samples than in arterial samples. As no difference in metabolism was observed between venous and arterial samples, the higher venous plasma activity values were only caused by a higher venous concentration of parent molecules. The reason for this finding is unclear. Possibly, the interstitial compartment together with EGFR molecules that are highly expressed at the epidermal tissue compartment act as a capacitator, by reversibly binding [^{11}C]erlotinib molecules. So, venous plasma collects not only the unbound [^{11}C]erlotinib molecules coming from the arterio-capillary route, but also the [^{11}C]erlotinib molecules being released from the interstitial and peripheral tissue compartments. This can also explain why patients on therapy, who have more EGFR saturation, have less veno-arterial activity difference. Another cause that may be considered is the fact that a single venous cannula was used for tracer injection and blood withdrawal, which implies that venous activity may increase due to the presence of tracer molecules that remained sticking to the cannula wall during injection. However, this mechanism is unlikely as it cannot explain why the veno-arterial difference was higher off therapy than on therapy. Nevertheless, venous sampling was found to be suitable for interlesional quantitative comparison using TBR, as long as venous values are not interchanged with arterial values.

Limitations

This study was limited by the fact that not all uptake values of [^{11}C]erlotinib and [^{15}O]H_2O and not all arterial and venous sampling values were present or evaluable in all patients; this was due to practical limitations as mentioned in Table 1. The small number of patients did not allow to establish the clinical role of [^{11}C]erlotinib PET during erlotinib therapy. Larger studies are needed to explore the clinical benefits of scanning during therapy, e.g. for evaluating interlesional differences within a single patient, preferably using TBR as validated in the current study.

Conclusion

Therapeutically dosed oral erlotinib decreases tumor [^{11}C]erlotinib V_T with high variability, independent of tumor perfusion. In patients on erlotinib therapy, quantitative tracer uptake analysis using V_T does not seem appropriate, however, it may be useful for intrapatient comparison of tumor lesions, which remains to be investigated. For protocol simplification, both arterial and venous TBR, in the time interval between 40-60 min post injection, could be used, however, arterial and venous TBR values should not be interchanged as venous values underestimate arterial values.

References

1. Bahce I, Smit EF, Lubberink M, van der Veldt AAM, Yaqub M, Windhorst AD, et al. Development of [(11)C]erlotinib positron emission tomography for in vivo evaluation of EGF receptor mutational status. Clin Cancer Res. 2013, 19: 183–93.

2. Mammatas LH, Verheul HM, Hendrikse NH, Yaqub M, Lammertsma AA, Menke-van der Houven CW, et al. Molecular imaging of targeted therapies with positron emission tomography: the visualization of personalized cancer care. Cellular Oncology. 2015, 38: 49–64.

3. Sharma SV, Bell DW, Settleman J, Haber DA. Epidermal growth factor receptor mutations in lung cancer. Nature Reviews Cancer. 2007, 7: 169–181.

4. Keedy VL, Temin S, Somerfield MR, Beasley MB, Johnson DH, McShane LM, et al. American Society of Clinical Oncology provisional clinical opinion: Epidermal growth factor receptor (EGFR) mutation testing for patients with advanced non-small-cell lung cancer considering first-line EGFR tyrosine kinase inhibitor therapy. Journal of Clinical Oncology. 2011, 29: 2121–2127.

5. Weber B, Winterdahl M, Memon A, Sorensen BS, Keiding S, Sorensen L, et al. Erlotinib accumulation in brain metastases from non-small cell lung cancer: visualization by positron emission tomography in a patient harboring a mutation in the epidermal growth factor receptor. Journal of Thoracic Oncology. 2011, 6: 1287–1289.

6. Memon AA, Weber B, Winterdahl M, Jakobsen S, Meldgaard P, Madsen HHT, et al. PET imaging of patients with non-small cell lung cancer employing an EGF receptor targeting drug as tracer. Br J Cancer. 2011, 105: 1850–5.

7. Mok TS, Wu YL, Thongprasert S, Yang CH, Chu DT, Saijo N, et al. Gefitinib or carboplatin-paclitaxel in pulmonary adenocarcinoma. New England Journal of Medicine. 2009, 361: 947–957.

8. Van Assche K, Ferdinande L, Lievens Y, Vandecasteele K, Surmont V. EGFR mutation positive stage IV non-small-cell lung cancer: treatment beyond progression. Frontiers in oncology. 2014, 4:

9. Surti S, Kuhn A, Werner ME, Perkins AE, Kolthammer J, Karp JS. Performance of Philips Gemini TF PET/CT scanner with special consideration for its time-of-flight imaging capabilities. J Nucl Med. 2007, 48: 471–80.

10. Gunn RN, Gunn SR, Cunningham VJ. Positron emission tomography compartmental models. Journal of Cerebral Blood Flow \& Metabolism. 2001, 21: 635–652.

11. Lammertsma AA, Bench CJ, Hume SP, Osman S, Gunn K, Brooks DJ, et al. Comparison of methods for analysis of clinical [11C]raclopride studies. J Cereb Blood Flow Metab. 1996, 16: 42–52.

12. Watabe H, Ikoma Y, Kimura Y, Naganawa M, Shidahara M. PET kinetic analysis—compartmental model. Annals of nuclear medicine. 2006, 20: 583–588.

13. Akaike. A new look at the statistical model identification. I E E E Trans Autom Control. 1974, 19: 716–23.

14. Van der Veldt AAM, Hendrikse NH, Harms HJ, Comans EFI, Postmus PE, Smit EF, et al. Quantitative Parametric Perfusion Images Using 15O-Labeled Water and a Clinical PET/CT Scanner: Test-Retest Variability in Lung Cancer. Journal of Nuclear Medicine. 2010, 51: 1684.

15. Iqbal R, Kramer GM, Verwer EE, Huisman MC, De Langen AJ, Bahce I, et al. Multiparametric analysis of the relationship between tumor hypoxia and perfusion using 18F-FAZA and 15O-H2O PET. Journal of Nuclear Medicine. 2015, jnumed–115.

16. Petrulli JR, Sullivan JM, Zheng M-Q, Bennett DC, Charest J, Huang Y, et al. Quantitative analysis of [11C]-erlotinib PET demonstrates specific binding for activating mutations of the EGFR kinase domain. Neoplasia. 2013, 15: 1347–53.

17. Abourbeh G, Itamar B, Salnikov O, Beltsov S, Mishani E. Identifying erlotinib-sensitive non-small cell lung carcinoma tumors in mice using [11C] erlotinib PET. EJNMMI research. 2015, 5:

18. Slobbe P, Windhorst AD, Stigter-van Walsum M, Smit EF, Niessen HG, Solca F, et al. A comparative PET imaging study with the reversible and irreversible EGFR tyrosine kinase inhibitors [11C] erlotinib and [18F] afatinib in lung cancer-bearing mice. EJNMMI research. 2015, 5:

19. Wang H, Yu J, Yang G, Song X, Sun X, Zhao S, et al. Assessment of 11C-labeled-4-N-(3-bromoanilino)-6, 7-dimethoxyquinazoline as a positron emission tomography agent to monitor epidermal growth factor receptor expression. Cancer science. 2007, 98: 1413–1416.

20. Lankheet NA, Knapen LM, Schellens JH, Beijnen JH, Steeghs N, Huitema AD. Plasma concentrations of tyrosine kinase inhibitors imatinib, erlotinib, and sunitinib in routine clinical outpatient cancer care. Therapeutic drug monitoring. 2014, 36: 326–334.

21. Li J, Zhao M, He P, Hidalgo M, Baker SD. Differential metabolism of gefitinib and erlotinib by human cytochrome P450 enzymes. Clinical Cancer Research. 2007, 13: 3731–3737.

22. Pao W, Chmielecki J. Rational, biologically based treatment of EGFR-mutant non-small-cell lung cancer. Nature Reviews Cancer. 2010, 10: 760–774.

23. Riely GJ, Politi KA, Miller VA, Pao W. Update on epidermal growth factor receptor mutations in non-small cell lung cancer. Clinical Cancer Research. 2006, 12: 7232–7241.

24. Han B, Zhou X, Zhang R-X, Zang W-F, Chen Z-Y, Song H-D, et al. Mutations of the epidermal growth factor receptor gene in NSCLC patients. Oncology letters. 2011, 2: 1233–1237.

25. Arcila ME, Nafa K, Chaft JE, Rekhtman N, Lau C, Reva BA, et al. EGFR exon 20 insertion mutations in lung adenocarcinomas: prevalence, molecular heterogeneity, and clinicopathologic characteristics. Mol Cancer Ther. 2013, 12: 220–9.

26. Wu J-Y, Wu S-G, Yang C-H, Gow C-H, Chang Y-L, Yu C-J, et al. Lung cancer with epidermal growth factor receptor exon 20 mutations is associated with poor gefitinib treatment response. Clinical Cancer Research. 2008, 14: 4877–4882.

27. Masago K, Fujita S, Irisa K, Kim YH, Ichikawa M, Mio T, et al. Good clinical response to gefitinib in a non-small cell lung cancer patient harboring a rare somatic epidermal growth factor gene point mutation; codon 768 AGC> ATC in exon 20 (S768I). Japanese journal of clinical oncology. 2010, 40: 1105–1109.

28. Ong M, Kwan K, Kamel--Reid S, Vincent M. Neoadjuvant erlotinib and surgical resection of a stage iiia papillary adenocarcinoma of the lung with an L861Q activating EGFR mutation. Current Oncology. 2012, 19: e222.

Chapter 6

Detecting resistance in EGFR-mutated non-small-cell lung cancer after clonal selection through targeted therapy

Justine L Kuiper

Idris Bahce

Charlotte Voorhoeve

Maqsood Yaqub

Daniëlle AM Heideman

Erik Thunnissen

Marinus A Paul

Pieter E Postmus

N Harry Hendrikse

Egbert F Smit

Personalized Medicine, 2015, 12(2): 63-66

Abstract

Tumor heterogeneity plays an important role in the development of treatment resistance, especially in the current era of targeted therapies. Although tumor heterogeneity is a widely recognized phenomenon, it is at present unclear how this knowledge should be incorporated into daily clinical practice. In this report, we describe an innovative nuclear imaging method that may play a role in detecting tumor heterogeneity in the future.

Tumor heterogeneity

It is believed that cancer arises from a single common ancestor cancer cell (1). The development of this one cell to metastatic cancer is a multifactorial process, influenced by clonal selection, according to historical evolution theories. Genetic instability and epigenetic events lead to the survival of the 'fittest' clones and at time of clinical presentation, tumours consist of multiple molecularly distinct tumour cell populations (2). The populations with the highest proliferation rate predominate in the tumour lesions. Consequently a tissue biopsy or cytological sample for diagnostic purposes will most likely be procured from this dominating part. Subsequently, this small sample from the dominating part will be considered to be representative for the whole tumour, primary and metastatic lesions. Even till very recently the initially obtained tissue was the only sample used for decision-making throughout the whole treatment period, even far beyond first line treatment, despite the well-known and well-described phenomenon of tumour heterogeneity (3, 4). Physiological and iatrogenic events, for instance anti-tumour therapy, may modify the clonal selection process. With modern therapies that are aimed at a specific target, nowadays described as 'targeted therapy', this effect is even more pronounced than with traditional chemotherapy.

The importance of tumor heterogeneity in the development of resistance to targeted therapies has extensively been described. Currently, the only way of detecting tumor heterogeneity is by sampling tumor tissue from different locations within the primary tumor and from different metastases, which is not feasible in daily clinical practice given the burden to the patient.

Epidermal growth factor receptor in non-small-cell lung cancer

Treatment of epidermal growth factor receptor (EGFR)-mutated non-small cell lung cancer (NSCLC) patients with tyrosine-kinase inhibitors (TKIs) results in high response rates and prolongation of progression free and overall survival. Unfortunately most patients develop progression after approximately 10 months, while on treatment. This pattern of progression is usually different from the behaviour prior to start of TKI-treatment. Several studies of rebiopsy at the time of tumour progression while on treatment, demonstrated that in more than half of the patients the new tissue sample differed from the initial sample (5). A common finding is presence of a different mutation at EGFR exon 20, the T790M mutation. This finding illustrates that in particular targeted therapies selectively eliminate sensitive clones, providing resistant populations of tumour cells the opportunity to outgrow. The outgrowth of certain tumour populations during a targeted

treatment increases tumour heterogeneity, allowing both resistant and sensitive clones to be present simultaneously. This demonstrates the need for continuous mapping of sensitivities and resistances of the tumour in order to be able to tailor treatment to the individual patient; the basis of the principle of 'personalized medicine'.

Radiolabeled TKI positron emission tomography scanning

Here, we describe a patient who underwent two positron emission tomography (PET)- scans using radiolabelled TKI ([^{11}C]erlotinib) as tracer (TKI-PET), a promising tumour imaging method (6). It has been demonstrated that NSCLC tumours that harbour an activating EGFR mutation have higher TKI binding affinity compared to tumours with wild-type EGFR (7). Therefore, increased [^{11}C]erlotinib uptake is indicative of (parts of the) tumour lesions that are sensitive to TKI-treatment (8).

A 46-year-old Asian woman was diagnosed with EGFR+ (exon 19 deletion) NSCLC (T3N3M1b), in the right upper lobe (RUL). Prior to treatment with erlotinib, an [^{11}C]erlotinib PET scan was performed (8) (Figure 1A). The overall tumour [^{11}C]erlotinib uptake was quantified by pharmacokinetic analysis in a 2-tissue reversible model using volume of distribution (VT) as a measure of uptake, as previously described (8). A tumour VT of 1.33 ± 0.03 and 1.90 ± 0.04 was measured during test and retest, respectively. Homogeneously increased uptake of [^{11}C] erlotinib was observed both in the tumour and in enlarged mediastinal lymph nodes. After start of erlotinib in standard dosage the patient obtained a partial response that lasted for 18 months. Then, there was progression in the primary tumour and a biopsy of this lesion showed the known EGFR exon 19 deletion, and a T790M mutation (molecular analysis performed by EGFR/KRAS high resolution melting (HRM) pre-screen with sequential analysis confirmation (9)). The [^{11}C]erlotinib scan was repeated after discontinuation of erlotinib for approximately 1 week (Figure 1B). This scan showed a VT value of 1.09 ± 0.02, indicating a decrease of 18% and 43%, as compared to test and retest, respectively. Also, by visual assessment, the intratumour [^{11}C]erlotinib uptake pattern had become heterogeneous, suggesting that also tumour affinity to TKI had become more heterogeneous. In retrospect the area where the new biopsy was taken, the dorsal part of the tumour, had little uptake of [^{11}C]erlotinib.

Applying this technique is not only a rather patient friendly method to illustrate the biological phenomenon of tumour heterogeneity and the limitations of the first generation targeted therapy drugs, but it may have consequences for guiding the clinician where to obtain a new biopsy in this specific situation. Although there is at

this stage no registered targeted drug available for treatment after development of resistance through selection of the T790M clone, in the very near future promising drugs – e.g. CO1686, AZD9192 - are expected, specifically targeted at T790M (10, 11). Switching to these next generation TKIs might again result in prolongation of progression free survival and survival. For today's situation, the [^{11}C] erlotinib PET scan may indicate residual TKI sensitivity, helping clinicians to decide whether the TKI should be continued while standard second-line chemotherapy starts or should be restarted after finishing chemotherapy.

Conclusion & future perspective

Although prospective evaluation is necessary before any final conclusions can be drawn, it is appealing to speculate on the possibilities that the use of PET scans in combination with radiolabeled TKIs (TKI-PET scans) may have in detecting tumor heterogeneity. Here, we decribed a patient in whom tumor heterogeneity was detected by these PET scans. In the future, TKI-PET scans could possibly be used to determine the optimal place to rebiopsy and/or guide therapeutic decisions.

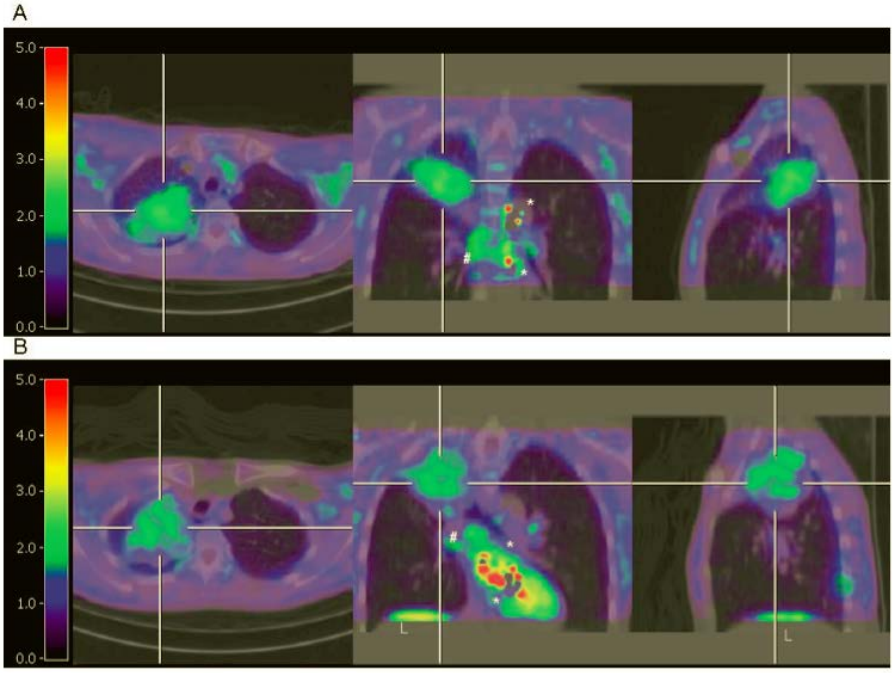

Fig 1 *Positron emission tomography scan showing [^{11}C]erlotinib uptake in the tumour (A) Prior to treatment, (B) After treatment with erlotinib*

References

1 Schepers AG, Snippert HJ, Stange DE et al. Lineage tracing reveals Lgr5+ stem cell activity in mouse intestinal adenomas. Science 337(6095), 730–735 (2012).

2 Burrell RA, McGranahan N, Bartek J, Swanton C. The causes and consequences of genetic heterogeneity in cancer evolution. Nature 501(7467), 338–345 (2013).

3 Meacham CE, Morrison SJ. Tumour heterogeneity and cancer cell plasticity. Nature 501(7467), 328–337 (2013).

4 Fisher R, Pusztai L, Swanton C. Cancer heterogeneity: implications for targeted therapeutics. Br. J. Cancer 108(3), 479–485 (2013).

5 Yu HA, Arcila E, Rekhtman N et al. Analysis of tumor specimens at the time of acquired resistance to EGFR-TKI therapy in 155 patients with EGFR-mutant lung cancers. Clin. Cancer Res. 19(8), 2240–2247 (2013).

6 Slobbe P, Poot AJ, Windhorst AD, van Dongen GA. PET imaging with small-molecule tyrosine kinase inhibitors: TKI-PET. Drug Discov. Today 17(21–22), 1175–1187 (2012).

7 Carey KD, Garton AJ, Romero MS et al. Kinetic analysis of epidermal growth factor receptor somatic mutant proteins shows increased sensitivity to the epidermal growth factor receptor tyrosine kinase inhibitor, erlotinib. Cancer Res. 66(16), 8163–8171 (2006).

8 Bahce I, Smit EF, Lubberink M et al. Development of [(11)C]erlotinib positron emission tomography for in vivo evaluation of EGF receptor mutational status. Clin. Cancer Res. 19(1), 183–193 (2013).

9 Heideman DA, Thunnissen FB, Doeleman M et al. A panel of high resolution melting (HRM) technology-based assays with direct sequencing possibility for effective mutation screening of EGFR and K-ras genes. Cell. Oncol. 31(5), 329–333 (2009).

10 Janne PA, Ramalingam SS, Chih-Hsin Yang J et al. Clinical activity of the mutant-selective EGFR inhibitor AZD9291 in patients (pts) with EGFR inhibitor-resistant non-small-cell lung cancer (NSCLC). Presented at: ASCO 2014. Chicago, IL, USA, 30 May–3 June 2014.

11 Sequist LV, Soria JC, Gadgeel SM et al. First in-human evaluation of CO-1686, an irreversible, highly selective tyrosine kinase inhibitor of mutations of EGFR (activating and T790M). Presented at: ASCO 2014. Chicago, IL, USA, 30 May–3 June 2014.

Chapter 7

Pilot study of ^{89}Zr-bevacizumab positron emission tomography in patients with advanced non-small cell lung cancer

Idris Bahce

Marc C. Huisman

Eline E. Verwer

Rogier Ooijevaar

Firdaouss Boutkourt

Danielle J. Vugts

Guus A.M.S. van Dongen

Ronald Boellaard

Egbert F. Smit

EJNMMI Research 2014, 4:35

Abstract

PURPOSE: The aim of this pilot study was to evaluate whether uptake of ^{89}Zr-bevacizumab in non-small cell lung cancer (NSCLC) tumors could be visualized and quantified. The correlation between tumor ^{89}Zr-bevacizumab uptake and tumor response to antitumor therapy with a bevacizumab based regimen was explored.

METHODS: Seven NSCLC patients underwent static PET scans at days 4 and 7 after injection of 36.4 ± 0.9 MBq (mean ± SD) ^{89}Zr-bevacizumab, prior to commencing carboplatin-paclitaxel-bevacizumab chemotherapy (CPB). Overall survival (OS) and Progression Free Survival (PFS) to CPB followed by bevacizumab maintenance therapy was correlated to tumor tracer uptake, quantified using peak standardized uptake values (SUV_{peak}).

RESULTS: ^{89}Zr-bevacizumab uptake (SUV_{peak}) was approximately 4 times higher in tumor tissues (primary tumor, metastases) than in non-tumor tissues (healthy muscle, lung, fat) on days 4 and 7. A positive trend, but no significant correlation could be found between SUV_{peak} and OS or PFS.

CONCLUSIONS: This pilot study shows that ^{89}Zr-bevacizumab PET imaging in NSCLC is feasible. Further investigation to validate this technique as a predictive biomarker for selecting patients for bevacizumab treatment, is warranted.

Background

Vascular endothelial growth factor (VEGF) is an important mediator in non-tumoral and tumoral angiogenesis. VEGF-A, one of the 5 members of the VEGF family and generally referred to as VEGF, is overexpressed in many tumors [1, 2]. In response to hypoxia, cells of mesenchymal, stromal and epithelial origin (e.g. myocytes, blood platelets, stromal cells in tumors) show paracrine secretion of VEGF-A. This increases VEGF-A concentrations locally in the tumor, causing a strong pro-angiogenic stimulus. The binding of VEGF-A to VEGF receptor subtypes 1 and 2 (VEGFR1 and VEGFR2), both transmembrane monomers expressed on vascular endothelial cells, causes dimerization of the VEGFR1/2 monomers, leading to activation of intracellular proangiogenic signaling pathways [3–6]. Also, non-angiogenic effects of increased VEGF-A have been described [3, 7, 8].

The addition of bevacizumab, a monoclonal antibody directed against VEGF-A, to cytotoxic chemotherapy improves tumor response rates and provides a survival advantage over chemotherapy alone in several malignancies [9–12]. A phase III study showed a survival benefit for patients with non-small cell lung cancer (NSCLC) treated with carboplatin-paclitaxel-bevacizumab compared with chemotherapy alone [13]. However, on an individual basis, it is unclear who would benefit from bevacizumab therapy, as predictive markers are lacking, despite a large body of clinical research available to date.

Imaging tumor uptake of radiolabeled bevacizumab in patients using positron emission tomography (PET) may provide such a predictive marker, as PET imaging enables *in vivo* monitoring of physiological processes.

To date, several clinical studies have been performed using antibodies with ^{89}Zr labeling. In these studies, positive image contrast is observed, and its relation to therapy response discussed [14–17]. The aim of this pilot study was to evaluate whether ^{89}Zr-bevacizumab enables visualization of NSCLC tumors, to assess the ranges of tumor-to-background ratios and standardized uptake values. Additionally, the correlation between ^{89}Zr-bevacizumab uptake and tumor response following treatment with a bevacizumab based regimen was assessed.

Methods

Patients

In this prospective pilot study, patients with stage IV adenocarcinoma of the lung who were scheduled for combined carboplatin–paclitaxel–bevacizumab treatment

were enrolled. Inclusion criteria were: histologic diagnosis of non-squamous NSCLC, age of 18 years or older, performance status of 0-2 (WHO), a life expectancy of at least 12 weeks and presence of at least 1 NSCLC lesion within the chest of at least 1.5 cm diameter as measured by CT. Exclusion criteria included: claustrophobia, pregnancy, lactation and use of concurrent or previous treatment with anti-cancer drugs within 30 days prior to scanning. Patients gave informed consent, and this study was approved by the Medical Ethics Review Committee of the VU University Medical Center.

Imaging

Prior to start of therapy, patients underwent positron emission tomography / computed tomography (PET/CT) scans using [^{18}F]fluorodeoxyglucose (FDG) and ^{89}Zr-bevacizumab.

Therapy

As scheduled prior to inclusion in this study, patients received treatment with carboplatin (area under the concentration time curve of 6.0 mg/mL/min) – paclitaxel (200 mg/m^2 of body surface area) – bevacizumab (15 mg/kg), and continuation maintenance bevacizumab upon non-progression after 4 cycles. Chemotherapy was given every 21 days, until disease progression or unacceptable toxicity [13].

Preparation of ^{89}Zr-bevacizumab

Bevacizumab was labeled with zirconium-89 using *N*-succinyl-desferrioxamine (*N*-suc-Df) as described previously [18, 19]. All procedures were performed under aseptic conditions in a shielded laminar flow cabinet. In short, desferrioxamine (desferal, Df, Novartis, Basel, Switzerland) was converted to *N*-succinyl-Df. Next, the hydroxamate groups were blocked with iron and the succinic acid group converted to its tetrafluorophenol ester. The resulting Fe-*N*-suc-Df-TFP ester was reacted with bevacizumab under basic conditions (pH 9.5-9.7) for 30 min at room temperature. Subsequently, iron was removed using an excess of ethylenediaminetetraacetic acid (EDTA) for 30 min at 35°C and the resulting *N*-suc-Df-bevacizumab was purified over a PD-10 column and radiolabeled with ^{89}Zr for 60 min in HEPES buffer at room temperature. Finally, ^{89}Zr-*N*-suc-Df-bevacizumab was purified over a PD-10 column using 5 mg/mL gentisic acid in 0.9% NaCl (pH 4.9-5.4). The mean labeling efficiency was 71.1 ± 5.3 %. The product was formulated and filter sterilized to 5 mg bevacizumab, 37 MBq Zr-89 per patient injection. These procedures resulted in a sterile final product with endotoxin levels < 2.5 EU/mL. The radiochemical purity was >97 % according to iTLC and HPLC and the

immunoreactivity as determined by an ELISA assay was >75 %, which is optimal for this assay.

PET scanning

All patients underwent a routine FDG PET/CT scan within 4 weeks prior to starting therapy. One week prior to therapy, patients were injected intravenously with 36.4±0.9 MBq ^{89}Zr-bevacizumab and 10-minute static PET/CT scans of the thoracic NSCLC lesion were performed on days 4 and 7 post injection.. These parameters were based on previous ^{89}Zr-trastuzumab analysis, showing appropriate doses and timing for visualization and quantification of uptake in HER2-positive tumors to be 37 MBq and days 4-5 after injection, respectively [20].

Scans were performed on a Gemini TF-64 PET/CT scanner (Philips Medical Systems, Cleveland, USA). PET data were normalized and all appropriate corrections were applied for dead time, decay, randoms and scatter. Reconstruction of PET data was performed using the BLOB-OS-TF reconstruction algorithm with CT based attenuation correction, resulting in a final voxel size of 4x4x4 mm^3, matrix 144x144x45 and a spatial resolution of 5-7 mm full width at half maximum [21]. Additional smoothing was performed, as this was shown to optimize quantitative accuracy and harmonized image quality [22].

^{89}Zr-bevacizumab uptake analysis

FDG PET/CT scans were used to identify the exact location of the tumors. PET data were analysed using in-house developed analysis tools within the IDL environment (IDL Virtual Machine 6.2, RSI). Volumes of interest (VOI) were drawn manually on the CT images around the contours of the primary tumor (PT), and, if present, lymph node metastases (LNM) and non-lymph node metastases (NLNM). Additionally, VOI were drawn within the descending aorta (AD) and non-tumor tissues muscle (M), healthy lung (HL) and fatty tissue (FT). Standardized Uptake Value (SUV) parameters were calculated by normalizing VOI activity concentrations to injected dose and patient weight: SUV_{peak} (spheric VOI of 1.2-cm diameter positioned around the voxel with the highest uptake), and SUV_{mean} (mean activity in VOI/cc) from the AD VOI to calculate the tissue-to-blood ratio (TBR). SUV_{peak} and TBR for the above-mentioned VOI were then compared for the scans at days 4 and 7.

Statistical analysis

Statistical analysis was performed using SPSS software (SPSS for Windows 15.0, SPSS, Inc.). Correlations were explored using the Spearman's correlation coefficient (r_s). A two-tailed probability value of $P < 0.05$ was considered significant. Values in

text and tables are presented as mean ± standard deviation (SD) unless stated otherwise.

Results

Seven patients were included in this study. Patient characteristics are summarized in table 1. Nine mediastinal LNM were identified using FDG PET/CT scans within the thoracic field of view. Six patients showed NLNM. All tumor lesions showed visible ^{89}Zr-bevacizumab uptake. To illustrate the findings as reported below, typical examples of fused PET/CT images using FDG and ^{89}Zr-bevacizumab in 3 NSCLC patients are provided in figure 1.

Table 1. Patient characteristics

Nr	Sex	Age (yrs)	Primary tumor	Evaluable metastasis	Histology	Bevacizumab Maintenance therapy	Best response	Site of progression	PFS (w)	OS (w)
1	F	56	RLL	-	AC	Yes	PR	LLL	56	79
2	M	51	RUL	Peritoneum	AC	Yes	PR	PC	13	17
3	M	59	RLL	Bone	AC	Yes	PR	RUL[a]	27	48
4	M	61	RLL	Bone	LCC	Yes	CR	RA	35	63
5	F	54	RLL	Bone	AC	Yes	PR	Brain	54	74
6	F	69	RH	Pericardium	AC	Yes	PR	MC	34	60

7	M	51	LH	Bone	AC	No	PD	Liver[a]	3	3

***Abbreviations**: AC: adenocarcinoma, CR: complete response, F: female, LCC: large cell carcinoma, LH: left hilum, M: male, MC: meningitis carcinomatosa, OS: overall survival, PC: peritonitis carcinomatosa, PD: progressive disease, PFS: progression free survival, PR: partial response, RA: right adrenal gland, RH: right hilum, RLL: right lower lobe, RUL: right upper lobe, SDC: salivary duct carcinoma, LLL: left lower lobe.*

Evaluable metastases are nonprimary lesions, located within the PET field of view. All patients received bevacizumab maintenance therapy, except for one patient, who died before bevacizumab maintenance therapy could be administered. The best tumor response to chemotherapy is shown. Progressive disease was seen in all patients. Two patients developed clinical disease progression ([a]) before radiological progression. One patient developed progression due to brain metastasis. Sites of radiological progression are shown. PFS and OS were calculated in weeks, between start of chemotherapy and date of progression and death, respectively.

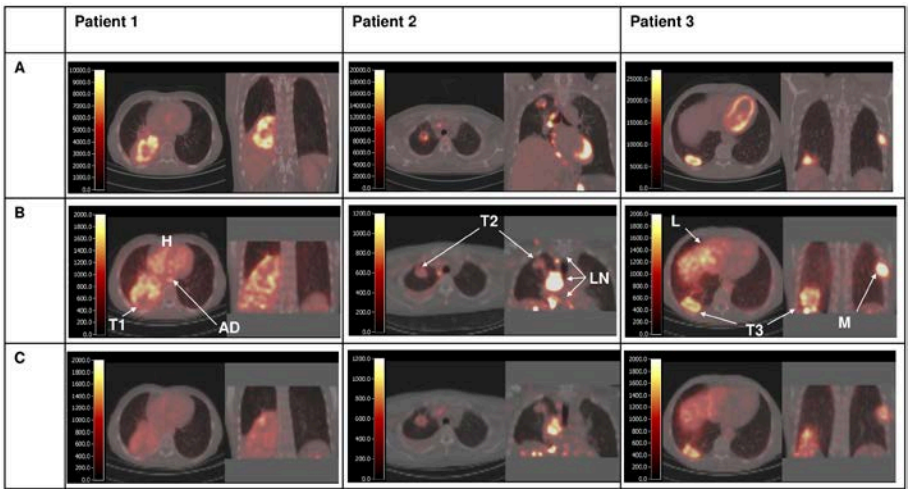

Fig.1 *Fused PET/CT images using FDG (A) and ^{89}Zr-bevacizumab at day 4 (B) and day 7 (C) are shown. Per scan an axial and coronal slice is shown. The color scale, indicating Bequerels per mL (BQML), ranges from 0 to a maximum value that corresponds with a SUV value of 6. In patient 1 a large tumor in the right lower lobe is seen. There is increased FDG uptake in the outer rims of the tumor, and reduced uptake in the center of the tumor (probably due to necrosis). The ^{89}Zr-bevacizumab*

image on day 4 also shows high uptake in the outer rims of the tumor (T1) and high blood activity concentration (aorta descendens (AD), heart chambers (H)). Low uptake is found in non-tumor tissues, such as healthy lung, fat and muscle. The ^{89}Zr-bevacizumab image on day 7 shows high uptake in the outer rims of the tumor, but low uptake in healthy tissues as well as low blood activity concentrations. In patient 2 the FDG scan shows increased uptake in both the primary tumor in the right upper lobe and the enlarged mediastinal lymph node metastases. Interestingly, the ^{89}Zr-bevacizumab images only show increased uptake in the lymph node metastases (LN), while the uptake in the primary tumor (T2) on both days 4 and 7 is faint. In patient 3, the primary tumor, the mediastinal lymph node metastases and rib metastasis all show increased FDG uptake. The ^{89}Zr-bevacizumab scans on days 4 and 7 show the highest uptake in the rib metastasis (M) and the primary tumor (T3), and moderate to high uptake is seen in the liver (L).

In all tumorous tissues (PT, LNM and NLNM), ^{89}Zr-bevacizumab uptake (SUV_{peak}) was approximately 4 times higher than in non-tumorous tissues (M, HL and FT) on days 4 and 7, as shown in table 2. For tumorous tissues, SUV_{peak} in NLNM and LNM was approximately 54% and 26% higher as compared to PT on day 4, and 49% and 19% higher on day 7, respectively (see Fig.2).

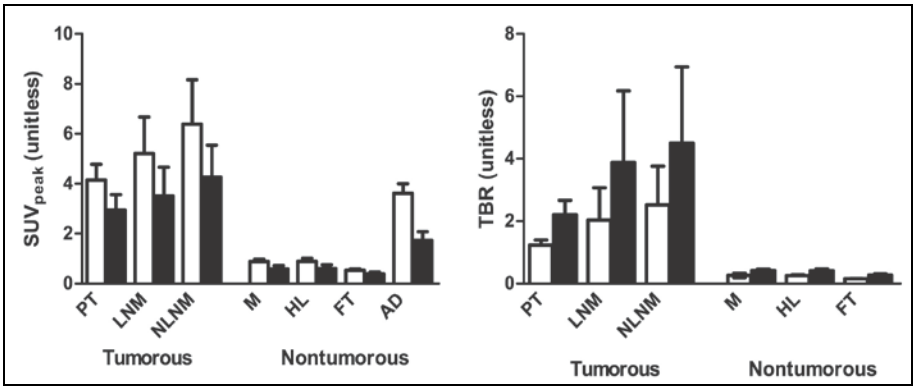

Fig 2. *Comparison of ^{89}Zr-bevacizumab SUV_{peak} and TBR in different tissues at day 4 (open bars) and day 7 (black bars).*

Abbreviations*: AD = aorta descendens, FT = fatty tissue, HL = healthy lung, LNM = lymph node metastasis, M = muscle, NLNM = non lymph node metastasis, PT = primary tumor, TBR = tumor-to-blood ratio.*

Table 2. 89Zr-bevacizumab uptake parameters

		Tumorous tissue			Blood (AD)	Nontumorous tissue		
		PT	LNM	NLNM		Muscle	Fat	Lung
Day 4	SUV_{peak}	4.3 (2.1-6.9)	4.0 (2.1-12.1)	5.0 (2.9-14.5)	3.9 (1.7-4.9)	1.0 (0.4-1.1)	0.6 (0.3-0.7)	0.8 (0.5-1.4)
	TBR	1.2 (0.7-1.8)	1.1 (0.8-7.2)	1.2 (0.7-8.6)		0.3 (0.1-0.3)	0.2 (0.1-0.2)	0.3 (0.2-0.3)
Day 7	SUV_{peak}	3.3 (0.7-4.9)	2.7 (1.0-9.0)	3.9 (1.1-9.7)	1.4 (0.9-3.5)	0.5 (0.2-1.3)	0.4 (0.1-0.6)	0.4 (0.2-1.1)
	TBR	1.8 (1.0-4.0)	1.6 (1.1-15.3)	1.9 (0.9-16.5)		0.5 (0.3-0.6)	0.3 (0.1-0.4)	0.4 (0.2-0.6)

***Abbreviations**: AD: aorta descendens, LNM: lymph node metastases, NLNM: non-lymph node metastases, PT: primary tumor, TBR: tumor-to-blood ratio. Median (range) is shown.*

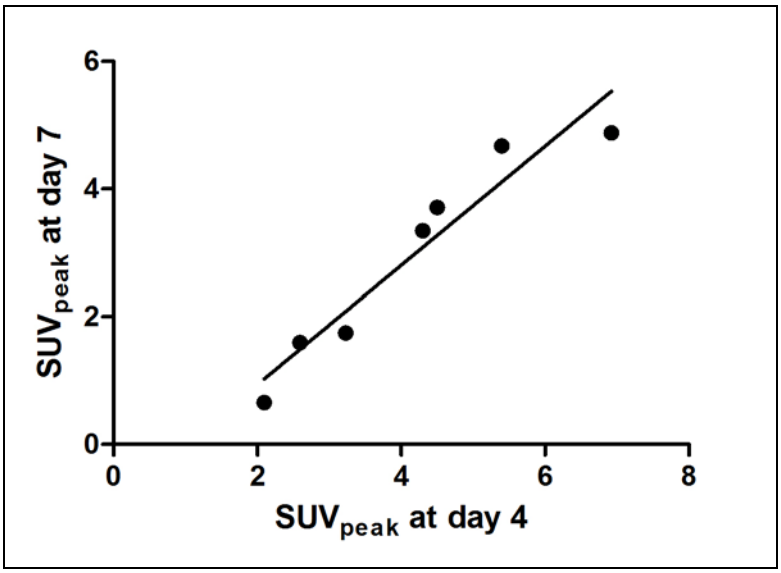

Fig.3 *Comparison of tumor ^{89}Zr-bevacizumab uptake (SUV_{peak}) on days 4 and 7. A correlation coefficient (r_s) of 1 ($P < 0.001$) was found.*

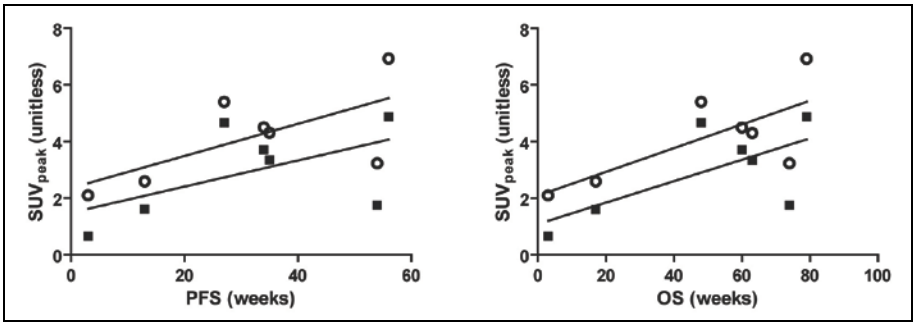

Fig.4 *Correlations between SUV_{peak} and clinical outcome (PFS, OS) for day 4 (open circles) and day 7 (black squares). Correlation coefficients were not statistically significant for both PFS and OS, with rs of 0.64 ($P = 0.139$) at days 4 and 7, respectively.*

Abbreviations*: PFS = progression free survival, OS = overall survival.*

Remarkably, on day 4 activity concentration in blood (AD) was approximately the same as in the primary tumor (PT), while the healthy tissue activity was clearly

lower than in PT (see table 2, Fig.1 and Fig.2). However, between days 4 and 7 tumor TBR increased from 1.23 ± 0.4 to 2.2 ± 1.2.

SUV_{peak} correlated strongly between days 4 and 7, as indicated by an rs of 1 ($P < 0.001$). Figure 3 shows the correlation between days 4 and 7 for SUV_{peak}.

As shown in Figure 4, correlations between tumor SUV_{peak} and outcome parameters showed a positive trend, but did not reach statistical significance. SUV_{peak} showed weak correlation with both PFS and OS on days 4 and 7. (rs was 0.64 with a $P = 0.139$ for both PFS and OS on days 4 and 7, respectively).

Discussion

Visualization of tumor lesions

Prior to this study, it was unclear whether NSCLC tumors could be imaged by ^{89}Zr-bevacizumab. The results of this pilot study show that all tumor lesions (PT, LNM, NLNM) had a higher ^{89}Zr-bevacizumab uptake as compared to non-tumor background tissues, allowing for visualization and analysis of tumor ^{89}Zr-bevacizumab uptake.

This increased uptake may be caused by accumulation of VEGF in the tumor, due to high paracrine expression and subsequent binding to extracellular matrix glycoproteins such as heparan sulfate proteoglycans (HSPG) and neuropilins (NRP). These glycoproteins act as non-signaling co-receptors that facilitate binding of VEGF to VEGFR molecules [6]. Another mechanism that may contribute is the internalization of ^{89}Zr-bevacizumab into cells within the tumor. After internalization, the ^{89}Zr-label may become trapped in the lysosomes and show up on the PET-scan [23].

Our findings are in accordance with the limited number of publications of previous preclinical and clinical data showing that high VEGF-A expressing tumors are associated with high tumor-to-background ^{89}Zr-bevacizumab uptake. Nagengast *et al.* showed that high VEGF-producing SKOV-3 ovarian tumor xenografts had a higher uptake of ^{89}Zr-bevacizumab than of ^{89}Zr labeled IgG, which served as a control. In a follow-up study the same researchers found that ^{89}Zr-bevacizumab uptake decreased in (NVP-AUY922 sensitive) A2780 ovarian tumor xenografts after 2 weeks of antitumor therapy (using NVP-AUY922), while in the therapy-resistant CP70 xenografts, ^{89}Zr-bevacizumab uptake did not change. Van der Bilt *et al.* showed a decrease in ^{89}Zr-bevacizumab uptake in A2780 ovarian tumor xenografts after 2 weeks of everolimus therapy, while ^{89}Zr-bevacizumab uptake remained

unchanged in other organs, matching ex vivo measures of VEGF-A levels [19, 24, 25]. Recently, a first clinical study using ^{89}Zr-bevacizumab was reported. In breast cancer patients, tumors with elevated VEGF-A levels showed higher ^{89}Zr-bevacizumab uptake than the background of healthy breast tissue [26].

We found that tumor-to-background ratios were high at days 4 and 7, however, tumor-to-blood ratios were higher on day 7, due to a relative decrease of blood activity concentrations as compared to tumor activity concentrations. However, image quality at day 7 was hampered due to physical decay of the tracer. The optimal time for ^{89}Zr-bevacizumab seems to be between 4 and 7 days post-injection.

Lymph node metastases and especially NLNM showed higher uptake than pulmonary lesions. This may be caused by the fact that pulmonary lesions suffered more from breathing-movement induced partial volume effects than LNM and NLNM, which were relatively fixed to bone and peritoneum. Although all tumoral lesions were visible in this study, the quantification of uptake in small-volume lesions needs to be interpreted with caution, as these tumors suffer even more from this partial volume-induced underestimation of tracer uptake.

Clinical outcome

Although our results did not show a significant correlation between tracer uptake and PFS, a positive trend was observed. As tumor ^{89}Zr-bevacizumab uptake may represent the level of tumor VEGF, this technique might offer a predictive biomarker for bevacizumab treatment efficacy. At present, there is an absence of clinically useful predictive biomarkers. For example, several blood biomarkers, such as VEGF-A and NRP-1 using newly developed sensitive assays, have been proposed to predict bevacizumab treatment efficacy, but their value is still the subject of debate [6], [27].

Limitations

As this was a pilot study, only a limited number of patients were included. However, the results obtained were consistent for all patients, indicating larger clinical trials are warranted.

Another limitation was the absence of arterial blood sampling for blood and plasma activity and metabolite analysis, which could have provided a more accurate quantification of tracer uptake. However, because patients already underwent several PET/CT-scans, additional blood sampling for research purposes was considered too high a burden. Furthermore, previously published data show a good correlation between image derived activity from ^{89}Zr-labeled antibodies and blood

activity [15, 17]. Additionally, ^{89}Zr-bevacizumab was found to be highly stable in plasma, as only a 6% decrease in protein-bound radioactivity was seen after 168 hrs (stored in serum at 37 ºC) [19].

Although NSCLC was initially diagnosed in all patients, no extra tumor biopsy was taken prior to scanning for VEGF-A staining, again because this was considered too burdensome.

Future perspectives

The results of this study show tumor specific uptake of ^{89}Zr-bevacizumab. Future studies should consider not to include small lesions that could suffer from partial volume effects. Furthermore, the optimal timing should be investigated, as this can be expected to be between day 4 and day 7 post injection. To better understand the physiological processes causing tracer accumulation, concurrent pathology data (e.g. angioproliferative markers) should be assessed by taking biopsies prior to scanning. Quantification of uptake may be improved by using blood sampling for plasma radioactivity assessment.

The effect of perfusion on ^{89}Zr-bevacizumab should be analyzed. In this study an assessment of tumor blood perfusion, e.g. with [^{15}O]H_2O PET scan, was not performed. Using [^{15}O]H_2O PET scans, Van der Veldt et al. showed that the intratumoral distribution of docetaxel followed the tumor perfusion patterns. Therefore, tumor perfusion data may have provided additional understanding of the distribution of tumoral ^{89}Zr-bevacizumab uptake.

^{89}Zr-bevacizumab PET may be used as an imaging agent, as tracer uptake showed a trend towards a positive correlation with PFS and OS. It should be noted that patients were treated with carboplatin-paclitaxel-bevacizumab (CPB) followed by bevacizumab maintenance therapy. PFS was the result of both CPB therapy and bevacizumab. In future studies ^{89}Zr-bevacizumab scans should ideally be performed at two time points, i.e. prior to CPB therapy, but also prior to bevacizumab maintenance therapy. This is because the post-CPB altered tumor VEGF status is unknown, however this new post-CPB VEGF status may be a better predictor for sensitivity to subsequent bevacizumab maintenance therapy.

Conclusions

This pilot study demonstrates that ^{89}Zr-bevacizumab PET imaging in tumors is feasible. Larger studies are needed to validate and substantiate these findings. ^{89}Zr-bevacizumab PET merits further investigation, aiming to evaluate its use as a predictive imaging biomarker.

References

1. Okines AFC, Reynolds AR, Cunningham D: Targeting angiogenesis in esophagogastric adenocarcinoma. Oncologist 2011, 16: 844–58.

2. Burger RA: Overview of anti-angiogenic agents in development for ovarian cancer. Gynecol Oncol 2011, 121: 230–8.

3. Maharaj ASR, D'Amore PA: Roles for VEGF in the adult. Microvasc Res 2007, 74: 100–13.

4. Kerbel RS: Tumor angiogenesis. New England Journal of Medicine 2008, 358: 2039–2049.

5. Maharaj ASR, Saint-Geniez M, Maldonado AE, D'Amore PA: Vascular endothelial growth factor localization in the adult. Am J Pathol 2006, 168: 639–48.

6. Wu FTH, Stefanini MO, Mac Gabhann F, Kontos CD, Annex BH, Popel AS: A systems biology perspective on sVEGFR1: its biological function, pathogenic role and therapeutic use. J Cell Mol Med 2010, 14: 528–52.

7. Lee S, Chen TT, Barber CL, Jordan MC, Murdock J, Desai S, Ferrara N, Nagy A, Roos KP, Iruela-Arispe ML: Autocrine VEGF signaling is required for vascular homeostasis. Cell 2007, 130: 691–703.

8. D'Amore PA: Vascular endothelial cell growth factor-a: not just for endothelial cells anymore. Am J Pathol 2007, 171: 14–8.

9. Presta LG, Chen H, O'Connor SJ, Chisholm V, Meng YG, Krummen L, Winkler M, Ferrara N: Humanization of an anti-vascular endothelial growth factor monoclonal antibody for the therapy of solid tumors and other disorders. Cancer Res 1997, 57: 4593–9.

10. Kim KJ, Li B, Winer J, Armanini M, Gillett N, Phillips HS, Ferrara N: Inhibition of vascular endothelial growth factor-induced angiogenesis suppresses tumour growth in vivo. Nature 1993, 362: 841–4.

11. Borgström P, Bourdon MA, Hillan KJ, Sriramarao P, Ferrara N: Neutralizing anti-vascular endothelial growth factor antibody completely inhibits angiogenesis and growth of human prostate carcinoma micro tumors in vivo. Prostate 1998, 35: 1–10.

12. Reck M, von Pawel J, Zatloukal P, Ramlau R, Gorbounova V, Hirsh V, Leighl N, Mezger J, Archer V, Moore N, Manegold C: Overall survival with cisplatin-gemcitabine and bevacizumab or placebo as first-line therapy for nonsquamous

non-small-cell lung cancer: results from a randomised phase III trial (AVAiL). Ann Oncol 2010, 21: 1804–9.

13. Sandler A, Gray R, Perry MC, Brahmer J, Schiller JH, Dowlati A, Lilenbaum R, Johnson DH: Paclitaxel-carboplatin alone or with bevacizumab for non-small-cell lung cancer. N Engl J Med 2006, 355: 2542–50.

14. Perk LR, Visser OJ, Stigter-van Walsum M, Vosjan MJWD, Visser GWM, Zijlstra JM, Huijgens PC, van Dongen GAMS: Preparation and evaluation of (89)Zr-Zevalin for monitoring of (90)Y-Zevalin biodistribution with positron emission tomography. Eur J Nucl Med Mol Imaging 2006, 33: 1337–45.

15. Rizvi SNF, Visser OJ, Vosjan MJWD, van Lingen A, Hoekstra OS, Zijlstra JM, Huijgens PC, van Dongen GAMS, Lubberink M: Biodistribution, radiation dosimetry and scouting of 90Y-ibritumomab tiuxetan therapy in patients with relapsed B-cell non-Hodgkin's lymphoma using 89Zr-ibritumomab tiuxetan and PET. Eur J Nucl Med Mol Imaging 2012, 39: 512–20.

16. Deri MA, Zeglis BM, Francesconi LC, Lewis JS: PET imaging with ^{89}Zr: from radiochemistry to the clinic. Nucl Med Biol 2013, 40: 3–14.

17. Börjesson PKE, Jauw YWS, de Bree R, Roos JC, Castelijns JA, Leemans CR, van Dongen GAMS, Boellaard R: Radiation dosimetry of 89Zr-labeled chimeric monoclonal antibody U36 as used for immuno-PET in head and neck cancer patients. J Nucl Med 2009, 50: 1828–36.

18. Verel I, Visser GWM, Boerman OC, van Eerd JEM, Finn R, Boellaard R, Vosjan MJWD, Stigter-van Walsum M, Snow GB, van Dongen GAMS: Long-lived positron emitters zirconium-89 and iodine-124 for scouting of therapeutic radioimmunoconjugates with PET. Cancer Biother Radiopharm 2003, 18: 655–61.

19. Nagengast WB, de Vries EG, Hospers GA, Mulder NH, de Jong JR, Hollema H, Brouwers AH, van Dongen GA, Perk LR, Lub-de Hooge MN: In vivo VEGF imaging with radiolabeled bevacizumab in a human ovarian tumor xenograft. J Nucl Med 2007, 48: 1313–9.

20. Dijkers EC, Oude Munnink TH, Kosterink JG, Brouwers AH, Jager PL, de Jong JR, van Dongen GA, Schröder CP, Lub-de Hooge MN, de Vries EG: Biodistribution of 89Zr-trastuzumab and PET imaging of HER2-positive lesions in patients with metastatic breast cancer. Clin Pharmacol Ther 2010, 87: 586–92.

21. Surti S, Kuhn A, Werner ME, Perkins AE, Kolthammer J, Karp JS: Performance of Philips Gemini TF PET/CT scanner with special consideration for its time-of-flight imaging capabilities. J Nucl Med 2007, 48: 471–80.

22. Makris NE, Boellaard R, Visser EP, de Jong JR, Vanderlinden B, Wierts R, van der Veen BJ, Greuter HJNM, Vugts DJ, van Dongen GAMS, Lammertsma AA, Huisman MC: Multicenter harmonization of 89Zr PET/CT performance. J Nucl Med 2014, 55: 264–7.

23. van Dongen GAMS, Visser GWM, Lub-de Hooge MN, de Vries EG, Perk LR: Immuno-PET: a navigator in monoclonal antibody development and applications. Oncologist 2007, 12: 1379–89.

24. Nagengast WB, de Korte MA, Oude Munnink TH, Timmer-Bosscha H, den Dunnen WF, Hollema H, de Jong JR, Jensen MR, Quadt C, Garcia-Echeverria C, van Dongen GAMS, Lub-de Hooge MN, Schröder CP, de Vries EGE: 89Zr-bevacizumab PET of early antiangiogenic tumor response to treatment with HSP90 inhibitor NVP-AUY922. J Nucl Med 2010, 51: 761–7.

25. van der Bilt ARM, Terwisscha van Scheltinga AGT, Timmer-Bosscha H, Schröder CP, Pot L, Kosterink JGW, van der Zee AGJ, Lub-de Hooge MN, de Jong S, de Vries EGE, Reyners AKL: Measurement of tumor VEGF-A levels with 89Zr-bevacizumab PET as an early biomarker for the antiangiogenic effect of everolimus treatment in an ovarian cancer xenograft model. Clin Cancer Res 2012, 18: 6306–14.

26. Gaykema SBM, Brouwers AH, Lub-de Hooge MN, Pleijhuis RG, Timmer-Bosscha H, Pot L, van Dam GM, van der Meulen SB, de Jong JR, Bart J, de Vries J, Jansen L, de Vries EGE, Schröder CP: 89Zr-bevacizumab PET imaging in primary breast cancer. J Nucl Med 2013, 54: 1014–8.

27. Maru D, Venook AP, Ellis LM: Predictive biomarkers for bevacizumab: are we there yet? Clin Cancer Res 2013, 19: 2824–7.

Chapter 8

Discussion and summary

Discussion

The studies described in this thesis aimed to investigate the potential of PET, using radiolabeled targeting agents directed against NSCLC tumors, as a modality to characterize these tumors and determine their sensitivity to the corresponding targeting agents. For these proof of concept studies [^{11}C]erlotinib was used as a TKI tracer and [^{89}Zr]bevacizumab as a labeled mAb. The selection of [^{11}C]erlotinib as a TKI PET tracer was based on the fact that erlotinib is one of the most commonly used TKI in NSCLC. Similarly, [^{89}Zr]bevacizumab was selected as a immunoPET tracer as it is commonly used in clinical practice.

Chapter 2

Chapter 2 comprises a review of the current literature on TKI PET and immunoPET in NSCLC. This review also includes all studies described in this thesis.

This review shows that in NSCLC patients, so far only EGFR TKIs were used in published TKI PET studies. The two most studied radiolabeled EGFR TKI are [^{11}C]PD153035 and [^{11}C]erlotinib. Preclinically, these tracers have consistently demonstrated high uptake in tumors with activating EGFR mutations, indicating that increased affinity of mutated EGFR to TKIs can be imaged. In clinical pilot studies, visualizing and quantifying tumor uptake was possible with both tracers. In addition, significant correlations were found between high tumor tracer uptake and improved therapeutic outcome on erlotinib treatment. However, as these tracers are labeled with the short-lived carbon-11 isotope, they are not suitable for widespread clinical use. To circumvent this limitation, fluorine-18 labeled second generation irreversibly binding EGFR TKI, e.g.[^{18}F]F-PEG6-IPQA and [^{18}F]afatinib, are being studied. In preclinical studies, these tracers did show better tumor-to-background ratios as compared to [^{11}C]PD153035 and[^{11}C]erlotinib, respectively. Clinical studies using these fluorine-18 labeled tracers are ongoing.

Furthermore, this review shows that preclinical immunoPET studies were performed using radiolabeled mAbs directed against all currently actionable mAb targets in NSCLC, i.e. EGFR, VEGF-A, VEGFR2 and PD-1. For all these targets, immunoPET showed its capacity to image target expression. Nevertheless, only a very limited number of clinical studies have been published using radiolabeled mAbs that are of interest in the treatment of NSCLC. In fact, nearly all clinical studies used [^{89}Zr]bevacizumab and demonstrated that tumor uptake could be visualized and quantified. Although various interesting correlations were found between tumor [^{89}Zr]bevacizumab uptake and clinical outcome, the predictive and prognostic value of imaging tumor VEGF-A with immunoPET is still unclear.

Chapter 3

The clinical study in chapter 3 describes the first-in-human TKI PET study that aimed to investigate the effect of activating EGFR mutations on tumor uptake of [^{11}C]erlotinib, by using full tracer kinetic modeling with continuous and discrete arterial sampling, and metabolite analysis. This elaborate analysis of the PET data was needed to establish the best tracer kinetic model and subsequently calculate the most accurate tracer accumulation value. The experimental design of this study included 10 patients with NSCLC, i.e. 5 with an EGFR exon 19 deletion and 5 without. Patients were scanned twice (to evaluate test-retest variability) on the same day. Each scanning procedure included a low dose CT scan, a dynamic [^{15}O]H_2O PET scan and a dynamic [^{11}C]erlotinib PET scan.

Tracer kinetic modeling showed a preference for the reversible two tissue compartment model with metabolite corrected arterial plasma input function (2T4k), with volume of distribution (V_T) as the quantitative measure of [^{11}C]erlotinib uptake. In this study, tumor V_T was significantly higher in tumors with activating EGFR mutations than in those without. Reproducibility of tumor V_T values was good. The higher tumor uptake in the mutated group is in accordance with preclinical studies, and was attributed to increased specific binding due to the increased affinity of the mutated EGFR molecule for erlotinib. Potential confounding variables, such as EGFR expression levels or tumor blood flow as measured with [^{15}O]H_2O, did not contribute to this effect, as they were not correlated with the intergroup V_T difference. This study highlights the potential capacity of TKI PET for imaging the affinity of target molecules for TKI.

Chapter 4

Chapter 4 provides an extensive tracer kinetic modeling study of [^{11}C]erlotinib. Compared with the tracer kinetic modeling aspect of the previous study, this methodological study included more patients, fitted the PET data using a larger number of kinetic models, and additionally evaluated simplified models to assess whether they could be used in future clinical whole body [^{11}C]erlotinib scans. Dynamic [^{15}O]H_2O and [^{11}C]erlotinib scans were available for 17 NSCLC patients, 8 with and 9 without an activating EGFR mutation. For 10 of the 17 patients, a retest scan on the same day was available. Kinetic modeling included single tissue and two tissue irreversible and reversible plasma input models. In addition, several advanced models that account for uptake of radiolabeled metabolites were evaluated, including a model where no correction for radiolabeled metabolites in plasma was performed. Simplified methods consisted of standardized uptake value (SUV) and tumor-to-blood ratio (TBR) for several scan intervals.

This study demonstrated that tumor kinetics were best described using the reversible two tissue compartment model without correcting the arterial plasma input function for radiolabeled metabolites (2T4k-WP), yielding optimal fits to the data, acceptable test–retest variability, no dependence on perfusion changes, and differentiating between the two clinical groups. V_T values, estimated using 2T4k-WP and 2T4k (used in Chapter 3), were highly correlated, and similar test–retest variability and separation between clinical groups were obtained. The 2T4k model did not perform better than the uncorrected model (2T4k-WP), which was probably caused by uncertainty in the estimation of true metabolite fractions. Investigation of simplified approaches showed that SUV curves did not reach equilibrium within the time of the scan. In contrast, TBR normalized to whole blood (TBR-WB) for the 40–60 min interval best correlated with V_T derived from 2T4k-WP. This indicates that static [^{11}C]erlotinib scans are best performed 40-60 minutes post injection using TBR-WB as semi-quantitative measure of uptake.

Chapter 5

Chapter 5 describes a study investigating the effects of oral erlotinib therapy on [^{11}C]erlotinib kinetics and tumor uptake. This study also looked at the effects of erlotinib therapy on tumor blood flow and its correlation with tumor [^{11}C]erlotinib uptake. In addition, the simplified uptake parameters SUV and TBR were investigated again. This time, however, also TBR values based on venous blood samples were compared with corresponding values based on arterial samples in order to investigate whether arterial cannulation can be omitted from the scanning procedure.

In this study, 10 out of the 13 patients included were scanned twice within a 1 to 2 weeks interval, i.e. on and off erlotinib therapy. Each procedure consisted of a low-dose CT scan, a dynamic [^{15}O]H_2O PET scan, and a dynamic [^{11}C]erlotinib PET scan with arterial and venous sampling at six time points. On therapy, tumor tracer kinetics again were best fitted using the 2T4k model, with V_T as measure of uptake. In all patients, tumor V_T was lower on therapy than off therapy. This finding, which is consistent with preclinical "blocking" studies, probably was due to a decrease in available binding sites under erlotinib therapy, because abundantly present non-labeled erlotinib occupies the ATP binding pockets of the EGFR molecules. This finding was independent of tumor perfusion, as perfusion measured by [^{15}O]H_2O remained unchanged during erlotinib therapy.

Both arterial and venous TBR values in the 40–50 and 50–60 min p.i. intervals were found to be strongly correlated with tumor V_T, whilst SUV did not correlate with V_T, confirming and extending the results of the previous chapter to a data set with

reduced V_T. Although there was a strong correlation between venous and arterial TBR, venous TBR was consistently lower than arterial TBR, indicating that arterial and venous values should not be interchanged.

Chapter 6

Chapter 6 presents a case report of a patient with a right upper lobe tumor, harboring an activating EGFR mutation, who underwent 2 dynamic [^{11}C]erlotinib scans over the course of her disease history. Her first PET scan, prior to initiation of erlotinib therapy, showed homogeneously elevated tracer uptake in the tumor. She responded well to erlotinib therapy and remained free of disease progression for 18 months, supporting the notion that elevated tumor [^{11}C]erlotinib uptake was associated with erlotinib efficacy. Then, she developed progression at the site of the primary tumor and a second [^{11}C]erlotinib scan was performed after discontinuation of erlotinib therapy. This latter scan showed an overall decrease in tumor [^{11}C]erlotinib uptake. In addition, the uptake pattern was heterogeneous. A biopsy from a low uptake region of the tumor revealed the presence of the secondary resistance mutation T790M. These findings support the concept that TKI PET can image (regional) tumor sensitivity and resistance to a TKI due to differences in EGFR affinity for that TKI.

Chapter 7

Chapter 7 describes the first-in-human immunoPET study using [^{89}Zr]bevacizumab in NSCLC patients who were scheduled to be treated with a bevacizumab containing regimen. This study aimed to assess whether [^{89}Zr]bevacizumab tumor uptake could be visualized and quantified, and to explore whether uptake was correlated with clinical outcome. Seven NSCLC patients underwent 2 static PET scans, i.e. at days 4 and 7 after injection of [89Zr]bevacizumab. Tumor tracer uptake, quantified using peak standardized uptake values (SUVpeak), was found to be approximately 4 times higher than in non-tumorous background tissues, both on days 4 and 7. This means that tumors could be clearly visualized within the non-tumorous background. Although VEGF-A, the target for [89Zr]bevacizumab, is considered to be a soluble and freely circulating ligand, the elevated tumor uptake supports the notion that VEGF-A concentrations are higher in tumor areas due to high paracrine expression and subsequent binding to extracellular matrix glycoproteins, such as heparan sulfate proteoglycans and neuropilins. These glycoproteins act as non-signaling co-receptors that facilitate binding of VEGF-A to VEGFR molecules. Another possible mechanism may be the internalization of [^{89}Zr]bevacizumab into cells within the tumor. After internalization, the ^{89}Zr label may become trapped in the lysosomes and show up on the PET scan. A positive trend but no significant correlation could be found between SUVpeak and overall

survival or progression free survival to bevacizumab containing chemotherapy. This indicates that more research is needed to clarify whether [^{89}Zr]bevacizumab uptake is predictive for bevacizumab efficacy.

Future aspects

[^{11}C]erlotinib and TKI PET

The studies in this thesis added new information to the existing literature on [^{11}C]erlotinib PET. Briefly, NSCLC tumors with EGFR mutations were shown to have a higher [^{11}C]erlotinib uptake as compared to those without. Also, tumor [^{11}C]erlotinib uptake was shown to decrease when patients were on erlotinib therapy. Furthermore, analysis of simplified uptake models have shown that TBR (arterial or venous) 40 to 60 min p.i. correlated best with V_T, measured with the gold standard method.

The advantage of using a simplified uptake measure such as TBR as opposed to V_T is the possibility of performing whole body PET scans. However, at present, it is unclear whether TBR is sufficiently accurate to discriminate between patient groups with different sensitivities to erlotinib. Another unclear item is whether TBR is able to identify heterogeneity in uptake between and within tumor lesions.

To address these items, a clinical study is currently ongoing at the VUmc. This study is including 3 groups of EGFR-mutated NSCLC patients with different sensitivities to erlotinib, i.e. (1) TKI-naïves prior to start of TKI, (2) after disease progression under TKI, and (3) after a TKI-holiday and prior to re-treatment with TKI. Only patients with at least 2 separate tumor lesions are included, the response to erlotinib therapy of each lesion is monitored. All patients undergo a static whole body scan using TBR 40-88 min p.i. as a measure of uptake. This study will allow to assess whether TBR can discriminate differences in erlotinib sensitivity between patient groups, and within patients.

Clinically, [^{11}C]erlotinib PET can be used in the initial diagnosis of patients with a suspicion of EGFR mutated NSCLC where no pathology proof is available. Also, whole body [^{11}C]erlotinib PET can be useful to assess residual sensitivity in different tumor lesions after disease (oligo)progression.

Although whole body [^{11}C]erlotinib PET may offer these advantages, its use will be limited to PET centers that can produce this tracer, as shipment to remote centers will not be possible due the rapid decay of carbon-11 radioactivity.

To circumvent this limitation, fluorine-18, an isotope with a longer radioactivity half-life, can be used to label EGFR TKI. Afatinib allows for the synthesis of an *in vivo* stable tracer, i.e. [^{18}F]afatinib, by substituting its constitutive fluorine atom for the fluorine-18 isotope. A clinical study using [^{18}F]afatinib is currently ongoing at the VUmc. Here, the optimal pharmacokinetic model, test-retest variability, the optimal simplified model for static scanning and the optimal timing for static scanning is assessed. Four groups of patients are being included, i.e. (1) TKI-naïve patients without EGFR mutations, (2) TKI-naïves with EGFR mutations, (3) TKI-resistant patients with EGFR and T790M mutations, and (4) TKI-resistant with EGFR and no T790M mutations. The accuracy of [^{18}F]afatinib for discriminating afatinib sensitivity (using full kinetic models and simplified models) will be assessed between patient groups and within patients.

Besides EGFR, future TKI PET studies should investigate TKIs directed against other NSCLC targets such as ALK, BRAF, ROS1, RET, and MET. For example, crizotinib is a very interesting candidate. It is a multi-target TKI used in the treatment of ALK rearranged NSCLC, however, it has also activity against ROS1 and MET. Theoretically, in these patients (harboring aberrations in ALK, ROS1 and MET), radiolabeled crizotinib and PET may predict therapy response irrespective of the sensitizing DNA aberration of the tumor. This could lead to a whole new way of personalizing therapy without necessarily performing tumor molecular analysis.

[^{89}Zr]bevacizumab and immunoPET

The [^{89}Zr]bevacizumab study in this thesis showed that uptake of [^{89}Zr]bevacizumab in NSCLC tumors could be visualized and quantified. Although there was an encouraging positive trend between tumor [^{89}Zr]bevacizumab uptake and therapy outcome using a bevacizumab containing regimen, the predictive value of tumor uptake is still unclear.

In this study, patients were scanned at 2 time points, for future studies that intend to scan at a single time point, the optimal timing needs to be determined. Also, whether additional blood sampling may help quantification is unclear. Furthermore, the level of tumor VEGF-A was not measured, so, this could not be correlated to tumor tracer uptake.

To assess the above raised items, particularly, to assess the prognostic and predictive value of tumor [^{89}Zr]bevacizumab uptake, a larger clinical trial is needed.

In routine clinical practice, [^{89}Zr]bevacizumab PET could provide for a predictive biomarker to identify patient subgroups or lesions within patients that are sensitive to bevacizumab therapy.

If validated as a predictive biomarker, its many practical advantages, such as easy to produce stable and shippable tracers, and the possibility for whole body scanning protocols using simplified parameters for easy uptake measurement, can facilitate a broad clinical application of this technique.

However, the clinical success of any immunoPET tracer will depend on how tracer uptake will relate to target expression and affinity, and how predictive target expression will be for therapy efficacy of the studied antibody. This seems very promising for cancer immuno therapy. For example, the expression levels of PD1 and PD-L1 on tumor infiltrating T-cells or tumor cells, respectively, although not exclusionary, are indicative of an improved immunotherapy outcome in patients with non-squamous NSCLC. ImmunoPET could provide a noninvasive means for repeated whole-body scanning to guide treatment decision management, hereby overcoming some of the limitations associated with the use of the current pathology-based PD1 and PD-L1 expression markers, such as variabilities in tissue preparation and processing, differences between primary tumor biopsies versus metastatic biopsies, and intrinsic versus induced PD1/PD-L1 expression levels that may change over time. This should be investigated in future immunoPET studies.

Nederlandstalige samenvatting

Discussie

De studies in dit proefschrift onderzoeken de tumorkenmerken van patiënten met NSCLC d.m.v. PET met radioactief gelabelde doelgerichte geneesmiddelen (*radiolabeled targeting agents*). Meer bepaald wordt er gekeken in hoeverre deze beeldvormende technieken in staat zijn om de gevoeligheid van tumoren voor een behandeling middels deze *targeting agents* te voorspellen. In deze *proof-of-concept* studies werden [^{11}C]erlotinib als TKI-PET *tracer* en [^{89}Zr]bevacizumab als immunoPET *tracer* gebruikt. Erlotinib en bevacizumab werden gekozen omdat ze vaak gebruikte middelen zijn in de dagelijkse praktijk.

Hoofdstuk 2

In hoofdstuk 2 wordt een overzicht gegeven van de huidige literatuur over TKI-PET en immunoPET bij NSCLC. In deze *review* werden ook de studies die in dit proefschrift zijn beschreven opgenomen.

Uit deze *review* blijkt dat de TKI-PET studies bij NSCLC patiënten tot nu toe alleen met EGFR-TKIs zijn gedaan. De 2 meest bestudeerde EGFR-TKIs waren [^{11}C]PD153035 en [^{11}C]erlotinib. In preklinisch onderzoek hebben deze *tracers* aangetoond dat tumoren met activerende EGFR-mutaties een hogere opname hadden, wat erop kan duiden dat de toegenomen affiniteit van gemuteerde EGFR moleculen voor TKIs kan worden afgebeeld. In klinische *pilot*-studies kon opname van beide *tracers* in tumoren worden gevisualiseerd en gekwantificeerd, ook werden significante correlaties gevonden tussen hoge tumor *tracer*opname en gevoeligheid voor erlotinib-therapie. Deze *tracers* die gelabeld zijn met koolstof-11 zijn (o.w.v. hun korte halfwaardetijd) niet geschikt voor routinematig gebruik in de dagelijkse klinische praktijk. Om deze beperking te kunnen overkomen werden EGFR-TKI onderzocht die gelabeld zijn met fluor-18, wat een langere halfwaardetijd heeft, bijv. [^{18}F]F-PEG6-IPQA en [^{18}F]afatinib. In preklinische studies toonden deze *tracers* een betere signaal/ruis verhouding van de tumor tot de achtergrond dan respectievelijk [^{11}C]PD153035 en [^{11}C]erlotinib. Klinische studies met deze fluor-18 gelabelde *tracers* zijn lopende.

Deze *review* laat ook zien dat er preklinisch immunoPET onderzoek gedaan is met radioactief gelabelde mAbs die gericht zijn tegen bijna alle behandelbare doelwitten in de behandeling van NSCLC, te weten EGFR, VEGF-A, VEGFR2 en PD-1. De expressie van deze *targets* kon middels immunoPET in beeld worden gebracht. Echter, slechts een zeer beperkt aantal klinische immunoPET studies zijn gepubliceerd bij patiënten met NSCLC. Bijna alle klinische studies gebruikten [^{89}Zr]bevacizumab en konden aantonen dat de *tracer*opname in tumoren kon worden gevisualiseerd en gekwantificeerd. Verder werden er verschillende

interessante correlaties gevonden tussen [^{89}Zr]bevacizumab-opname in de tumor en de klinische uitkomst van bevacizumab-behandelingen, echter, deze waren niet conclusief en blijft de predictieve en prognostische waarde van [^{89}Zr]bevacizumab PET nog onduidelijk.

Hoofdstuk 3

De studie in hoofdstuk 3 beschrijft de resultaten van de eerste klinische [^{11}C]erlotinib PET-studie naar de invloed van activerende EGFR mutaties op de opname van [^{11}C]erlotinib in NSCLC tumoren. In deze studie werd a.h.v. de PET data eerst het model bepaald wat het best overeenkwam met het farmacokinetisch gedrag van deze *tracer,* hierbij werd gebruik gemaakt van arteriële bloed*sampling* en metabolietenanalyse. Deze uitgebreide analyse was nodig om de meest accurate maat voor het kwantificeren van de *tracer*opname te bepalen. In deze studie werden 10 patiënten met NSCLC geïncludeerd, te weten 5 patiënten met een EGFR exon 19 deletie en 5 zonder. Patiënten werden tweemaal gescand (om de test-retest variabiliteit te beoordelen) op dezelfde dag. Elke scanprocedure omvatte een CT-scan, een dynamische [^{15}O]H_2O PET-scan (voor het beoordelen van de tumorperfusie) en een dynamische [^{11}C]erlotinib PET-scan.

Het *reversible 2-tissue compartment* model met metaboliet-gecorrigeerde arteriële plasma *input* (2T4k) kwam het best overeen met de PET-data met daarbij het distributievolume (V_T) als beste maat voor het kwantificeren van de [^{11}C]erlotinib-opname in tumoren. Deze studie toonde aan dat de V_T van alle tumoren met een activerende EGFR mutatie significant hoger was dan de V_T van de tumoren zonder activerende mutaties. De V_T-waarden waren goed te reproduceren. De verhoogde *tracer*opname in de gemuteerde groep werd toegeschreven aan de toegenomen specifieke binding door de verhoogde affiniteit van het gemuteerde EGFR voor de TKI. Andere variabelen zoals EGFR expressie of tumorperfusie waren gelijk tussen de groepen en konden het verschil in V_T tussen de groepen niet verklaren. Deze studie toont aan dat TKI-PET de potentie heeft om de specifieke TKI-affiniteit van de receptoren te *imagen*.

Hoofdstuk 4

Hoofdstuk 4 toont de resultaten van een uitgebreide methologisch onderzoek naar het beste farmacokinetisch model voor [^{11}C]erlotinib. Vergeleken met de vorige studie omvatte deze methodologische studie meer patiënten, bovendien werd de PET-data vergeleken met een groter aantal kinetische modellen en werden er correlaties onderzocht met vereenvoudigde modellen. Dit laatste is nodig voor het kunnen uitvoeren van statische PET scans, bv voor *whole body* (WB) scans. Voor deze methodologische analyse, werd PET-data gebruikt van dynamische [^{15}O]H_2O

en [^{11}C]erlotinib scans, verkregen bij 17 NSCLC patiënten, waarvan 8 patiënten met en 9 zonder een activerende EGFR mutatie. In 10 van de 17 patiënten, was een retest scan op dezelfde dag beschikbaar. De PET-data werd vergeleken met *1-tissue* en *2-tissue* modellen met reversibele en irreversibele plasma *input*. Daarenboven werden verschillende geavanceerde modellen onderzocht, waaronder varianten zonder correctie voor de metabolieten-fracties in het plasma. Vereenvoudigde modellen zoals *standardized uptake value* (SUV) en *tumor-to-blood ratio* (TBR) werden geëvalueerd voor meerdere scan-intervallen.

Deze methodologische studie toonde aan dat de tracerkinetiek het beste beschreven werd a.h.v. het *reversible 2-tissue* model met metaboliet-ongecorrigeerde arteriële plasma *input* (2T4k-WP). De V_T-waarden geschat volgens 2T4k-WP en 2T4k (van de eerdere studie, Hoofdstuk 3) waren sterk gecorreleerd, ze vertoonden een vergelijkbare test-retest variabiliteit en konden een vergelijkbaar klinisch groepsonderscheid maken tussen gemuteerde en niet-gemuteerde tumoren. Op dit laatste punt deed het 2T4k model het niet beter dan het ongecorrigeerde model (2T4k-WP), dit berustte waarschijnlijk op een onzekerheid in de schatting van de ware metabolietenfracties in het plasma. Bij de vereenvoudigde modellen bleken de SUV waarden geen evenwicht te bereiken binnen het tijdsbeloop van de scan en konden daarom niet worden gebruikt. Daarentegen, was TBR genormaliseerd t.o.v. *whole blood* (TBR-WB) in het interval van 40-60 minuten na de injectie (p.i.) best gecorreleerd met V_T (afgeleid van 2T4k-WP). Dit geeft aan dat statische [^{11}C]erlotinib scanprotocols best uitgevoerd worden in het 40-60 minuten p.i. interval met behulp van TBR-WB als kwantitatieve maat voor opname.

Hoofdstuk 5

Hoofdstuk 5 onderzoekt het effect van orale erlotinib-therapie op het farmacokinetisch gedrag van [^{11}C]erlotinib, de [^{11}C]erlotinib-opname in de tumor en de tumorperfusie. Daarnaast is in deze studie (vergelijkbaar met het vorige hoofdstuk) ook gekeken naar de bruikbaarheid van vereenvoudigde modellen (SUV en TBR), waarbij deze keer TBR o.b.v. veneus bloed werd vergeleken met TBR waarden o.b.v. arteriële *input.* Als veneuze bloednames gebruikt kunnen worden i.p.v. arteriële samples, kan de arterielijn achterwege gelaten worden.

Tien van de 13 geïncludeerde patiënten werden 2 maal gescand binnen een periode van 1 à 2 weken, te weten 1 keer met en 1 keer zonder erlotinib-therapie. Elke scanprocedure omvatte een CT-scan, een dynamische [^{15}O]H_2O PET-scan (tumorperfusie) en een dynamische [^{11}C]erlotinib PET-scan met arteriële en veneuze sampling op 6 tijdstippen. De tracerkinetiek van [^{11}C]erlotinib tijdens

therapie kwam het beste overeen met het 2T4k model met V_T als maat voor *tracer*opname. De V_T van de tumor was bij alle patiënten lager tijdens de erlotinib-therapie. Dit wordt waarschijnlijk veroorzaakt door een afname in de beschikbare bindingsplaatsen onder erlotinib-therapie, d.w.z. dat de ATP binding*spockets* van de EGFR-moleculen bezet worden door de overvloedig aanwezige ongelabelde erlotinib-moleculen. Dit effect wordt niet veroorzaakt door veranderingen in de tumorperfusie, omdat deze onveranderd bleef onder erlotinib-therapie.

De analyse van de vereenvoudigde modellen toonde aan dat zowel arteriële als veneuze TBR-waarden in de 40-50 en 50-60 min p.i. intervallen sterk correleerden met V_T-waarden, terwijl deze correlatie niet werd gezien tussen V_T en SUV-waarden. Dit bevestigde de conclusies van het vorige hoofdstuk in een nieuwe dataset. Er werd een sterke correlatie gezien tussen TBR-waarden op basis van arteriële en veneuze samples, echter, de veneuze sampling toonde een lagere opname, dit maakt het direct uitwisselen van veneuze en arteriele TBR-waarden met elkaar niet mogelijk.

Hoofdstuk 6

In hoofdstuk 6 wordt de casus beschreven van een patiënte met een NSCLC tumor met een activerende EGFR-mutatie, die 2 maal een dynamische [^{11}C]erlotinib PET-scans onderging over het beloop van haar ziekte. Haar eerste PET-scan, voorafgaand aan haar behandeling met erlotinib, toonde een homogeen toegenomen *tracer*opname in alle delen van de tumor. Hierna startte ze met de erlotinib-therapie en zij bleef vrij van progressie voor 18 maanden. Vervolgens was er ziekteprogressie t.p.v. de primaire tumor en een tweede [^{11}C]erlotinib PET-scan werd gemaakt na het staken van de erlotinib-therapie. Deze PET-scan toonde aan dat de *tracer*opname over het geheel van de tumor was afgenomen en dat het opnamepatroon meer heterogeen was geworden. Een biopsie uit een gebied met lage *tracer*opname toonde de aanwezigheid aan van de secundaire resistentiemutatie T790M. Deze bevindingen ondersteunen het concept dat TKI-PET de (regionale) tumorgevoeligheid voor TKIs kan *imagen*, waarbij ook nog heterogeniteit kan worden vastgesteld binnenin een tumorlesie. Verder illustreert deze casus dat de gevoeligheid van de tumor over verloop van tijd kan veranderen en dat dit ook in beeld gebracht kan worden met deze techniek.

Hoofdstuk 7

Hoofdstuk 7 beschrijft de eerste klinische immunoPET studie met [^{89}Zr]bevacizumab in een populatie van NSCLC patiënten. In deze studie werden de patiënten na de PET-scan behandeld met bevacizumab en chemotherapie. De studie onderzocht of opname van [^{89}Zr]bevacizumab in de tumor zou kunnen

worden gevisualiseerd en gekwantificeerd. Er werd ook gekeken of deze opname kon worden gecorreleerd met de tumorrespons op de behandeling middels bevacizumab en chemotherapie. Zeven NSCLC patiënten ondergingen 2 statische PET-scans, te weten op dag 4 en 7 na *tracer*injectie. *Tracer*opname in de tumor werd gekwantificeerd d.m.v. SUVpeak. De *tracer*opname in de tumor was gemiddeld ongeveer 4 maal hoger dan in het niet-tumoreus achtergrondweefsel, zowel op dag 4 als op dag 7. Dit betekent dat de tumoren duidelijk zichtbaar waren tegen de niet-tumoreuze achtergrond. Hoewel VEGF-A, de *target* van [^{89}Zr]bevacizumab, wordt beschouwd als een vrij circulerende solubele ligand, kon deze studie aantonen dat er verhoogde *tracer*opname was bij de tumor. Dit ondersteunt het idee dat VEGF-A concentraties hoger zijn in de tumorgebieden als gevolg van hoge paracriene expressie en binding aan extracellulaire matrixglycoproteïnen zoals heparansulfaat proteoglycanen en neuropilines. Deze glycoproteïnen fungeren als niet-signalerende co-receptoren die de binding van VEGF aan VEGFR vergemakkelijken. Een ander mogelijk mechanisme is de internalisering van [^{89}Zr]bevacizumab in tumorcellen, waarbij de zirconium-89-labels gevangen raken in de lysosomen en een signaal blijven afgeven op de PET-scan. Verder werd er een positieve trend gezien tussen enerzijds de *tracer*opname en anderzijds de *overall survival* en de progressievrije overleving na bevacizumab en chemotherapie. Deze bemoedigende resultaten geven aan dat meer onderzoek nodig is om te bepalen wat de voorspellende waarde is van [^{89}Zr]bevacizumab-opname in tumoren voor wat betreft de werkzaamheid van bevacizumab-behandelingen.

Toekomstige aspecten

[^{11}C]erlotinib en TKI-PET

De onderzoeken in dit proefschrift hebben nieuwe informatie opgeleverd m.b.t. [^{11}C]erlotinib-PET. In het kort, er werd aangetoond dat de opname van [^{11}C]erlotinib hoger was bij patiënten met een EGFR-gemuteerde tumor. Tijdens erlotinib-therapie daalde de opname van [^{11}C]erlotinib in de tumor. Het vereenvoudigde model wat het beste correleerde met de V_T-waarden van [^{11}C]erlotinib was de TBR (arterieel en veneus) in het 40 tot 60 min p.i. interval.

TBR biedt het voordeel dat het gebruikt kan worden om *whole body* PET-scans te maken. Echter, het is onduidelijk of TBR voldoende nauwkeurig is om onderscheid te kunnen maken tussen groepen met verschillende gevoeligheden voor erlotinib. Het is ook onduidelijk of TBR voldoende heterogeniteit kan herkennen in de sensitiviteit voor erlotinib tussen tumorlesies en binnenin de tumorlesies.

Er is momenteel een klinische studie lopende in het VUmc om deze onduidelijkheden te onderzoeken. Drie groepen van EGFR-gemuteerde NSCLC patiënten worden geïncludeerd, te weten (1) TKI-naïeve patiënten vooraf aan het starten van een TKI, (2) na ziekteprogressie op een TKI en (3) na een TKI-*holiday* vooraf aan herbehandeling met een TKI. Alleen patiënten met minstens 2 tumorlesies worden geïncludeerd, de respons van elke aparte lesie op de behandeling wordt gevolgd. Alle patiënten ondergaan een *whole body* PET-scan met TBR tussen 40 en 88 min p.i. als maat voor opname. Deze studie zal kunnen beoordelen of TBR de verschillen in erlotinib-gevoeligheid kan onderscheiden tussen verschillende patiëntengroepen en tussen lesies binnen de patiënt.

In de routinematige patiëntenzorg kan [^{11}C]erlotinib-PET gebruikt worden om een eventuele verhoogde gevoeligheid van een tumor voor erlotinib-therapie aan te tonen, bijv. bij patiënten waar geen weefselbewijs voorhanden is om een EGFR mutatie aan te tonen. Een *whole body* [^{11}C]erlotinib-PET kan ook nuttig zijn om residuele erlotinib-gevoeligheid in de diverse lesies op te sporen i.g.v. ziekteprogressie. Echter, het gebruik van *whole body* [^{11}C]erlotinib-PET zal beperkt blijven tot PET-centra die deze tracer kunnen produceren, omdat het transport ervan naar centra op afstand niet mogelijk is vanwege de korte halfwaardetijd van koolstof-11.

Om deze beperking te omzeilen kan fluor-18, een isotoop met een langere halfwaardetijd, worden gebruikt als label voor EGFR-TKI-*tracers*. Door substitutie van de eigen fluoratoom voor het fluor-18 isotoop kan afatinib worden gelabeld tot de *in vivo* stabiele tracer [^{18}F]afatinib. Een klinische studie met [^{18}F]afatinib is momenteel aan de gang in het VUmc. Hierbij worden het optimale farmacokinetisch model, de test-retest variabiliteit, het optimale vereenvoudigd model voor het statisch scannen en het optimale tijdstip voor het statisch scannen beoordeeld. Vier groepen van patiënten worden geïncludeerd, te weten (1) TKI-naïeve patiënten zonder EGFR mutaties (2) TKI-naïeven met EGFR mutaties (3) TKI-resistente patiënten met EGFR en T790M mutaties, en (4) TKI-resistenten met EGFR zonder T790M mutaties. De nauwkeurigheid van de [^{18}F]afatinib-PET voor het onderscheiden van afatinib-gevoeligheid zal worden beoordeeld tussen deze patiëntengroepen en tussen tumorlesies binnen de patiënt.

Maar naast EGFR dient toekomstig TKI-PET onderzoek zich ook te richten op andere NSCLC *targets* zoals ALK, BRAF, ROS1, RET en MET. Crizotinib is hierbij een zeer interessante kandidaat. Het is een multi-target TKI wat actief is tegen DNA abberaties in ALK, maar ook actief is tegen ROS1 en MET. Theoretisch zou het gelabelde crizotinib bij deze patiënten de kans op respons kunnen voorspellen

ongeacht welke sensibiliserende DNA aberratie er in de tumor gevonden wordt. Deze gedachte illustreert dat deze techniek in potentie een leidraad kan bieden voor de keuze van een TKI-behandeling zonder dat er vooraf moleculaire analyse van de tumor gedaan is of kon worden.

TKI-PET-tracers hebben het potentieel vermogen om in vivo de affiniteit en daarmee de gevoeligheid van een receptor voor de bijbehorende TKI af te beelden. Dit biedt een unieke meerwaarde voor de diagnostiek wat niet kan worden verkregen met een andere techniek. Echter, het vergt nog veel onderzoek om TKI-PET in de routine klinische praktijk te krijgen.

[^{89}Zr]bevacizumab en immunoPET

De [^{89}Zr]bevacizumab studie in dit proefschrift toonde aan dat de opname van [^{89}Zr]bevacizumab in NSCLC tumoren kon worden gevisualiseerd en gekwantificeerd. Hoewel er een bemoedigende positieve trend was tussen enerzijds de *tracer*opname en anderzijds de *overall survival* en de progressievrij overleving met bevacizumab en chemotherapie, blijft de voorspellende waarde van tumoropname onduidelijk. In deze studie werden patiënten gescand op 2 tijdstippen, echter, voor toekomstige studies die op één tijdstip zullen scannen moet het optimale tijdstip nog worden bepaald. Verder is het nog onduidelijk of een aanvullende bloedafname nog kan helpen bij de kwantificering van de *tracer*opname. Het niveau van VEGF-A in de tumoren werd niet gemeten en dit kon ook niet worden gecorreleerd met tumor *tracer*opname.

Er is meer klinisch onderzoek nodig om hierbovengenoemde onduidelijkheden te onderzoeken en m.n. ook de prognostische en predictieve waarde van [^{89}Zr]bevacizumab-opname in tumoren te beoordelen.

In de klinische praktijk zou [^{89}Zr]bevacizumab-PET een voorspellende biomarker kunnen zijn om subgroepen van patiënten te identificeren die gevoelig zijn voor bevacizumab-therapie.

Mocht [^{89}Zr]bevacizumab gevalideerd worden als predictieve marker, kunnen de vele praktische voordelen zoals het feit dat de tracer makkelijk te produceren en stabiel is, dat het makkelijk verzendbaar is naar andere centra en het de mogelijkheid biedt voor whole body scans de implementatie van deze techniek in de klinische praktijk vergemakkelijken.

Echter, het klinische succes van immunoPET zal uiteindelijk afhangen van enerzijds hoe goed een specifieke gelabelde mAb de expressie van diens *target*-moleculen in de tumor kan *imagen* en anderzijds hoe goed het *target*-expressieniveau in de

tumor uiteindelijk de werkzaamheid van de mAb-behandeling kan voorspellen. Dit laatste lijkt veelbelovend voor immunotherapie. De expressie van PD1 en PD-L1 in tumor infiltrerende T-cellen en tumorcellen kunnen voorspellend zijn voor respons op immunotherapie bij patiënten met niet-squamous NSCLC. Indien PD1- of PD-L1-expressie succesvol gereflecteerd kan worden door immunoPET zou dit een nuttige, noninvasieve methode kunnen zijn voor *whole body* scanning wat over het ziektebeloop vaker herhaald kan worden en wat leidend kan zijn voor het nemen van behandelbeslissingen rondom immunotherapie. Dit zou in toekomstige immunoPET studies onderzocht moeten worden.

Dankwoord

Dankwoord

Dankzij de bijdrage en steun van vele betrokkenen kon dit proefschrift tot stand komen. Enkelen wil ik hieronder in het bijzonder bedanken.

Allereerst wil ik de patiënten en families bedanken die deelnamen aan de studies in dit proefschrift. "Dan helpt het een ander" was meestal de motivatie voor deze patiënten om toch de inspanning te doen en uren onder de scanner stil te liggen. Voor hun belangeloze inzet ben ik zeer dankbaar.

Omdat dit proefschrift op het raakvlak ligt tussen nucleaire geneeskunde, klinische fysica en longziekten is het ook niet te verwonderen dat ik 3 promotoren en 1 co-promotor heb. Prof. dr. Hendrikse, beste Harry, ik dank je voor de prettige samenwerking. Je interesse en betrokkenheid (ook voor persoonlijke omstandigheden) waardeer ik enorm. Prof. dr. Lammertsma, beste Adriaan, dankzij jouw inzichten en messcherpe analyses heb ik veel geleerd over *kinetic modeling* en basisprincipes van de klinische fysica die hierop toegepast worden. In de beginperiode kon ik je helaas niet altijd volgen en moest ik zelfs geluidsopnames maken om het allemaal nog eens na te luisteren en na te zoeken, dat hoefde later gelukkig niet meer. Prof. dr. Smit, beste Egbert, je doortastende aanpak, heldere visie en kritische houding als wetenschapper en als clinicus zijn inspirerend. Mijn co-promotor en tevens mijn persoonlijke fysicus ir. dr. Yaqub, beste Maqsood, dankjewel voor je inzet. Ik ben erg blij met onze abstracte discussies over farmacokinetische *modeling*, de naloopsessies van foutgelopen scans, de run-sessies van matlab-scripts, input curves maken, etc, ze waren voor mij niet alleen leerzaam maar ook erg gezellig.

Vele collega's deden hun best om dit promotietraject voor mij mogelijk te maken. Hierbij denk ik aan mijn opleiders in het Rijnstate ziekenhuis, m.n. Frank van den Elshout en Hans Smit, maar ook Eric Ullmann. Ik wil jullie danken voor jullie begeleiding en tussenkomst om de brug te slaan naar het Vumc. Prof. dr. Postmus, beste Piet, dank je wel voor het vertrouwen en de ruimte die ik kreeg om aan dit traject te beginnen. En uiteraard prof. dr. Vonk-Noordegraaf, beste Anton, als huidige afdelingshoofd heb je me net als Piet de ruimte gegeven om dit promotietraject op mijn eigen ritme af te maken, waarvoor dank. Mijn directe onco-collega's Annemarie Becker, Sayed Hashemi en Joop de Langen, dank jullie voor jullie geduld en steun waardoor ik vrij werd gespeeld om dit proefschrift te kunnen afronden in een periode waarin de drukte op de polikliniek alleen maar toenam.

De leden van de leescommissie, beste prof.dr. Stroobants, prof.dr. Wolf, prof.dr. Groen, prof.dr. Hoekstra, dr. Menke-van der Houven van Oordt, dr de Langen. Ik wil U bedanken voor de tijd en moeite die u nam voor het kritisch beoordelen van dit proefschrift.

De medewerkers van de "PET"-afdeling, in het bijzonder Judith van Es, Femke Jongsma, Amina el Ouahmani, Nasserah Sais, Cemile Karga,Tamara Kraal-van Beaumont, Kitty Mascini, Suzette van Balen, Henri Greuter, Robin Hemminga, Nghi Pham en anderen die ik nu vergeten ben te noemen, jullie deden altijd het uiterste om de PET-scans te laten slagen. Jullie inspanningen in de planning, de patiëntenbegeleiding, het scannen en de verwerking van de PET- en bloeddata waren enorm. AnnaLarissa Niemeijer, jij hoort bij de longafdeling, maar ik wil je voor nu bij de PET-collega's noemen, omdat je me vaak uit de nood hielp als stand-in. Ik ben jullie allen zeer dankbaar voor jullie harde werk.

Mijn lieve ouders, jullie dank ik voor jullie steun in moeilijke tijden, jullie tomeloze liefde en de vanzelfsprekendheid van alle opofferingen die jullie deden voor mijn broer en ik.

Mijn liefste betere helft, jij en onze zoons zijn mijn grootste zegeningen. Ik ben zeer dankbaar voor jou, voor jouw steun en liefde, zonder jullie zou ik hier niet kunnen of willen staan.

List of Publications

List of Publications

1. Yaqub M, Bahce I, Voorhoeve C, Schuit RC, Windhorst AD, Hoekstra OS, et al. Quantitative and simplified analysis of 11C-erlotinib studies. Journal of Nuclear Medicine. 2016, 57: 861–866.

2. Bahce I, Yaqub M, Errami H, Schuit RC, Schober P, Thunnissen E, et al. Effects of erlotinib therapy on [11C] erlotinib uptake in EGFR mutated, advanced NSCLC. EJNMMI research. 2016, 6: 1–13.

3. Bahce I, Yaqub M, Smit E, Lammertsma A, van Dongen G, Hendrikse N. Personalizing NSCLC therapy by characterizing tumors using TKI-PET and immuno-PET. Lung Cancer. 2016. doi:10.1016/j.lungcan.2016.05.025.

4. Kuiper JL, Hendriks LE, van der Wekken AJ, de Langen AJ, Bahce I, Thunnissen E, et al. Treatment and survival of patients with EGFR-mutated non-small cell lung cancer and leptomeningeal metastasis: A retrospective cohort analysis. Lung cancer. 2015, 89: 255–261.

5. Dingemans A-M, Groen H, Herder G, Stigt J, Smit E, Bahce I, et al. A randomized phase II study comparing paclitaxel-carboplatin-bevacizumab with or without nitroglycerin patches in patients with stage IV nonsquamous nonsmall-cell lung cancer: NVALT12 (NCT01171170). Annals of Oncology. 2015, 26: 2286–2293.

6. Kuiper JL, Bahce I, Voorhoeve C, Yaqub M, Heideman DA, Thunnissen E, et al. Detecting resistance in EGFR-mutated non-small-cell lung cancer after clonal selection through targeted therapy. Personalized Medicine. 2015, 12: 63–66.

7. Iqbal R, Kramer GM, Verwer EE, Huisman MC, De Langen AJ, Bahce I, et al. Multiparametric analysis of the relationship between tumor hypoxia and perfusion using 18F-FAZA and 15O-H2O PET. Journal of Nuclear Medicine. 2016, 57: 530–535.

8. Bahce I, Vos C, Dickhoff C, Hartemink K, Dahele M, Smit E, et al. Metabolic activity measured by FDG PET predicts pathological response in locally advanced superior sulcus NSCLC. Lung Cancer. 2014, 85: 205–212.

9. Vos C, Dahele M, de Koste J van S, Senan S, Bahce I, Paul M, et al. Semiautomated volumetric response evaluation as an imaging biomarker in superior sulcus tumors. Strahlentherapie und Onkologie. 2014, 190: 204–209.

10. Bahce I, Huisman MC, Verwer EE, Ooijevaar R, Boutkourt F, Vugts DJ, et al. Pilot study of 89Zr-bevacizumab positron emission tomography in patients

with advanced non-small cell lung cancer. EJNMMI Research. 2014, 4: 35. doi: 10.1186/s13550-014-0035-5.

11. Bahce I, Smit EF, Lubberink M, van der Veldt AAM, Yaqub M, Windhorst AD, et al. Development of [(11)C]erlotinib positron emission tomography for in vivo evaluation of EGF receptor mutational status. Clin Cancer Res. 2013, 19: 183–93.

12. Kramer G, Yaqub M, Bahce I, Smit E, Lubberink M, Hoekstra O, et al. CT-perfusion versus [15O] H2O PET in lung tumors: Effects of CT-perfusion methodology. Medical physics. 2013, 40: 052502. doi: 10.1118/1.4798560.

13. Verwer EE, van Velden FH, Bahce I, Yaqub M, Schuit RC, Windhorst AD, et al. Pharmacokinetic analysis of [18F] FAZA in non-small cell lung cancer patients. European journal of nuclear medicine and molecular imaging. 2013, 40: 1523–1531.

14. Van der Veldt AA, Lubberink M, Bahce I, Walraven M, de Boer MP, Greuter HN, et al. Rapid decrease in delivery of chemotherapy to tumors after anti-VEGF therapy: implications for scheduling of anti-angiogenic drugs. Cancer cell. 2012, 21: 82–91.

15. Petrulli JR, Hansen SB, Abourbeh G, Yaqub M, Bahce I, Holden D, et al. A multi species evaluation of the radiation dosimetry of [11C]erlotinib, the radiolabeled analog of a clinically utilized tyrosine kinase inhibitor. Nucl Med Biol. 2017 Apr;47:56-61. doi: 10.1016/j.nucmedbio.2016.12.009.